12-31-2019

Cerebro-vascular disruption mediated initiation and propagation of traumatic brain injury in a fluid percussion injury model

Xiaotang Ma
New Jersey Institute of Technology

Copyright Warning & Restrictions

The copyright law of the United States (Title 17, United States Code) governs the making of photocopies or other reproductions of copyrighted material.

Under certain conditions specified in the law, libraries and archives are authorized to furnish a photocopy or other reproduction. One of these specified conditions is that the photocopy or reproduction is not to be "used for any purpose other than private study, scholarship, or research." If a, user makes a request for, or later uses, a photocopy or reproduction for purposes in excess of "fair use" that user may be liable for copyright infringement,

This institution reserves the right to refuse to accept a copying order if, in its judgment, fulfillment of the order would involve violation of copyright law.

Please Note: The author retains the copyright while the New Jersey Institute of Technology reserves the right to distribute this thesis or dissertation

Printing note: If you do not wish to print this page, then select "Pages from: first page # to: last page #" on the print dialog screen

ABSTRACT

CEREBRO-VASCULAR DISRUPTION MEDIATED INITIATION AND PROPAGATION OF TRAUMATIC BRAIN INJURY IN A FLUID PERCUSSION INJURY MODEL

by
Xiaotang Ma

Traumatic brain injury (TBI) is a major health problem for over 3.17 million people in the US. There is no FDA-approved drug for the treatment because the injury mechanisms have not been clearly identified. The knowledge gap is addressed here by the lateral fluid percussion injury (FPI) rat model, through the understanding of layer-structured mechanisms from physical vascular rupture to acute necrosis, as well as biochemical changes in perivascular space as secondary events.

Firstly, the cerebrovascular hemorrhage and related infarct volume are investigated as the primary events in moderate FPI, which is found to be increased with injury severity in FPI. The extent of coagulation is validated by the bio-distribution of fluorescent tracer in the cerebrospinal fluid (CSF) pathway after the injury. Bio-distribution of the tracer is specifically diminished at the site of coagulation, which blocks the CSF movement in subarachnoid and interstitial spaces. The pattern of coagulation is associated with the CSF blockage and correlates to necrotic cell death in and around the impact site. Different biomarkers for immune cells, neuronal death and tight junction proteins show that physical disruption of vasculature plays an important role for the acute induction of neuroinflammation and neurodegeneration in blunt TBI.

Additionally, free radicals generation is found to be significantly increased in the injured hemisphere immediately post FPI and decreases over time. Upregulation of radical-generating enzymes, NADPH oxidase 1 as well as inducible nitric oxide synthase,

initiates biochemical damage of the injured brain. As a result, the signatures of oxidative/nitrosative damage markers 4-HNE and 3-NT are observed in the blood brain barrier (BBB) post-TBI, with temporal changes in the injury site. Oxidative/nitrosative damage and immune cells infiltration correlate with gliosis at 4 hours and 7 days post moderate FPI. Examination of apoptosis, tau phosphorylation, and neuronal survivability at day 7 post FPI further validate neurodegeneration. Thus, it is confirmed that the acute and long-term neuroinflammation and neurodegeneration are correlated with cerebral vascular disruption.

Finally, novel regenerative medicines are explored for in-situ repair with angiogenesis and neuroprotection mechanisms in the injured brain post-TBI. An injectable self-assembling peptide-based hydrogel (**SAPH)** appended with vascular endothelial growth factor (VEGF) mimic is used to create a regenerative microenvironment for neovascularization at the injury site. VEGF is an angiogenic and neuroprotective growth factor that is involved in the process of brain repair. Supramolecular assembly allows for thixotropy; the injectable drug delivery system provides sustained *in vivo* efficacy. Application of the angiogenic SAPH directly in the injury site promotes disrupted vasculature repair in and around the hydrogel implant at day 7 post-TBI. Upregulation of VEGF-receptor 2 is observed, demonstrating an angiogenic response in the presence of angiogenic SAPH. Moreover, vascular markers von-Willebrand factor (vWF) and α-smooth muscle actin (α-SMA) show a concomitant increase with blood vessels in response to the angiogenic SAPH. The neuronal rescue examination by NeuN and myelin basic protein shows that the SAPH has the potential to provide neuroprotective benefits in the long-term recovery.

CEREBRO-VASCULAR DISRUPTION MEDIATED INITIATION AND PROPAGATION OF TRAUMATIC BRAIN INJURY IN A FLUID PERCUSSION INJURY MODEL

by
Xiaotang Ma

A Dissertation
Submitted to the Faculty of
New Jersey Institute of Technology
And Rutgers University Biomedical and Health Sciences - Newark
in Partial Fulfillment of the Requirements for the Degree of
Doctor of Philosophy in Biomedical Engineering

Department of Biomedical Engineering

December 2019

.

APPROVAL PAGE

CEREBRO-VASCULAR DISRUPTION MEDIATED INITIATION AND PROPAGATION OF TRAUMATIC BRAIN INJURY IN A FLUID PERCUSSION INJURY MODEL

Xiaotang Ma

Dr. James Haorah, Dissertation Advisor — Date
Associate Professor, Department of Biomedical Engineering, NJIT

Dr. Namas Chandra, Committee Member — Date
Distinguished Professor, Department of Biomedical Engineering, NJIT

Dr. Bryan J. Pfister, Committee Member — Date
Professor & Chair, Department of Biomedical Engineering, NJIT

Dr. Vivek Kumar, Committee Member — Date
Assistant Professor, Department of Biomedical Engineering, NJIT

Dr. Kevin Pang, Committee Member — Date
Professor, Department of Pharmacology, Physiology & Neuroscience,
Rutgers New Jersey Medical School

Dr. Joshua Berlin, Committee Member — Date
Professor, Department of Pharmacology, Physiology & Neuroscience,
Rutgers New Jersey Medical School

BIOGRAPHICAL SKETCH

Author: Xiaotang Ma

Degree: Doctor of Philosophy

Date: December 2019

Undergraduate and Graduate Education:

- Doctor of Philosophy in Biomedical Engineering,
  New Jersey Institute of Technology, Newark, NJ, 2019

- Master of Science in Biomedical Engineering,
  New Jersey Institute of Technology, Newark, NJ, 2015

- Bachelor of Science in Bioengineering,
  Northwest A&F University, Shaanxi, People's Republic of China, 2013

Major: Biomedical Engineering

Presentations and Publications:

Ma, X., Aravind, A., Pfister, B. J., Chandra, N., Haorah, J. (2019). "Animal Models of Traumatic Brain Injury and Assessment of Injury Severity". Molecular neurobiology, 1-14.

Ma, X., Cheng, Y., Garcia, R., Haorah, J., (2019). "Hemorrhage Associated Mechanisms of Neuroinflammation in Experimental Traumatic Brain Injury". Journal of NeuroImmune Pharmacology, 1–15.

Ma, X., Agas, A., Siddiqui, Z., Kim, K., Iglesias-Montoro, P., Kalluru, J., Kumar, V., Haorah, J., "Angiogenic Peptide Hydrogels for treatment of Traumatic Brain Injury". Bioactive Materials (2019 In revision)

Ma, X., Cheng, Y., Haorah, J., "Oxidative/nitrosative damage mediated cerebrovascular neuroinflammation and neurodegeneration after traumatic brain injury". (2019 in preparation)

Sarkar, B.[1], Ma, X.[1], Iglesias-Montoro, P., Siddiqui, Z., Haorah, J., Kumar, V., "Self-assembling Peptide Hydrogel for Neuroprotection after Traumatic Brain Injury". Scientific Reports. (2019 Submitted).

Ma, X., Sarkar, B., Kumar, .V, Haorah, J., Society of Neuroscience (2019), Chicago, IL, "Vascular Pathology Mediated Traumatic Brain Injury and The Regenerative Treatment Using Peptide Hydrogel".

Ma, X., Agas, A., Sarkar, B., Iglesias-Montoro, P., Siddiqui, Z., Kumar, V., Haorah, J., Biomedical Engineering Society 2019 Annual Meeting, Philadelphia, PA, "Self-assembling Peptide Hydrogel for Neuroprotection after Traumatic Brain Injury".

Ma, X., Agas, A., Sarkar, B., Iglesias-Montoro, P., Siddiqui, Z., Kumar, V., Haorah, J., Biomedical Engineering Society 2019 Annual Meeting, Philadelphia, PA, "Self-assembling Peptide Hydrogel for Angiogenesis after Traumatic Brain Injury".

Ma, X., Cheng, Y., Garcia, R., Haorah, J.., Biomedical Engineering Society (2018), Atlanta, GA," Focal Hemorrhage Initiated Perivascular Inflammation and Neurodegeneration in Fluid Percussion Animal Model"

Cheng, Y., Liu, X., Ma, X., Garcia, R., Belfield, K., Haorah, J., Alcohol promotes waste clearance in the CNS via brain vascular reactivity. Free Radical Biology and Medicine. 2019 Nov 1;143:115-26.

Abdul-Muneer, PM., Alikunju, S., Schuetz, H., Szlachetka, AM., Ma, X., Haorah, J., Impairment of thiamine transport at the GUT-BBB-AXIS contributes to Wernicke's encephalopathy. Molecular neurobiology. 2018 Jul 1;55(7):5937-50.

This thesis is dedicated to my parents Hailong Ma and Wenli Li, and my husband, Biao Leng; it was their support that gave me the ability to complete this work.

ACKNOWLEDGMENT

First and most importantly, I would like to thank my Ph.D. advisor Dr. James Haorah for his immense kindness and support. I cannot tell how grateful I am to be his graduate student for all these years. He has always helped me to make progress with the kindest hearts, and to guide me step by step. I feel so blessed to have him as my mentor in my Ph.D. career.

As our collaborator, Dr. Vivek Kumar designed and provided the novel regenerative treatment for my project. He gave me a lot of help and support to make my research better. He taught me the presentation and scientific writing skills that will benefit my future.

I also want to thank Dr. Namas Chandra for providing support for my research, allowing me to perform some of the most important experiments for my research in his lab. I enjoyed talking to him and listening to his insightful comments.

I still remember when I took Dr. Bryan Pfister's course in my first semester as a graduate student. I was bad at writing and research at that time, so I withdrew at the end. Then it became my goal to be a qualified researcher and keep developing myself to be better. I've always appreciated his encouragement as my committee member and chair of our department.

I want to thank Dr. Joshua Berlin for his patience and guidance throughout my dissertation progress. His comments and advice has made me a more qualified young researcher. I want to let him know how appreciative I am for his help in science. His feedback at the final stages of my research was invaluable.

And it was my great pleasure to have Dr. Kevin Pang on my committee. Since I took his course in UMDNJ at the beginning of my Ph.D. program, I know he is a very good scientist and professor. His scientific input in my dissertation lead it to be a more thorough study.

I would like to thank Department of Biomedical Engineering for their financial support. I express my heart-felt gratitude to my lab mates: Yiming Cheng and Agnieszka Agas; it would be significantly more difficult without their scientific inputs and personal helps to finish my experiments. I'd like to take the chance to thank all my colleagues in Dr. Chandra and Dr. Pfister's lab, who work closely with me and became my friends over the years. It's my pleasure to work with all of them. Aswati Aravind, Matthew Kuriakose, Millie Swietek, Ningning Shao, Daniel Younger, Matthew Long, Jose Rodriguez, their help and support is the light to hold me through the dark days. And of course my previous lab mate Pamela Hitscherich, her help and encouragement is with me in the past and the future.

Finally, I would like to thank my husband and my parents for their love; their support is my greatest motivation.

TABLE OF CONTENTS

TABLE OF CONTENTS
(Continued)

Chapter **Page**

TABLE OF CONTENTS
(Continued)

Chapter **Page**

TABLE OF CONTENTS
(Continued)

Chapter **Page**

TABLE OF CONTENTS
(Continued)

Chapter **Page**

LIST OF TABLES

LIST OF FIGURES

LIST OF FIGURES
(Continued)

Figure **Page**

CHAPTER 1

INTRODUCTION

1.1 Traumatic Brain Injury

Traumatic brain injury (TBI) is a major cause of death and disability in the world, particularly caused by an external insult in the battlefield or in civilian life [1]. There are about 2.2 million people who suffer TBI each year in the US, which accounts for more than 3.2-5.3 million people living with a life-long disability [2]. Incidence of TBI is still rising with 2.8 million TBI-related emergency hospital visits and deaths in 2013 in the US. These TBI patients consist of about 54% children and 79% seniors that resulted from falls [3]. The incidence of motor vehicle accidents, athletic sports head injury, and blast-wave diffuse injury are also major causes of TBI [4]. Many of these brain injuries when left untreated or without properly management, lead to development of cognitive/behavioral impairment [5, 6], PTSD [7-9], chronic encephalopathy [10-12], epileptic seizure [13, 14], and neurodegenerative Alzheimer's disease [15-17].

TBI is a complex disease process causes structural damage and functional impairment due to primary and secondary injury mechanisms. The primary injury is immediately caused by a mechanical pulse on the brain tissue at the time of exposure; this process includes surface contusion, damage to blood vessels, laceration, and axonal shearing. Secondary injury happens minutes to months after the primary injury, resulting from cascades of metabolic, cellular and molecular events that lead to brain cell death, tissue damage and atrophy [18]. Common features are apnea and hypoxia, which leads to ischemia of the brain. Many biochemical mechanisms

underlying TBI pathophysiology have been confirmed, such as oxidative stress, glutamate excitotoxicity, inflammation, apoptosis and necrosis in animal model studies [19]. Cell death happens within minutes to months post TBI, and necrotic and apoptotic cell death occurs specifically in contused areas and the boundaries, leading to cognitive deficits and neurodegeneration [20].

Over the past decades, despite numbers of phase III clinical trials of TBI pathophysiology modulating candidates, no treatment has been shown to be efficacious [21, 22]. The reasons of failures were complicated, and the underlying mechanism of TBI is not well understood yet, as the patients are always present with complicated lesions of different severity and regional distribution. There are two main types of TBI insults; focal and diffuse injuries. Focal injuries are localized damages at the site of the impact, characterized by contusions and lacerations, leading to local hematoma. Diffuse injuries are with brain swelling, diffuse axonal injury (DAI) and ischemic brain injury both at the impact site and remote sites [23]. But some brain injuries are mixed injuries with focal and diffuse injury patterns.

1.2 Experimental Methodology in Traumatic Brain Injury

Animal models have been used to recapitulate salient features of TBI pathophysiology. Although there is no specific animal model that can accurately mimic human brain injury [24]. Notwithstanding, these animal models of TBI offer a viable alternative to examine the biomechanical, cellular and molecular mechanisms of TBI-associated neuropathological progression and the time-dependently effects. **Table 1.1** shows current animal models of TBI, the types of injury, the clinical relevance, and the

strengths or the weaknesses of each TBI model within the category of focal, diffuse, and mixed mechanisms of injury.

Table 1.1 Animal models of experimental TBI.

Model	Injury	Clinical Relevance	Strength	Weakness
Fluid-Percussion Midline Lateral	Mixed Mixed	Direct brain deformation. Cerebral concussion Example: Sports related TBI: Boxing, Football	Severity of injury can be adjusted; inflicted injury is highly reproducible within one laboratory	Requires craniotomy that may compensate for ICP increases; no immediate post-injury neuroscoring; possible inflicted injury is variable between different laboratories; high mortality rate due to apnea
Controlled Cortical Impact Open-skull Closed-skull	Mainly focal	Direct brain deformation. Cerebral concussion with subarachnoid hemorrhage. Example: Sports related TBI: Boxing, Football	Severity of injury can be adjusted, inflicted injury is highly reproducible	Requires craniotomy; no immediate post-injury neuroscoring
Weight Drop Feeney Shohami Marmarou	Mainly focal Mainly focal Mainly diffuse	Hemorrhage and diffuse axonal injury. Example: Falling down, Motor vehicle accidents	Mechanism is similar to human TBI, severity of injury can be adjusted; well characterized neuroscoring; immediately after injury allows randomization; inexpensive	High mortality rate due to apnea and skull fractures; not highly reproducible; high variability in injury severity
Blast Wave Model Shock/blast tube	Diffuse	Blast Wave induced TBI (Battle field)	Similar to soldiers in battle field.	Not so precise mimicking human TBI

Source: [25]

To evaluate the efficacy of therapeutic treatments, the assessment of injury severity post TBI has played a critical role. In clinical settings, Glasgow Coma Scale (GCS) [26, 27] or improved/extended GCS (GCSE) [27] is used for the severity of

TBI diagnosis and prognosis. The GCS is based on a 15-point neurological scale according to eye, verbal and motor movements. The clinical guidelines incorporating duration of loss of unconsciousness and structural imaging with GCS, classify human TBI into mild, moderate and severe level. However, there is no established guideline or standard to assess injury severity in experimental TBI, making it challenging to translate animal models to clinical studies. For decades researchers have discussed different parameters to grade injury severity according to each model: the mechanical parameters such as the peak pressure or duration; neurological changes including apnea, righting reflex time and pinna reflex; physiological changes with weight loss or intracranial pressure increment; behavioral changes in neurological severity score (NSS) or motor function tests; histological changes indicated by infarct volume and neuronal loss. But untill now, there is no consensus because of the different mechanisms from these animal models.

Each experimental model of TBI has its own mechanical properties for the physical insult. To summarize, the principal causes of focal brain injury producing localized tissue damage resulted from a blow to the head, car accidents or violent assaults, while diffuse injury is caused by acceleration or deceleration impact including the unrestricted head movement in motor vehicle accidents or blast-wave propagation [28]. The mixed injury model represents the types of head injury resulting from falls or athletic sports injury. The rat model of fluid percussion injury (FPI) typifies the mixed injury, the open-skull controlled cortical impact (CCI) model approximates focal injury, and shock-wave blast model represents diffuse injury.

1.3 Fluid Percussion Injury

Mixed Injury Model- Lateral fluid percussion injury model (FPI): FPI is one of the best characterized and most often used animal models of TBI. The injury in FPI is induced by a pendulum striking the piston at the end of a tube filled with fluid, shown in **Figure 1.1**. The fluid pressure impulse then hits the exposed dura directly through the Luer-Lock that has been implanted surgically by craniotomy [29]. Briefly, a Luer-Lock is positioned above a 3.0 mm diameter opened skull circular window, which is connected to FPI device fluid impulse outlet and fluid pressure detector. In this way, the fluid pressure delivered on the exposed dura is accurately measured by the detector at the time of injury. The location of the craniotomy defines the types of injury in FPI models. Thus, when craniotomy is performed at the center of the sagittal suture, it is known as Midline FPI [30]. But the mortality of MFPI is higher than other models, which is believed to be due to brainstem-compromised apnea [31]. In Lateral FPI, craniotomy is performed at 3.5 mm lateral to midline [32], and for parasagittal FPI, the Luer-Lock is implanted less than 3.5 mm lateral to midline [33, 34]. Brain tissue deformation, displacement, and severity of the injury in these types of FPI are resulted from fluid pressure pulse [32]. The pathophysiological changes in FPI are correlated with the pressure transients, in which upper mild, moderate or severe type of pressure impulse causes focal and diffuse injury, while the lower threshold of mild pressure impulse produces diffuse injury [35].

Figure 1.1 Fluid percussion injury model. The fluid pulse impacts at the exposed dura by craniotomy. *Source: [25].*

The application of FPI model is used for replicating the human TBI without skull fracture that generates edema, hemorrhage and gray matter damage [29]. The primary type of injury in fluid pressure impulse includes contusion, shearing/stretching of tissue, subdural hematoma, and hemorrhage as seen in concussive sports injury [36]. Such primary injury is followed by secondary mechanisms of molecular, biochemical, and cellular changes arising from focal and diffuse injury. The vascular disruption like hemorrhage and on-site necrotic cell death are likely an outcome of primary injury, while activation of inflammatory glial cells and neuronal cell death could be resulted predominantly from secondary mechanisms of injury. The Lateral Fluid Percussion Injury (LFPI) model has the advantage of comparing the extent of damage in ipsilateral (injured side) and

contralateral (non-injured side) of the brain hemisphere. LFPI produces focal cortical contusion and diffuse subcortical neuronal injury in the ipsilateral side of the brain [37], which is also believed to be not extended in contralateral hemisphere. A post-injury lesion scar is generated around glial cells at the impact site, which appears to result from continuous chronic cell death [38]. This progressive neurodegeneration that begins from seconds up to a year post-injury at the ipsilateral side of brain region appears to occur predominantly at the cortex, hippocampus, thalamus, striatum and amygdala [39].

Such differential regional neurodegeneration in LFPI is able to reproduce neurobehavioral impairments that are observed in TBI patients, such as reflex suppression, vestibulomotor function and cognitive function [23, 40]. Such impairments are believed to continue for years after severe LFPI [41]. The reliability and reproducibility of FPI-induced neurodegeneration, neurological impairments, and mortality rate are dependent on the location of craniotomy because a small shift from the midline FPI (MFPI) can cause significant changes in brain infarct volume and neurological outcomes. The evolution of recent computer-controlled LFPI device that can monitor the fluid-percussion waveforms with adjustable rise times, peak pressures, and durations is an advanced reliable improvement to the model [42].

Injury Severity in FPI model: Perhaps the definition of mild, moderate and severe injury is the best established in animal model of FPI. The strength of the injury classification lies in the combination of mortality rate, the pressure exposure range, the righting reflexes, and reliable reproducibility of the injury model. For example, Alder et al. (2011) performed mild to moderate injury in a mouse model of

LFPI on the basis of mortality rate, pressure range, and righting reflexes [36]. Injury pressures are delivered in the range of 0.9 - 2.1 atmosphere (atm) pressure that produces mild injury with 0 - 5% mortality rate and a righting reflex time of 2 - 4 min, or moderate injury with a mortality rate of 10 - 20 % and a righting reflex time of 6 - 10 min.

Kabadi et al. (2010) described mild, moderate and severe injury at 1.8–2.2 atm, 2.4–2.8 atm and pressures greater than 2.8 atm, respectively in standard lateral FPI model (Amscien Instruments) [43]. They also established these classifications in a new developed rat model of microprocessor-controlled, pneumatically driven instrument, micro-FP device. With micro-FPI, pressures of 2.2–2.4 atm, 2.6–2.8 atm and > 3.0 atm correspond to mild, moderate and severe magnitudes of injury, respectively. They observed that mortality rates were 0% at 2.4 atm, 12% at 2.6 atm, 20% at 2.8 atm, 33% at 3.0 atm and > 65% above 3.2 atm. The cognitive performance, lesion volume and neuronal loss were significantly different between mild and moderate level. Similarly, Prins et al. (1996) classified the types of injuries in a rat model of FPI through a comparative study on mortality rate, morphology, intracranial pressure and mean arterial blood pressure [44]. They investigated mild pressure range from 1.35-1.45 atm, moderate injury pressure range from 2.65–2.75 atm, and severe injury pressure range from 3.65–3.75 atm. The mortality rate corresponding to mild, moderate, severe injury pressure range was respectively 27%, 36%, 100% for postnatal 17 days, and 0%, 20%, 55% mortality for adult rats [44]. They reported that the duration of apnea for adult rat was 10.4 secs; 20.3 secs; 24.9 secs and duration of unconsciousness was 97.8 secs; 183.0 secs; 291.2 secs for mild,

moderate, severe, respectively. The increment of intracranial pressure and mean arterial blood pressure appeared to contribute the mortality rate in the corresponding mild, moderate, severe injuries. Moreover, weight loss post injury is also correlated with injury severity. Mild, moderate and severe injury was found to result in 0-10%, 15-20%, 25-30% weight loss, respectively [45]. Meanwhile, the injury severity range was summarized after a literature research from FPI studies on mild, moderate and severe level, separately. After incorporating the data from the literature and the work established in our laboratory, it was defined here that mild FPI range at 0.9-1.5 atm [46-48], moderate FPI at 1.6-2.5 atm [49-51] and severe injury above 2.5 atm [52-54].

The suppression time of reflexes such as pinna, cornea, and righting has been established as a standard indicator of neurological evaluation in animal model immediately after FPI. The pinna reflex is defined as a head shake or twitching of ear when touching the inside of the pinna with a cotton-tip applicator. The corneal relax is when there is a blink response after touching the cornea gently with a saline-moistened wisp of cotton. The righting reflexed is examined by recording the time for the animal to roll over on their feet when they are placed on their back, for three times [55]. The non-invasive righting reflex appears to correlate with injury severity, thus it is used commonly as an indicator of injury severity [40, 56]. Apart from righting, apnea, and pinna reflexes, the types of injury severity are also assessed by physiological functions such as arterial blood gases, vital signs, intracranial pressure, and electrophysiology.

1.4 Specific Aims and Significance

In this study, I have examined the sequence of injury events of injury for a moderate LFPI pressure pulse exposure in experimental TBI. Tissue deformation at the site of impact includes rupturing the subarachnoid and pial vessels that leads to intracranial hemorrhage of the ventricle area on the impact side. The subsequent event of hemorrhage is likely to produce subarachnoid coagulation preventing effective cerebrospinal fluid (CSF) clearance and thrombotic vessel occlusion. Such hemorrhage and coagulative thrombosis resulting from primary focal contusive injury causes necrotic cell death that is different from the secondary mechanisms of injury/cell death as depicted in the two arms of schematic pathways (**Figure 1.2)**. The critical role of coagulation after cerebrovascular damage in trauma patients after TBI has become a reality that a majority of TBI patients are treated with novel oral anticoagulant therapy [57]. The primary injury leads to the propagation of secondary mechanisms of injury. It involves the alterations of molecular, biochemical, and cellular components that are mostly regulated by a sequence of signaling pathways. For example, there is immediate induction of oxidative stress and infiltration of immune cells at the deformed and vascular rupture area. In TBI, myeloid cells like microglia and astrocytes are anticipated to active in response of ongoing immune cell infiltration (right arm) and changes in brain microenvironment (left arm) as depicted in the pathways (**Figure 1.2**). These cascades of inflammatory processes like the oxidative stress, neuroimflammation, and apoptotic cell death comprise the secondary mechanisms of brain injury and neurodegeneration.

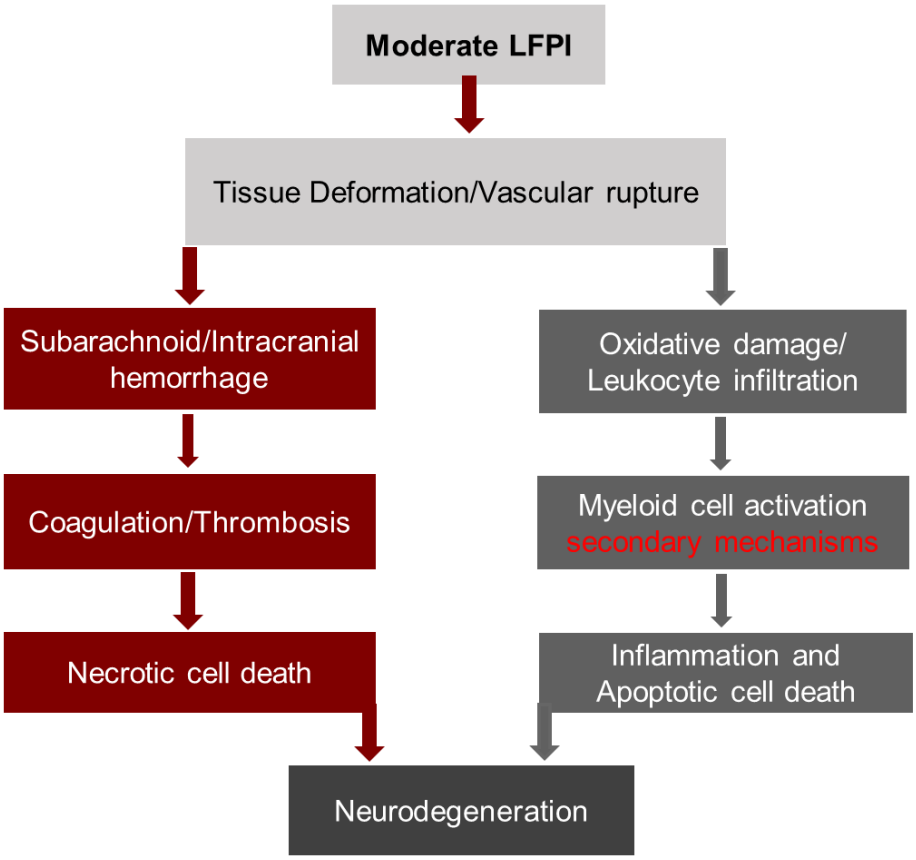

Figure 1.2 Schematic of moderate lateral fluid percussion injury. *Source: [25].*

The overarching objective in this dissertation is to uncover the mechanisms of TBI in layer structured neurovascular units in preclinical measures as reliable predictors for clinical assessments, as well as development of regenerative treatments targeting the cerebrovascular repair. The objective was achieved by examining the hypothesis that cerebrovascular damage post FPI leads to acute necrosis, then develops to neuroinflammation and neurodegeneration, and angiogenic modulation may have the potential for neuroprotection. Success of this goal rests on three Specific Aims:

Aim 1: To establish that physical disruption of cerebro-vasculature post TBI leads to coagulation, necrotic cell death and onsite inflammation. First, it was

established that hemorrhage at the side of injury causes necrotic cell death around the site of injury. Hemorrhagic infarct area of the brain was analyzed by histology staining, and then followed by imaging of fluorescent tracer contrast (high 2000 kDa and low 3 kDa MW) bio-distribution to determine the thrombotic blockage at the cerebrospinal fluid (CSF) clearance routes following intracisterna magna or intravenous injection. Second, staining of coagulation factor XII, thrombin and blood platelets confirmed thrombotic sites, and histological evaluation identified necrosis in and around thrombotic site. Third, acute infiltration of immune cells around the injury sites validated the onsite inflammation resulted from acute vascular damage or subarachnoid hemorrhage. The extent of immune cell infiltration in specific brain area, injured side or non-injured side was correlated with the hemorrhagic brain infarct volume.

Aim 2: To examine the prolonged secondary events after cerebral disruption, including oxidative/nitrosative damage in blood brain barrier (BBB), as well as gliosis in response of acute immune cells infiltration. First, the generation of free radicals at hemorrhagic site immediately post-injury was examined, as well as the activation of the free radical generation enzymes and oxidative/nitrosative damage markers. Second, in response of acute immune cells infiltration, microglia and astrocytes activation was assessed in short and long-term post injury, particularly in the injured brain side compared with non-injured side. Third, a delayed wound healing is expected to induce apoptotic cell death correlated with tau hyperphosphorylation and neuronal loss for neurodegeneration.

Aim 3: To evaluate the efficacy of regenerative treatment targeting angiogenesis and neuroprotection by injectable self-assembling peptide hydrogels. Cerebrovascular disruption slows down wound healing, while thrombosis and neuroinflammation are expected to cause prolonged neuronal loss. Injection of self-assembling angiogenic/neurogenic at the site of injury can promote in situ repair by angiogenesis and neuroprotection longitudinally.

A better understanding of the injury mechanisms is expected to contribute successful regenerative therapy for millions of trauma patients. Such effective neuroprotective therapy is much needed for alarming incidence of 69 million individuals worldwide who sustain TBI each year as per recent epidemiological reports [4].

CHAPTER 2

CEREBRAL VASCULAR RUPTURE IN THE MODERATE FLUID PERCUSSION MODEL

2.1 Introduction

Traumatic brain injury TBI is clinically classified as mild TBI [58-60], moderate TBI [61], severe TBI [62, 63], and vegetative state TBI [64] according to the 15-point Glascow Coma Scale in humans. TBI leads to a high risk for neurological diseases including post-traumatic stress disorder (PTSD) [65], chronic traumatic encephalopathy (CTE) [66, 67], and Alzheimer's disease (AD) [10, 15-17]. Most frequently observed concussive TBI (88%) involves the development of brain pathology induced by traumatic mechanical forces [68], resulting in temporary neurological dysfunction that is not associated with brain structural changes [69]. About 25-42% of concussive brain injury arising from contact sports [70-72], and vehicular accidents [73, 74] are alarmingly not reported. Therefore, the benefit in understanding the injury mechanisms and possible remedial approach will have significant impact for TBI patients.

Extensive research has been conducted to identify potential therapeutic targets for TBI, but none have translated into successful clinical treatments. One major consequence of TBI that has not been extensively investigated is cerebral vasculature dysfunction. The disruption of vasculature causes the primary injury in the form of blood-brain barrier (BBB) damage, hemorrhage, and coagulation, which can trigger the progression of the inflammatory neuropathogenesis [75, 76]. Hemorrhage occurs in 46% of all TBIs and is increasingly prevalent in moderate and severe injuries [77, 78]. The effects of hemorrhage will result in increased intracranial hypertension, compression of

brain structures, neuroinflammation, and even cognitive impairments in long-term [79, 80]. Hemorrhagic bleeding and subsequent coagulative thrombosis appears to be the most challenging management for TBI patients in critical emergency care [81-83]. Thrombosis in cerebral microcirculation is known to cause ischemia, reduction in blood flow, and accumulation of neurotoxic ferritin/hemosiderin [84-86]. In fact, a predicator of worse outcome in TBI is believed to be a reduction of pericontusional blood flow arising from thrombotic coagulation [87, 88]. In previous clinical studies, anticoagulation treatments were attempted on TBI patients with moderate to severe trauma, the results showed a marginal reduction of hypercoagulation when there was no significant difference in mortality or outcomes [89-91]. These clinical observations strongly indicate the importance of hemorrhage and thrombosis in managing the care of TBI patients in the emergency room. In agreement with these clinical observations, Stein et. al. (2002, 2009) reported that human cerebral contusions, lateral fluid-percussion injury (LFPI) in rats, and rotational acceleration head injury in pigs, all led to a universal intracranial thrombin accumulation [92], and that therapeutic use of erythrocyte-bound tissue plasminogen activator was effective in improving thrombin associated brain injury [93]. Yet, the mechanisms of coagulation and secondary propagated neuroinflammation and neurodegeneration in TBI remain elusive.

It is well established that neuropathology and clinical features of blunt head injury can be reproduced in an animal model of lateral/midline fluid percussion injury (LFPI/MFPI) [23, 25, 94, 95]. The insult is caused by a pendulum striking the fluid reservoir to generate a pressure pulse to the exposed dura at a 3 mm window, resulting in intracranial hemorrhage, contusion, neuronal injury and all pathophysiological

hallmarks of human brain injuries without skull fracture [94, 96]. Here, this aim is focused on understanding the sequential mechanisms of moderate brain injury in LFPI model for possibly aligning the injury pathology and therapeutic approach in human TBI. The novelty of the present work includes the layer-structured understanding of the underlying mechanisms at different timeframes post-TBI: 1) cerebral vascular disruption to hemorrhage mediated coagulation as the cause of primary injury, 2) instant CSF pathway blockage, necrotic cell death and activation of immune cells as the short-term secondary injury; 3) prolonged blockage of the CSF pathway correlating to sustained coagulation generation. The uniqueness of these findings will pave the path for understanding the mechanisms and developing a therapeutic treatment of TBI.

2.2 Methods and Materials

2.2.1 Reagents

All primary antibodies were purchased from Abcam (Cambridge, MA). Secondary Alexa Fluor conjugated antibodies were purchased from Invitrogen (Carlsbad, CA). Table 2.1 summarizes the details of the antibodies, including source, catalog numbers, and dilutions factors that were used for immunofluorescence or immunohistochemistry staining and western blot analyses. Dextran-conjugated Fluorescein, 2,000,000 MW (FITC-d2000) was purchased from Thermo Fisher (Waltham, MA).

Table 2.1 Antibody Source, Catalogue Numbers, and Dilution Factors for Immunohistochemical Staining and Western Blot Analysis

Antibody	Marker for	Company	Catalogue #	Dilution for Immunostaining	Dilution for WB
Coagulation factor XII	Coagulation factor XII	Abcam	ab196670	1:100	1:1000
Thrombin	Thrombin	Abcam	ab92621	1:200	1:1000
CD42d	Blood platelets adhesion	Abcam	ab65017	1:500	1:1000
NeuN	Neurons	Abcam	ab104225	1:500	--
RIP1	RIP1 kinase	Abcam	ab72139	1:200	1:1000
CD11b	CD11b	Abcam	ab52478	1:200	--
CD68	CD68	Abcam	ab955	1:200	--
ZO1	Tight junction protein	Abcam	ab96587	1:200	--
β-actin	actins	Abcam	ab8226	--	1:1000

2.2.2 Experimental Animals

Adult male Sprague–Dawley rats (250-300 g; 8–10 weeks old) were purchased from Charles River Laboratory (Wilmington, MA), and maintained in sterile cages under pathogen-free conditions. All procedures followed the National Institutes of Health guidelines for the ethical care of laboratory animals, and the Institutional Animal Care and Use Committee (IACUC) at the animal facility of Rutgers-Newark University. Rats were randomly selected and treated with different conditions as follows: 1) Determination of optimal working pressure by brain infarct volume variations in FPI (n=24): 4 rats per pressure (sham, 0.5 atm, 1.0 atm, 1.6 atm, 2.0 atm, 2.6 atm), and sacrificed the rats immediately after injury, without any transcardial perfusion of paraformaldehyde (PFA) or PBS wash. Following the injury-severity dependent study, 1.8-2.0 atm was used as the working pressure, to generate a moderate injury with visible hemorrhage and infarct volume, but with a low mortality rate of 7.5%. The recorded apnea time was 15-20 s, and the righting reflex time was

8-10 mins. 2) Tracer bio-distribution under different pressure of FPI (n=20), 4 rats per pressure (sham, 0.5 atm, 1.0 atm, 2.0 atm) at 4 hrs, and 4 rats for tracer distribution in moderate FPI (2.0 atm) at 7 days post injury to check if there was any repair mechanism. 3) Histological and biochemical changes in moderate FPI at 4 hrs (n=12), 6 rats per sham control and FPI groups.

2.2.3 Fluid Percussion Injury

The fluid percussion injury (FPI) model (Amscien Instruments) is the most commonly used animal model of traumatic brain injury. Briefly, the rats were anesthetized with a mixture of ketamine and xylazine (10:1 (100 mg/10 mg/kg), 0.1 mL/100 g) and placed in a stereotaxic frame. Craniotomy was performed by drilling a 3mm hole on the left parietal skull, 2.5 mm lateral from the sagittal suture and 3.0 mm caudal from the coronal suture, with the dura intact. A Luer-lock hub was glued on the skull over the exposed dura with cyanoacrylate gel, and secured by application of methyl-methacrylate (Henry Schein, Melville, NY, USA). One day after surgery, animals were anesthetized by isoflurane to receive either sham or lateral FPI. Different injury severity levels were used in the preliminary studies according to our previous publication [25]. Sham animals were anesthetized and attached to the device without the injury. After removing the injury hub, the rats' heads were sutured and the rats were returned to their cages.

2.2.4 Intracisterna CSF Tracer Infusion

Fluorescent FITC tracer (Dextran, Fluorescein, 2,000,000 MW, (Thermo Scientific, Rockford, IL) reconstituted in artificial CSF (5 mg/ml) was infused into anesthetized

rats via intracisterna magna [97], 2 hours before sacrifice. Anesthetized rats were fixed in a stereotaxic frame and 10 microliters of CSF tracer was infused by a 30-gauge needle at a rate of 1 μl/min for 10 mins with a syringe pump (Harvard Apparatus). Small molecule tracer (Texas red, Thermo Scientific) was injected through tail vein at the same time. To visualize the movement of tracer in the CSF flow and into the brain parenchyma, animals were transcardially perfused with 4% paraformaldehyde after 4 hrs of intracisterna infusion.

2.2.5 Anti-coagulant Treatment

Five rats were treated with tissue plasminogen activator (tPA, Sigma Aldrich) after 24 hrs post moderate FPI. Single dose of 5 μL dose (1mg/ml) was injected intracranially through the impact site. Then the rats were sacrificed at day 3 post FPI after FITC tracer injection through cisterna magna.

2.2.6 Tissue Processing

Animals were sacrificed at 4 hrs and 7 days at post-injury to harvest the brain tissue for analysis. Blood samples were collected from the bleeding out of the Luer-lock hub at the injury site for FPI rats, and from the carotid artery for sham controls. Anticoagulant-treated tubes with sodium citrate were used for collection of blood samples (10 μl sodium citrate/100 μl blood sample), and centrifuged at 2100 x g for 10 mins to get blood plasma. Brain tissues were immersed in 4% paraformaldehyde overnight, followed by cryoprotection in 30% sucrose in PBS. Brain tissues were snap frozen in Tissue-Tek OCT compound (Thermo Scientific, Rockford, IL) and coronal sliced by Leica CM3050 cryostat into 20μm thick sections.

2.2.7 Histological Staining

Cresyl Violet staining. The brain sections were stained in 0.1% cresyl violet solution for 10 mins and then rinsed quickly in distilled water. Then the slides were immersed in 95% ethyl alcohol for 10 mins, and dehydrated in 100% alcohol for 5 mins and then cleared in xylene for 5 mins. *H & E staining.* The brain sections were stained in hematoxylin for 15 mins, washed in running tap water for 15 mins, placed in distilled water for 30 s, then counterstained in Eosin for 30 s. Afterwards the sections were dehydrated with 95% EtOH and100% EtOH for 4 mins. They were then cleared with xylene for 4 mins. All the stained sections were finally mounted with DPX mounting medium.

2.2.8 Immunostaining and Microscopy Analysis

Brain tissue sections (20 μm thickness) were fixed in acetone-methanol (1:1 v/v) fixative for 10 minutes at -20°C. This was followed by washing the tissue slides with PBS, and blocking with 5% bovine serum albumin in 0.1% Triton X-100 PBS at 25°C for 1 hr. Tissues slides were then incubated at 4°C overnight with either of the following primary antibodies: rabbit anti-Thrombin, rabbit anti-CD42d, rabbit anti-CD11b, rabbit anti-NeuN, mouse anti-RIP1, mouse anti-CD68, rabbit anti-ZO-1 (Abcam, Cambridge, MA). After rinses with PBS, sample slides were incubated with Alexa Fluor 488/594 conjugated with anti-mouse/rabbit immunoglobulin-G (IgG) for 1 hr. After washing with PBS, sample slides were mounted by Golden DAPI mounting medium (Thermo Scientific, Rockford, IL). For immunohistochemistry labeling of Coagulation factor XII, a biotinylated rabbit anti-coagulation factor XII

antibody (Abcam, Cambridge, MA) and streptavidin-HRP were used and amplified by DAB kit (Thermo Scientific, Rockford, IL). **Table 2.1** summarizes the details of the antibodies, catalogue numbers and dilution factors that were used. Whole brain tissue section images were scanned (20x magnification) by Leica Aperio Versa 200 digital pathology grade slide scanner, and detailed regional fluorescence images were captured by a fluorescence microscope (IX81 DSO; Olympus, Somerset, NJ). Cell counting were performing by using Image J to measure positive stained neurons, and presented as numbers/ square mm.

2.2.9 Western Blotting

Brain tissues were homogenized on ice using a sonicator with probe, lysed with CellLytic-M (Sigma) for 30 mins at 4°C, then centrifuged at 14,000 x g. Protein concentrations from brain tissue homogenates and blood plasma were estimated by the bicinchoninic acid (BCA) method (Thermo Scientific, Rockford, IL). Protein load was 20μg/lane in 4-15% SDS-PAGE gradient gels (Bio-Rad, Hercules, CA). The separated proteins were then transferred onto PVDF membranes, blocked with superblock (Thermo Scientific), and incubated overnight with the respective primary antibody listed in **Table 2.1** at 4°C, followed by washes and incubation with horse-radish peroxidase conjugated secondary antibodies for 1 hr at room temperature. Immunoreactive bands were detected by West Pico chemiluminescence substrate (Thermo Scientific). Data were quantified as arbitrary densitometry intensity units using the Image J software.

2.2.10 Statistical Analysis

SPSS Statistics 24 software (IBM) was used for all statistical analysis. Data are presented as mean ± standard error of the mean (SEM, n = 6). Shapiro-Wilk test revealed no significant deviations from normality in either group, and Levene's test for homogeneity of variance revealed no significant differences in variance between groups. Then between-group comparisons were made by independent t-test to determine individual group differences. Differences between means were considered to be significant at the probability level of $p < 0.05$ or 0.001.

2.3 Results

2.3.1 Brain Infarct Volume and Hemorrhage Increase Dose-dependently in Fluid Percussion Injury

In previous studies, injury severity was established in the range of mild hemorrhage (0.5 – 1.4 atm pressure), moderate hemorrhage (1.5 - 2.4 atm pressure), and severe hemorrhage TBI (> 2.5 atm pressure) in animal models of lateral fluid percussion injury (FPI) [25]. Brain tissues were removed without PFA perfusion or PBS washing immediately after injury to examine the extent of hemorrhage and infarct volume as a proof-of-concept in FPI. **Figure 2.1** upper panels showed the tissue insulted area at the site of impact at different fluid pressure range, and **Figure2.1** lower panels revealed the internal hemorrhage and brain infarct in the whole brain tissue cross-sections compared with control. It was observed that increment of hemorrhagic lesions and brain infarct volume is related to injury severity. In the moderate range of FPI, the type of internal injury appeared to be localized in the injured side of the brain (ipsilateral side) with clear dura membrane damage, but did

not extent to the non-injured side of brain (contralateral side). In the mild injury level (0.5 -1.4 atm), the contusion was small with minor visible subarachnoid and intracranial hemorrhage in the ipsilateral hemisphere. In the severe injury level (> 2.5 atm), the cortex was physically damaged by the fluid pulse with visible intracranial hemorrhage expanded to the thalamus region and contralateral side. The mortality rate exceeded 33% at the severe injury level, **Figure 2.1** showed representative images of rats' brain gross observation, with death right after FPI. The hemorrhage was significantly larger than other injury levels, and expanded throughout the entire brain. Here, it was addressed if the infarct volume and hemorrhagic lesions in moderate injury correlate with the demarcation of coagulation and thrombosis in the ipsilateral side of the brain. The rationale for selecting moderate injury severity is that it has a clearly visible brain infarct volume and hemorrhagic lesions with mortality rate less than 10%, as such, successful preventive measures for such injuries would be clinically meaningful. The injury in the lower mild pressure range is not well defined; as such the injury is self-repaired with time perhaps without compromising the changes in neurocognitive behavior. Mortality rate in the severe injury type is extremely high; as such it may not be relevant clinically. In **Table 2.2**, parameters were summarized for FPI injury severity from the pathophysiological data collected in this study, and with the incorporation from literature [25]. Thus, 1.8-2.0 atm was used as the moderate injury working condition for hemorrhage.

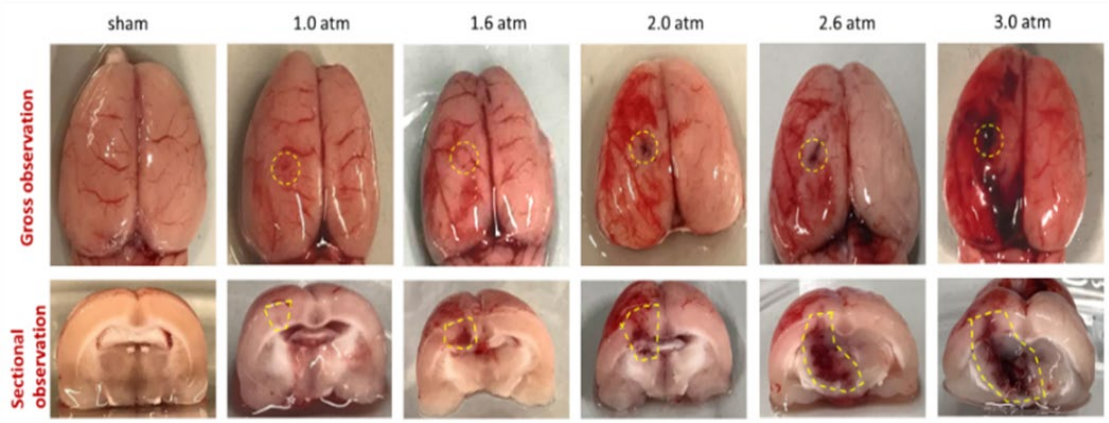

Figure 2.1 Gross observation of the injured brain. Pathomorphological changes in rat brains at different pressures induced by Fluid Percussion Injury. *Source: [98]*

Table 2.2 Parameters to Assess Injury Severity Levels for Fluid Percussion Injury.

Injury Model	Injury severity	Parameters to assess injury severity			
		Pressure range (atms)	Mortality rate	Righting reflex time (min)	Apnea (secs)
Fluid percussion injury (Lateral FPI)	Mild	0.9-1.5	0-5%	2-4	~10.4
	Moderate	1.6-2.5	5-20%	6-10	~20.3
	Severe	>2.5	>33%	>10	~24.9

2.3.2 Bio-distribution of Tracer is Blocked at the Site of Injury

An increase in FITC tracer accumulation was expected at the impact site resulted from tissue deformation. Thus, large size molecular weight fluorescence tracer (Dextran, FITC, 2000 kDa) was injected into the CSF via intracisterna magna to track the bio-distribution of this tracer. The distribution of this tracer in the brain parenchyma and CSF clearance pathway were examined by whole-brain tissue sections from sham controls and injured rat brain at different pressure ranges. As expected, tracer was distributed clearly in subarachnoid space and perivascular space along the arterial vessels in sham controls and in the very mild range of fluid pressure injury (**Figure 2.2A**). But unlike the sham controls, there was no flow through in the subarachnoid space at the site of impact and surrounding area in moderate pressure

injury (**Figure 2.2A**). **Figure 2.2B** showed a significant difference of tracer distribution in the perivascular space by enlargement of the contralateral and ipsilateral cortex. Distribution of the tracer was not observed in the brain interstitial space due to its large size of the molecule. The combined images of the large molecule tracer FITC (CSF pathway) with small molecule tracer Texas red (blood circulation) indicated blood vessel disruption. In the contralateral site, vasculature was intact with FITC distributed in the perivascular space, but in ipsilateral site, FITC distribution was blocked and vascular disruption was observed (**Figure 2.2C**). Interestingly, the observed blockage area in moderate or severe injury pressure ranges was correlated to the hemorrhage and infarct volume increment in gross observation. The temporal and spatial distribution of FITC tracer in sham (**Figure 2.3A**), moderate FPI at 4 hrs (**Figure 2.3B**) and 7 days (**Figure 2.3C**) post-injury showed a consistent blockage of subarachnoid flow at the injury site, frontal and caudal site, even though the distances were sectioned about 2.5 mm away from the injury site (**Figure 2.3**). The data led us to further investigate if the blockage of tracer movement in the interstitial space and subarachnoid space was due to coagulation.

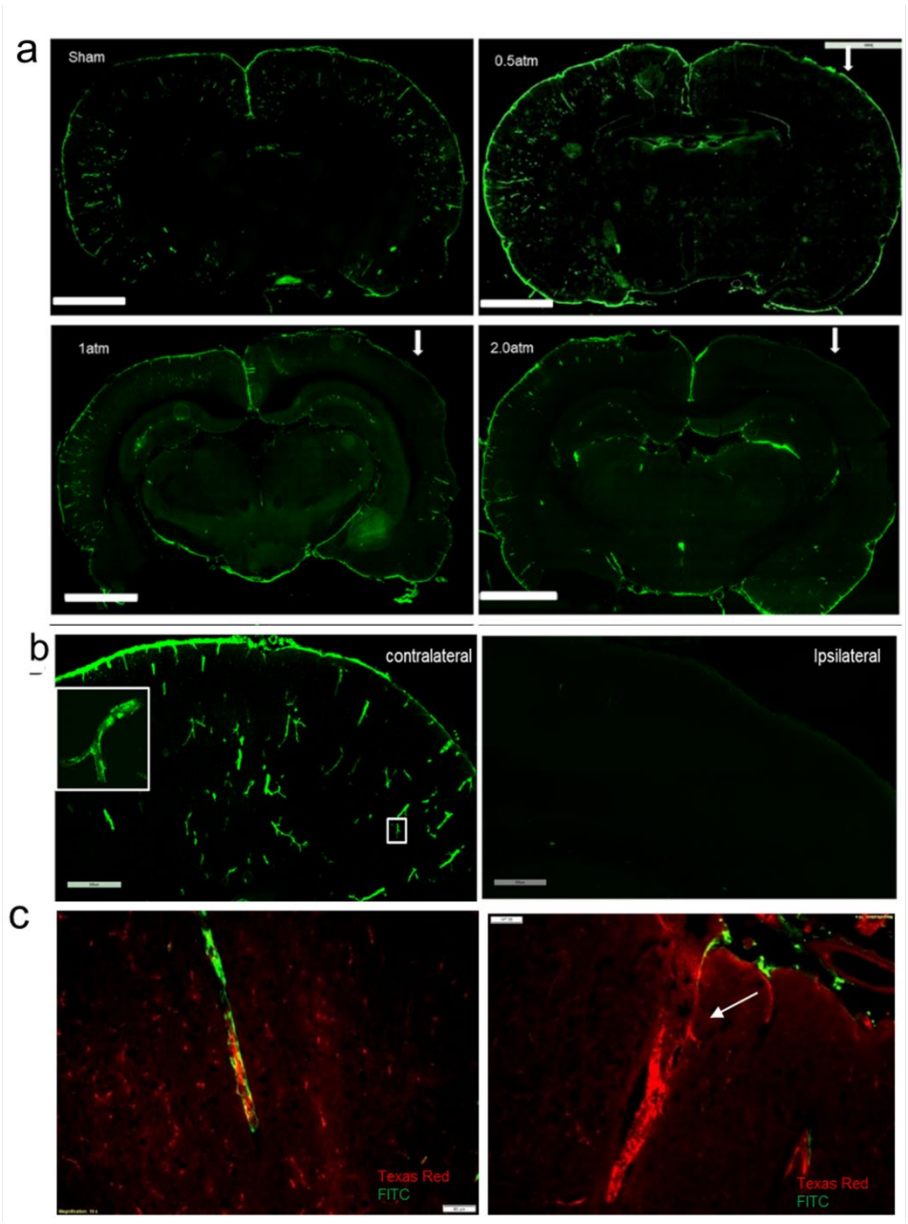

Figure 2.2 Representative image of blockage of FITC (2000 kDa) tracer bio-distribution in the brain sections. (a)Increased blocked region with FPI pressure increment was observed. The injury site is indicated by the white arrow. Scale bar: 3 mm. (b) Enlarged tracer bio-distribution at the contralateral site and ipsilateral site in FPI brain sections. Scale bar: 500 μm. (c) Merged image of the large molecule tracer FITC (in CSF pathway) and small molecule tracer Texas red (in blood circulation) in the contralateral site (Left) and ipsilateral site (Right). T=4 hrs post-injury.

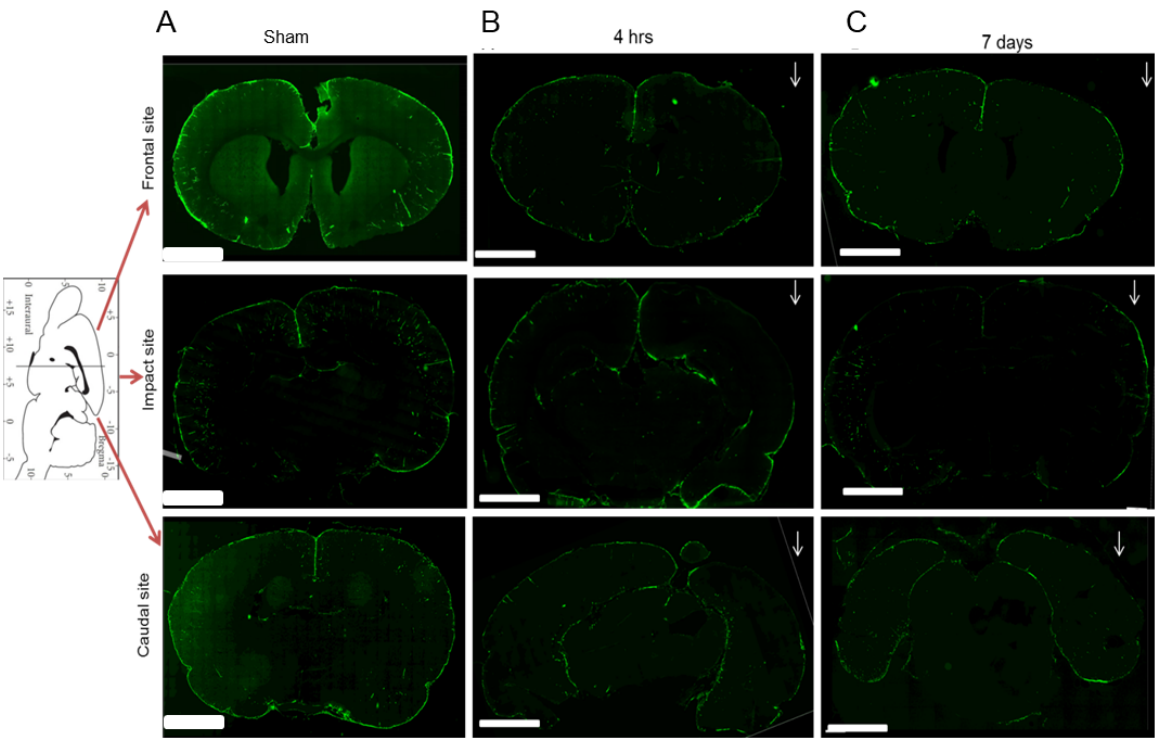

Figure 2.3 Temporal and spatial distribution of FITC tracer. Rat brain coordinates indicates the location of tracer distribution at the frontal and caudal site away from impact site in sham control (a), at 4 hrs (b) and 7 days (c) post-injury. Scale bar is 3mm.

2.3.3 Hemorrhagic Infarct Area and Necroptosis Were Pronounced in the Injury Side

To evaluate whether blockage of FITC tracer distribution in the subarachnoid and interstitial was *in sync* with hemorrhage and hemolytic cell death, the accumulation of red blood cells (RBC) and necrotic cell death were examined by H&E histological staining as the first step in injured (**Figure 2.4C)** and sham brains (**Figure 2.4A)**. H&E staining validated the localization of hemorrhage indicated by RBC aggregation and hemolytic cell death in these brain regions (**Figure 2.4**). Sham control brain tissue section did not show any of these changes, hemolytic cell death was found around the hemorrhagic area (yellow arrow in **Figure 2.4D**) that were identified as the deeply eosinophillic necrotic

cells that lost their nuclei, while necrosis of small neurons was characterized by basophilic nuclear pyknosis in H&E staining (blue arrow in **Figure 2.4D**).

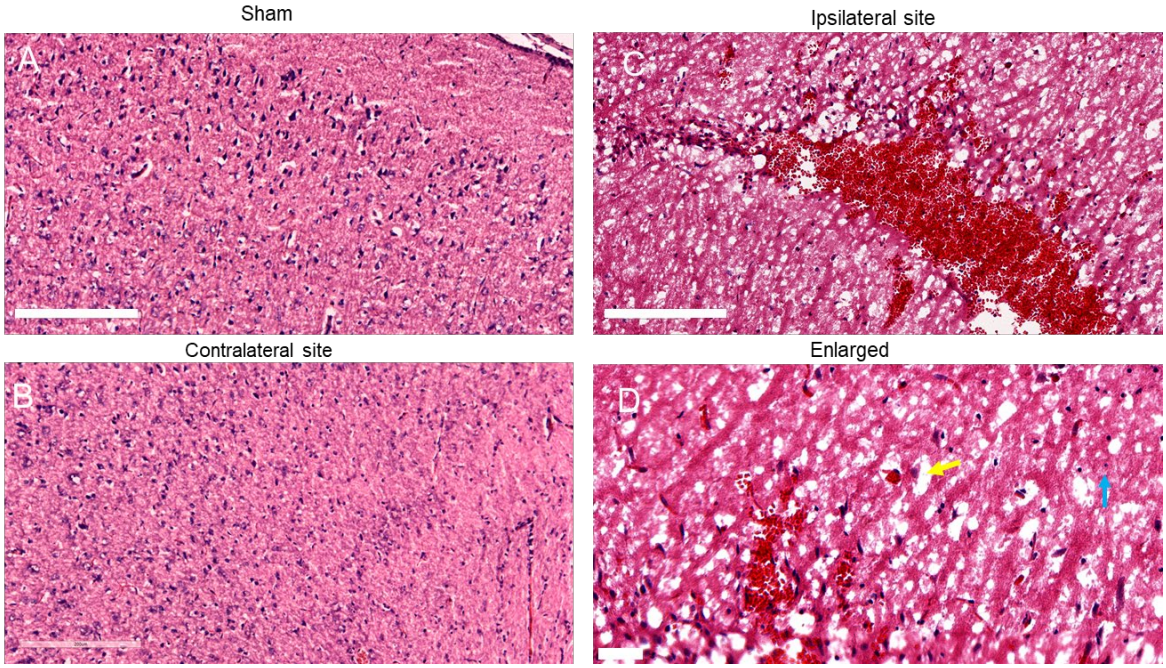

Figure 2.4 Representative H&E staining indicating hemorrhage and cell death after FPI. (a) Sham, (b) FPI contralateral site and (c) FPI ipsilateral site scale bar is 200 μm. (d) Enlarged image shows eosinophillic necrotic cells (yellow arrow) & basophilic nuclear pyknosis (blue arrow) near coagulation, scale bar is 30 μm. T=4 hrs post-injury.

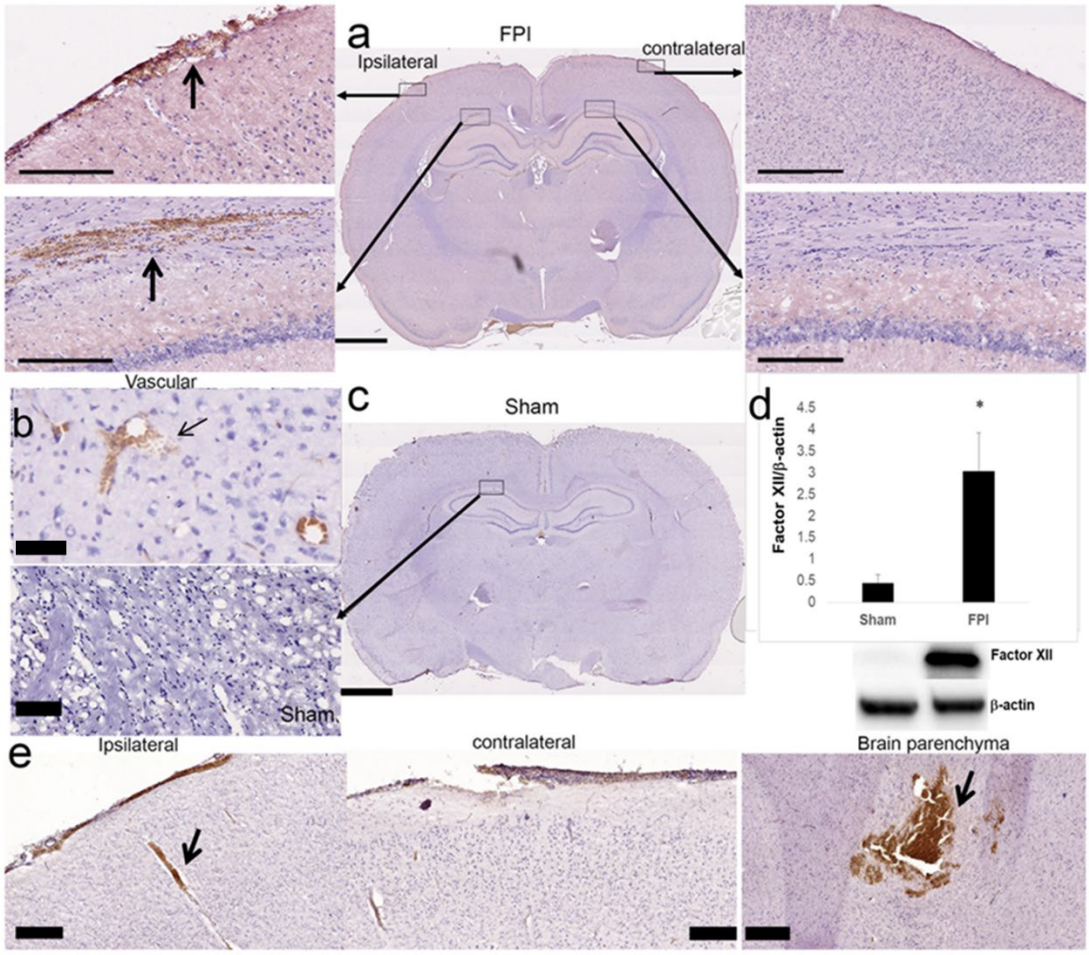

Figure 2.5 Representative expression of Coagulation factor XII in whole brain sections: (a: middle panel), injured ipsilateral site (a: left panel), contralateral site (a: right panel), and sham control whole brain section (c). Scale bar of whole brain section is 2 mm. Enlarged cortex and hippocampus at ipsilateral site show a significant higher expression of coagulation factor XII and (b) coagulation in perivascular space (scale bar: 90 μm), compared with the contralateral site and sham (c). (d) Western Blot shows higher expression of coagulation factor XII in blood plasma from injured rats than sham control, collected at T=4 hrs post-injury. Values are mean ±SEM (n = 6), independent t-test, $t(10)=-2.31$, $*p < 0.05$. (e) Immunohistochemistry staining of coagulation factor XII at 7 days post injury shows that coagulation was not cleared. Black arrow shows the blood vessel with coagulation. Scale bar: 90 μm. *Source: [98]*

2.3.4 Validation of Tracer Blockage Due to Coagulation at the Injury Site

To evaluate if blockage of tracer distribution in the injured subarachnoid region was due to coagulation, the possible involvement of specific coagulation factors was

screened by ELISA kits. Coagulation factor XII and thrombin were highly expressed out of 14 coagulation factors screened. Expression of coagulation factor XII was examined in brain tissue sections of injured and sham control animals. Coagulation factor XII was detected by immunohistochemistry staining in brain tissue sections. Strong positive expression of coagulation factor XII was observed in subarachnoid space, brain parenchyma near ventricle and in perivascular space on the injured side of the brain compared with the non-injured side (**Figure 2.5 A-C)**. This observation confirmed the notion that blockage of tracer flow in subarachnoid at the injured side was due to coagulation. The increased levels of coagulation factor XII in blood plasma (**Figure 2.5D)** collected in the Luer-lock from injured rats compared with sham controls further confirmed the argument that an intrinsic coagulation factor XII formation was a subsequent event of hemorrhage in blunt brain injury. Interestingly, immunohistochemistry staining of coagulation factor XII showed that coagulation persisted even at day 7 post-injury (**Figure 2.5E).** Our results suggest the need for prevention of coagulation in post-TBI in order to ameliorate the progression of neurological complication in TBI.

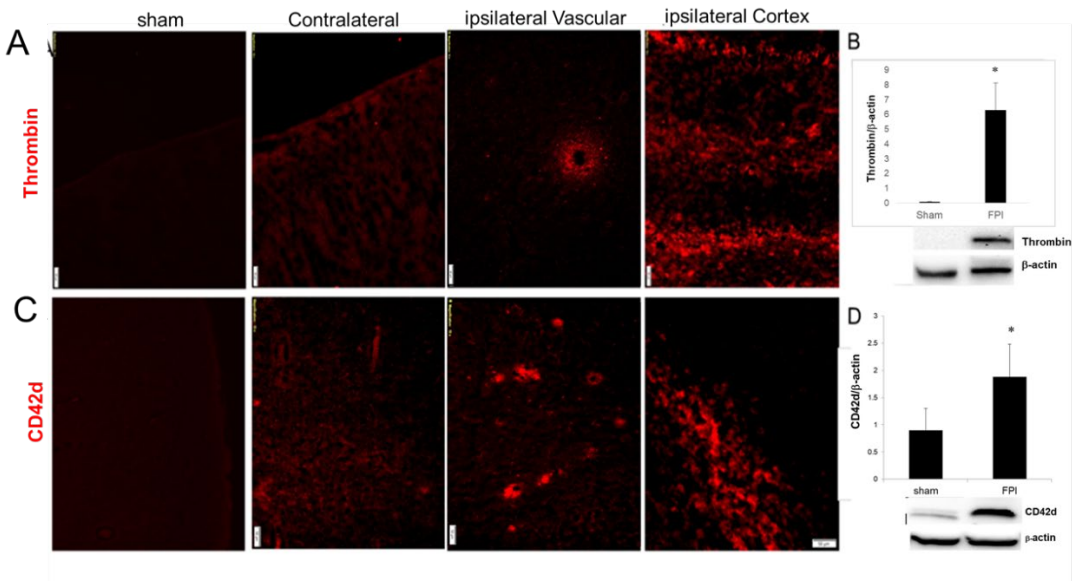

Figure 2.6 Significantly higher expression of thrombin and blood platelets in the injured brain than sham or contralateral brain, T=4 hrs. Immunofluorescence staining of thrombin (a) and CD42d (c) indicate thrombosis and blood platelets adhesion in the injured brain section, compared with sham. Scale bar is 50 μm. Western Blot shows higher expression of thrombin (b) in blood plasma and CD42d (d) in brain tissue from the injured brain than sham. Values are mean ±SEM (n = 6), *p < 0.05.

2.3.5 High Levels of Thrombin and Platelets in Hemorrhagic Area

Since formation of intrinsic coagulation factor XII can lead to extrinsic cerebral thrombus formation, then the role of thrombin (that converts fibrinogen to fibrin) was examined and identified by the protein marker for cross-linkage of fibrin clots with blood platelets. Thus, expression of thrombin and glycoprotein V (by anti-CD42d antibody) was detected by immunofluorescence staining in whole brain tissue cross-sections. Similar to the expression of coagulation factor XII, a positive immunoreactive staining of thrombin was localized in the subarachnoid space, and ipsilateral cortex on the injured side compared with the non-injured side (**Figure 2.6A**). In agreement with the expression of thrombin in the brain tissue, the level of thrombin in the blood plasma from the injured brain was significantly higher than the sham control, as shown by Western blot (**Figure 2.6B**). As expected from thrombin

results, the levels of the platelets clotting factor marker glycoprotein V (CD42d) in the brain tissue (**Figure 2.6C**) or in the brain tissue samples (**Figure 2.6D**) were significantly higher in the injured brain than the sham controls.

2.3.6 Necroptosis Is Prevalent around Thrombin Positive Areas

Then the association of coagulation and neuronal cell death was examined in the hemorrhagic region. **Figure 2.7A** showed the presence of Cresyl Violet Nissl staining in sham control (left panel) and absence of Nissl staining in FPI injured animal (right panel) of whole brain scanned sections. **Figure 2.7B-C** showed the enlarged Nissl staining images on the contralateral and ipsilateral side that clearly indicated the difference in the severity of cell death between the non-injured and injured brain hemispheres of the same injured animal. To further confirm the necrotic cell death in such a short-time (4 hrs), receptor-interacting serine/threonine-protein kinase 1 (RIP1) was used as the marker for necroptosis. **Figure 2.8A-B** indicated the significant higher expression of RIP1 at the ipsilateral site in FPI brain section, compared with the sham brain. Co-localization of NeuN with RIP1 positive cells in the brain cortex showed necrotic cell death in neurons at the ipsilateral site, compared with sham control and contralateral site (**Figure 2.8C).** The evidence of neuronal loss was validated quantitatively by counting the NeuN positive stained cells in both sham control and impact site cortex (**Figure 2.8D)**. RIP1 expression was significantly higher in the injured brain ipsilateral than sham control (**Figure 2.8E),** by quantitative analysis of RIP1 protein levels. Our data suggest that necrotic cell

death arising from coagulation and hemolysis could significantly contribute to neuronal loss.

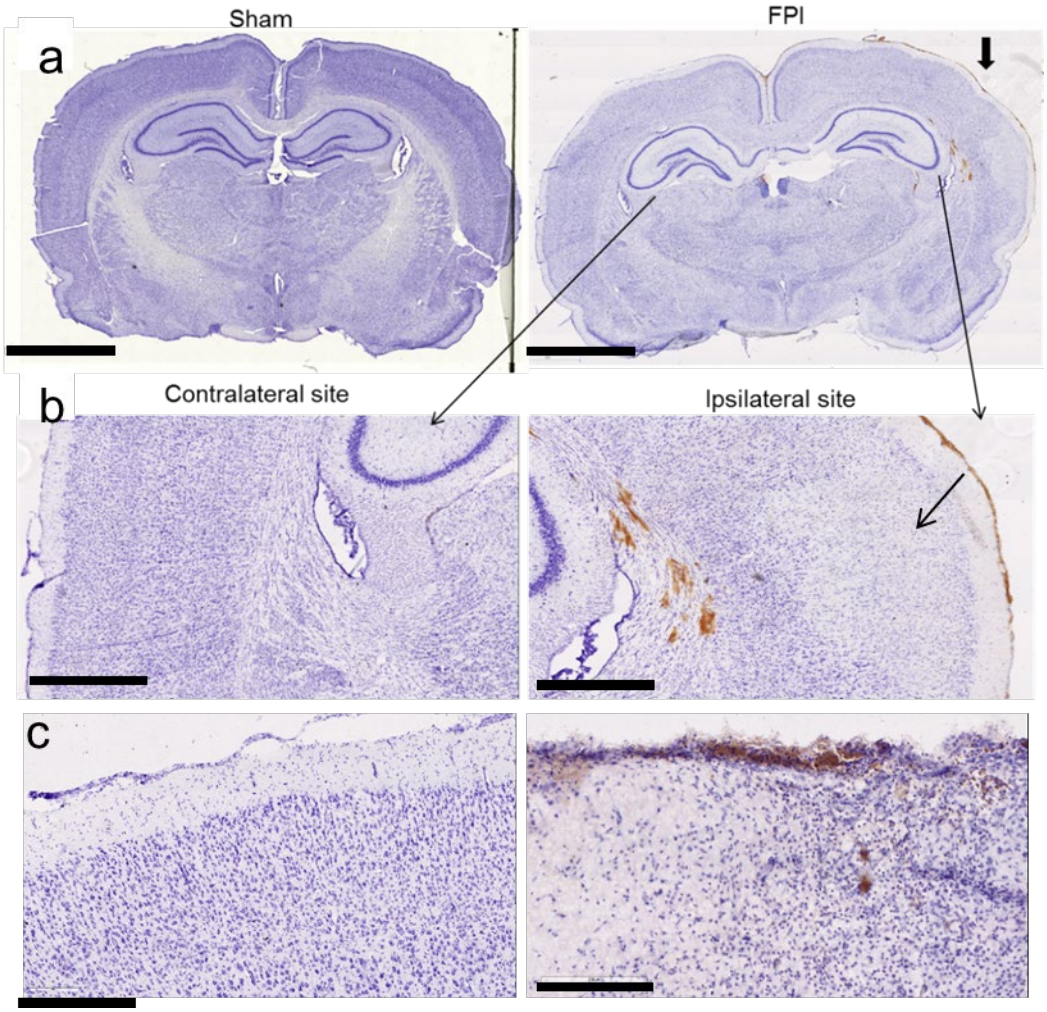

Figure 2.7 Neuronal loss shown by Nissl staining at T=4 hrs post-injury. (a) Nissl staining of whole brain sections for sham control and FPI (scale bar is 3mm). Enlarged Nissl staining images near the ventricle area (b) and at the impacted cortex (c) indicates the neuronal cell loss in and around the hemorrhage region at the contralateral and ipsilateral site. Scale bar in (b) is 300 μm, scale bar in (c) is 200 μm.

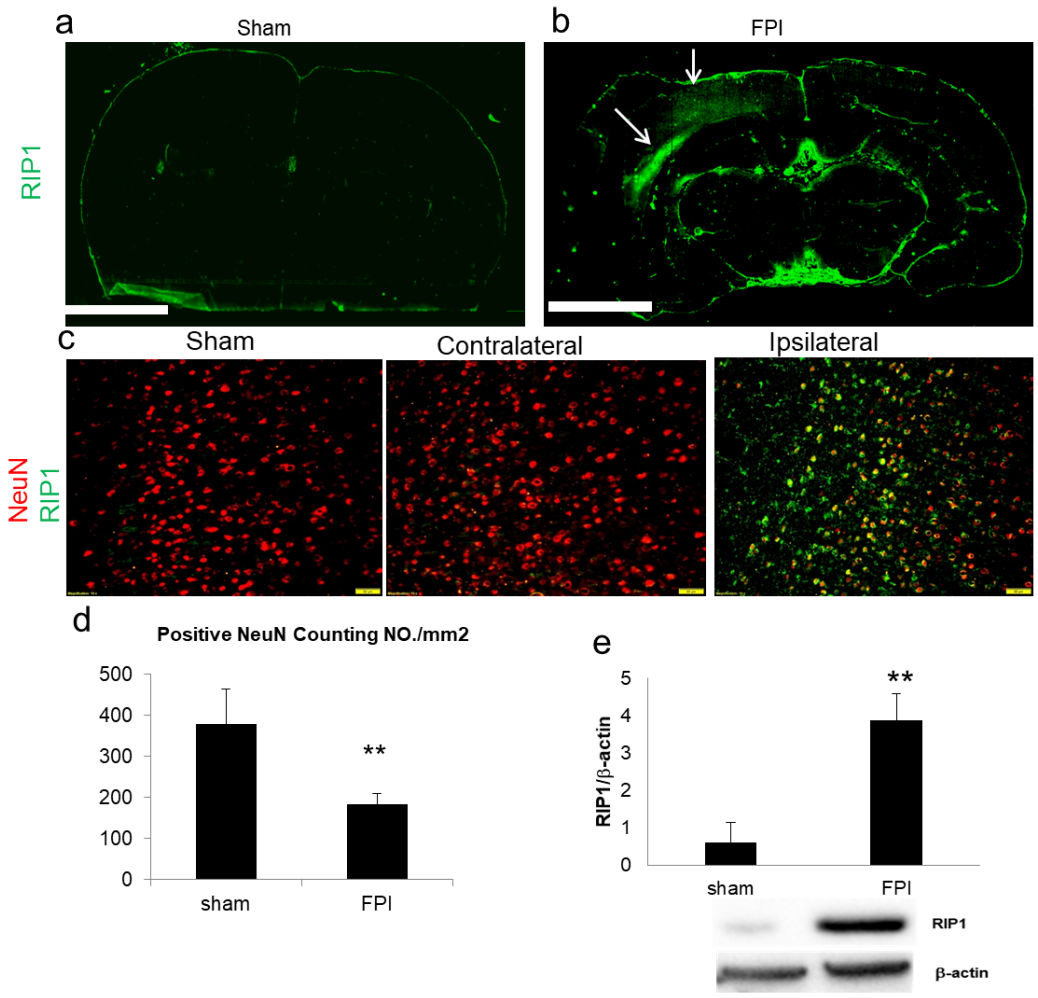

Figure 2.8 Necrotic cell death at T=4 hrs post-injury. Necrotic cell loss was further examined by RIP1 staining in sham (a) and FPI (b) brain sections (scale bar is 3 mm), as well as the co-localization of RIP1 with NeuN staining (c) (scale bar is 50 μm). (d) Number of NeuN-immunopositive cells in FPI and sham groups. Values are mean ±SEM (n = 6). **p < 0.001. Western blot (e) of RIP1 show FPI lead to necrotic cell death at T=4 hrs post injury. Values are mean ±SEM (n = 6), Independent t-test, t(10)=-2.75, **p < 0.001.

2.3.7 Immune Cells Infiltration at the Site of Hemorrhage

The infiltration and accumulation of immune cells were then investigated by antibody CD11b and CD68, at the hemorrhage site. CD11b is expressed on the surface of many leukocytes including neutrophils, monocytes, macrophages and microglia in the brain, but mostly on neutrophils in the acute stage of the injured

brain, with the rounded cell morphology infiltrating through vasculature. **Figure 2.9A** showed an enhanced infiltration of immune cells in the cortex and around arterial blood vessels compared with sham controls. CD68 is a protein highly expressed on the monocytes lineage, including circulating macrophages and tissue macrophages (microglia in the brain). An increased infiltration of monocytes/macrophages in brain tissue sections was observed from 4 hrs post-TBI compared with sham controls (**Figure 2.8B)**. The infiltration of immune cells was seen to be mostly in the hemorrhagic lesions and around the tissue deformed areas, as depicted by the enlarged CD68 positive area at the actual impact site. These results suggest that tissue deformation initiated the onsite inflammation of immune cells because infiltration of immune cells was confined to the hemorrhagic lesions that penetrated deep down into the ventricle and hippocampus area of the brain. These data suggest that deformation or even rupture of cerebral vascular integrity may play an initial vital role for induction of the hemorrhagic inflammatory process, subsequent coagulative hemolysis, and progression of neurodegeneration in post-TBI.

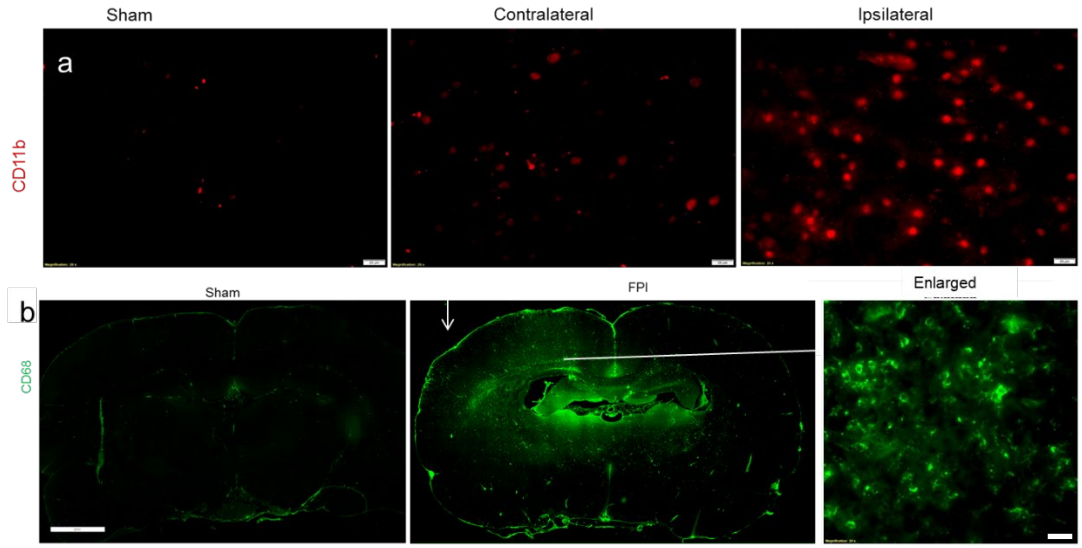

Figure 2.9 Aggregation and accumulation of immune cells at 4 hrs after FPI. (a) Expression of neutrophils by immunofluorescence staining of CD11b in sham & FPI contralateral and ipsilateral cortex. Scale bar: 20 μm. (b) Expression of macrophages/monocytes by CD68 immunostaining in sham and FPI whole brain section. Scale bar: 2 mm. Enlarged image shows accumulated macrophages/monocytes in the injury site. Scale bar: 20 μm.

2.3.8 Anti-coagulant Treatment Reverses CSF Pathway

As the proof of concept, anti-coagulant drug tissue plasminogen activator (tPA) was used after FPI, to examine if removal of coagulation can restore the FITC tracer bio-distribution in CSF. As anticipated, FITC tracer bio-distribution was restored at the impact site, and accumulated at the injection site, compared with FPI brain without treatment (**Figure 2.10A**). IHC images of coagulation factor XII further confirmed the clearance of coagulation at the impact site (**Figure 2.10A**). The anti-coagulant can be a potential treatment for TBI patients with the clearance of coagulation and the recovery of CSF pathway.

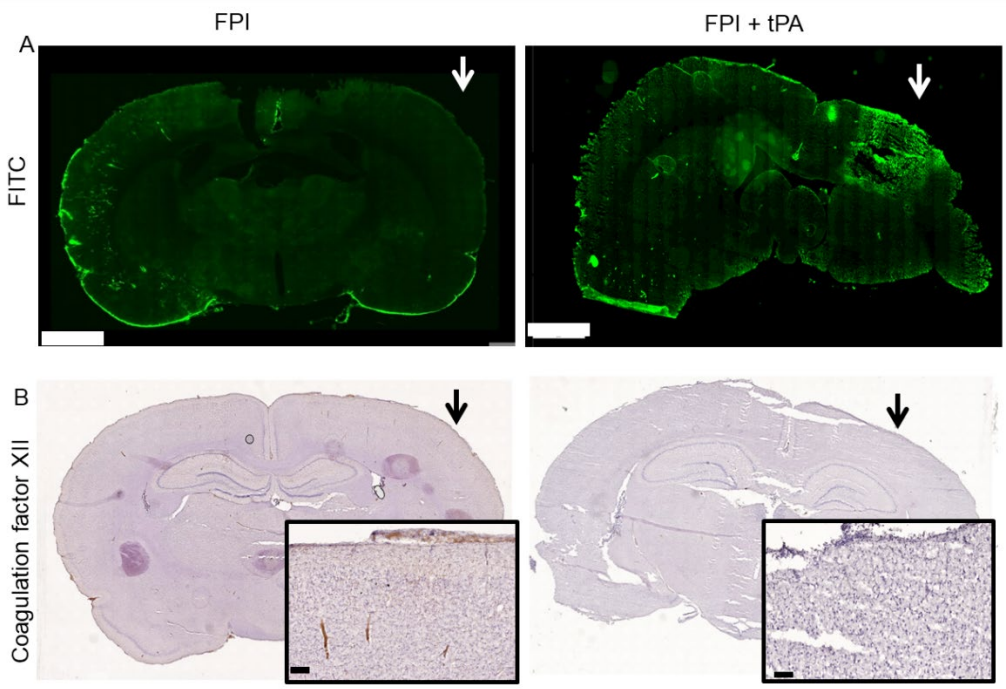

Figure 2.10 Anti-coagulant drug reduced coagulation post FPI. Scale bar: 3 mm. (A) FITC tracer indicated CSF blockage in FPI brain and reverse in tPA treated FPI brain. (B) Immunohistochemistry staining of Coagulation factor XII in FPI brain and tPA treated FPI brain. Enlarged image shows the clearance of coagulation by tPA treatment (scale bar 70 µm). T=3 days.

2.4 Discussion

This discussion will focus on three unique observations post TBI. a) Fluid Percussion injury is associated with hemorrhagic infarct volume, b) coagulative thrombosis is developed at the hemorrhagic site, and c) neuroimmune cells activation is prevalent at the hemorrhagic site as an initial step of inflammation. The findings revealed that hemorrhage of cerebral vascular and subarachnoid mediated coagulation play an important role in injury development.

Hemorrhage and subsequent thrombosis management is the severest issue in emergency care after TBI [81-83], and coagulation can be minimized by resuscitative care of optimizing cerebral perfusion [99, 100]. This clinical evidence revealed the

importance of treatment for hemorrhage and thrombosis in TBI. However, effective care of hemorrhagic bleeding and coagulative thrombosis in TBI patients remained challenging, partly due to uncovering the elusive mechanisms. Thus, the distinctive findings of intracranial hemorrhage, CSF pathway blockage, necrosis and immune cells infiltration observed in the present study appeared to be *in* sync with clinical observations in neurotrauma patients in critical emergency care [81-83].

The "dose-dependent" related internal hemorrhage with infarct volume immediately post-injury (**Figure 2.1**) was a clear indication of physical tissue damage impacted by mechanical force. Similar intraventricular hemorrhage and thrombin level increase post-TBI in moderate rat LFPI was shown by Lyeth's group [101]. They found that activation of Src kinase signaling pathway caused by thrombin results in hippocampal neuronal loss and cognitive dysfunction. However, the importance of hemorrhage associated coagulation and subsequent necrotic cell death in **Figures 2.4** and **2.5** had not been well documented in experimental FPI model. Necrotic cell death was examined in **Figure 2.8** by the presence of RIP1, which was a necroptosis marker [102, 103] around the brain area of hemorrhage and coagulation sites, and this neurotoxic necroptosis could be contributed by elongated coagulation as shown in **Figure 2.5** and **Figure 2.6**. Further investigation of other necrosis marker, RIP3 and MLKL are needed to confirm the pathway of necrosis.

Recently, an early impairment of pericyte-endothelium interaction was demonstrated to result in BBB dysregulation in a FPI model [75]. And the dynamics of T-cell infiltration into brain parenchyma post FPI was shown to be a contributing factor to post-injury impairment and poor recovery [104]. Moreover, age is another

important factor for TBI experimental model. It was found that most TBIs occur in males among the adult population [105], and age can determine the survival rate following isolated TBI [106], by resulting in more severe secondary brain damage [107], increased neuroinflammation with significantly higher monocytes infiltration [108], and age-dependent production of inflammation cytokines and chemokines [109]. Thus 8-10 weeks male rats were used in this study, to replicate human adult TBI scenario and reduce the age-dependent effects on inflammation response.

Further, the event of hemorrhage and coagulation is capable of triggering the activation of microglial cells as seen in Alzheimer's disease [110]. These unchartered events of hemorrhage and coagulation at post-injury are likely to bridge the missing piece for proper management of TBI related neurological disorders, because cerebrovascular damage, hemorrhage, and pro-inflammatory clotting factors are found to be closely associated with neurological diseases like Alzheimer's disease [111, 112]. Therefore, preventive measure targeting cerebrovascular disruption and coagulation in post-TBI could potentially serve as regenerative approach to slow down the progression of neurological disease in TBI. To this end, the present findings may bridge the knowledge gap between clinical observations and animal studies for a successful therapeutic treatment in TBI patients.

These findings also shed important light on immune cells infiltration and glial cells activation as the secondary mechanisms of neuroinflammation and neurodegeneration post TBI. The infiltration of immune cells was mostly localized in hemorrhage and coagulative area and penetrated deep inside the ventricle and hippocampus area similar to the track path of infarcted brain volume. These data

suggest that neuroinflammation and neurodegeneration in the demarcated brain area were initiated by hemorrhage and aftermath coagulation. The significant aggregation of immune cells around the hemorrhagic region where the arterial vessels (the BBB) were ruptured, further validated the point that hemorrhage and coagulation regulated the immune cell infiltration, neuroinflammation and neurodegeneration post-TBI. It is strongly suggested here that proper management of coagulation at the site of injury may promote hemorrhagic wound healing, prevent neuronal loss, and should be considered for post-TBI therapeutic treatment.

CHAPTER 3

OXIDATIVE/NITROSATIVE DAMAGE MEDIATED CEREBRAL VASCULAR INFLAMMATION AND NEURODEGENERATION AFTER TRAUMATIC BRAIN INJURY

3.1 Introduction

Traumatic brain injury (TBI) can be described as a physical intracranial injury which occurs when there is an external mechanical force, including impact, blast wave, penetration and sudden acceleration-deceleration [60]. About 10 million people are affected by TBI worldwide, and 5.3 million people experience TBI in the USA [2]. Most of the TBI cases are caused by motor vehicle accidents, falls and strikes or blows to the head, such as sports injuries or blast injuries [18, 113]. TBI leads to physical, cognitive and behavioral impairment, and a high risk of the later development of neurodegeneration, including Alzheimer's disease (AD) [10, 15-17]. Over the past decades, despite there have been numbers of phase III clinical trials, no treatment has been shown to be efficacious [21, 22].

Disruption of blood brain barrier (BBB) is found to be involved in TBI and neurological disorders [75, 76, 114]. Some studies have shown that the induction of free radical generating enzymes, oxidative damage, and BBB leakage are the main factors leading to perivascular inflammation [115, 116]. Reactive oxygen species (ROS) are the major sources of oxidative stress in brain injury, including superoxide (O2-), hydroxyl radical (HO-), hydrogen peroxide (H_2O_2), and hypochlorousacid (HOCl) [117]. Superoxide causes tissue damage by promoting hydroxyl radicals from hydro-gen peroxide (H_2O_2) and peroxynitrite (−ONOO) when combined with

nitric oxide (NO). RNS includes NO and the product of NO, $O2^{-}$ and peroxynitrite (ONOO−) [117]. It was demonstrated that the production of ROS/RNS is significantly enhanced by TBI [118]. ROS/RNS can further accumulate the condition and lead to BBB disruption via degradation of the extracellular matrix and tight junction proteins, and activates caspase-1/3, resulting in cell apoptosis [119]. Moreover, ROS/RNS also activate different inflammatory cytokines and growth factors such as IL-1β, IL-6, and TGF-β [120], which further aggravate neuroinflammation in TBI.

Interestingly, neuropathological analysis [67] of postmortem brains from young athletes revealed a significant neurodegeneration in the form of phosphorylated tau protein localized around the perivascular region. This distinctive localization of tau neuropathy around perivascular region showed evidence that vascular BBB oxidative injury and inflammation may lead the foundation for neuroinflammation initiation and neuronal degeneration propagation within the neurovascular layers. Growing evidence suggests that microvascular damage is involved in neuropathogenesis of TBI and Alzheimer's disease [121]. A number of studies have demonstrated that microglial activation is found in the brains of TBI patients and in the animal models of TBI [122]. It has been demonstrated that activated microglia also produce reactive oxygen species (ROS) such as superoxide ($O2^{-}$) and $O2^{-}$ derived oxidants, which may induce or exacerbate neurotoxicity by causing oxidative stress to neurons [123].

From previously published data of our laboratory, oxidative damage of the blood-brain barrier (BBB) was found to be the major mechanism of TBI in blast wave animal model [124]. The present study examined the temporal changes of the

NADPH oxidase (NOX) 1 and inducible nitric oxide synthase (iNOS), as well as levels of superoxide/nitrosative and formation of protein adducts 4-hydroxynonenal (4-HNE) and 3-Nitrotyrosin (3-NT). Cerebral vascular oxidative damage is associated with reduction in the BBB tight junction proteins and enhanced immune cell infiltration through perivascular units [116]. Thus destruction of the barrier leads to neuroinflammation and neurodegenerative disease [116].

Microglial activation was examined in this chapter to identify neuroinflammation footprint, especially for the M1 pro-inflammatory state at different time points. M1 phenotype is the pro-inflammatory state that releases cytokines, chemokine and ROS/RNS which further exacerbate neural injury. M2 state is related to a phagocytic role and the release of neurotrophic factors that promote repair and [125, 126]. But it is rare to specify M1 or M2 microglial phenotypes in chronic diseases, since these states are transitory and commonly mixed [127]. In this study, M1 phenotype was examined as the pro-inflammatory phenotype lies at one extreme of the reactivity spectrum, and can contribute to chronic neuroinflammation and long-term neurological impairments [128]. Co-localization of IBA-1 with RNS generation enzyme iNOS and pro-inflammatory/anti-inflammatory cytokine IL-6 was attempted to indicate the M1 phenotype of microglia at 4 hrs and 7 days post FPI. IL-6 is an interleukin that acts as both a pro-inflammatory cytokine and an anti-inflammatory myokine, and it has been established as a marker to identify M1 phenotype of microglia in rats [128-130].

3.2 Methods and Materials

3.2.1 Fluid Percussion Injury

All the use of experimental animals and Fluid Percussion injury model protocol was same as described in Chapter 2.2 Methods.

3.2.2 Real-time NO and Superoxide Detection

The method for free radical analysis in brain tissue was established in the previous study [131]. Freshly isolated brain tissues was prepared in ice-cold oxygenated (95% O2 and 5% CO2) artificial cerebrospinal fluid (aCSF). NO/O_2^- was measured using free radical analyzer with a specific NO or O_2^- probe (TBR4100, World Precision Instruments, Sarasota, FL). The probe is able to polarographically measure the concentration of NO/O_2^- in solutions. The NO detection system was calibrated daily using different concentrations of NO donor S-Nitroso-N-acetyl-DL-penicillamine (SNAP) to generate a standard curve, and the O_2^- detection system was calibrated using different concentrations of H_2O_2 solution. Baseline of NO/O_2^- release was determined by evaluation of NO/O_2^- release in aCSF without any treatments. The concentration of NO/O_2^- in solution was measured in real time. Each experiment was simultaneously performed with a control brain to exclude experimental drift in NO/O_2^- release unrelated to the study.

3.2.3 Tissue Processing

At different time points after TBI, the rats were deeply anesthetized and euthanized via slow transcardiac perfusion with ice cold phosphate buffered saline (PBS), followed by ice cold 4% paraformaldehyde in PBS. Brain areas involved in the

traumatic foci were recut from the whole brain and immersed in 4% paraformaldehyde overnight, followed by cryoprotection in 30% sucrose containing PBS. Coronal sections of 10μm thickness were sectioned from each sample and stored at −80°C for further analysis.

3.2.4 Immunofluorescence and Microscopy

This procedure was same as described in Chapter 2.2 Methods. Cell counting were performing by using Image J to measure positive stained Neurons, and presented as numbers/ square mm.

3.2.5 Western Blotting

This procedure was same as described in Chapter 2.2 Methods. All information about the source of antibodies, intended biomarker, catalogue numbers, and dilutions factors for immunohistochemical staining and western blotting analyses are listed in **Table 3.1**. Densitometry analysis of target marker was performed in a blinded way using ImageJ software. The levels of the marker detected are normalized with β-actin as loading control as a ratio.

Table 3.1 Antibody Source, Catalogue Numbers, and Dilution Factors for Immunohistochemical Staining and Western Blott Analysis

Antibody	Marker for	Company	Catalogue #	Dilution for Immunostaining	Dilution for WB
iNOS	iNOS	Abcam	ab15323	1:200	1:1000
NOX1	NOX1	Abcam	ab55831	1:200	1:1000
3-NT	3-NT	Abcam	ab61392	1:200	1:1000
4-HNE	4-HNE	Abcam	Ab46545	1:200	1:1000
GFAP	Astrocytes	Abcam	ab7260	1:500	--
IBA-1	Microglia	Abcam	ab5076	1:200	--
IL-6	IL-6	Abcam	ab6672	1:400	--
Claudin-5	Claudin-5	Abcam	Ab15106	1:200	--
Occludin	Occludin	Thermo Fisher	OC-3F10	1:200	--
Tau	Tau-5	Abcam	ab80579	--	1:1000
Caspase 3	Caspase-3	Abcam	ab4051	1:200	--
PHF-Tau	Ser202	Thermo Fisher	MN1020	1:200	1:1000
CD11b	CD11b	Abcam	ab52478	1:200	--
CD68	CD68	Abcam	ab955	1:200	--
ZO1	Tight junction protein	Abcam	ab96587	1:200	--
β-actin	actins	Abcam	ab8226	--	1:1000

3.2.6 Statistical Analysis

All results are expressed as the mean ± SEM. Statistical analysis of the data was performed using GraphPad Prism 7(Sorrento Valley, CA, USA). Comparisons between samples were performed by one-way ANOVA with Tukey's multiple comparison tests, two-way ANOVA with Sidack's multiple comparisons test, and independent t-test. Differences were considered significant at *$p<0.05$, **$p<0.01$, ***$p<0.001$, ****$p<0.0001$.

3.3 Results

3.3.1 Free Radicals Generation Increases Significantly Post TBI

Real-time free radicals production of the injured brain tissue was first examined by a free radical analyzer. Reactive oxygen species (ROS) superoxide (O_2^-) and reactive nitrogen species (RNS) nitric oxide (NO) were investigated at different time frames, including immediately after FPI (0 hr), after 4 hrs and 7 days post FPI, compared with sham control brain **(Figure 3.1)**. Each brain tissue was also separated into the ipsilateral and contralateral site, to compare the injured hemisphere with non-injured hemisphere. Two-way ANOVA was used to compare each time frame as well as the ipsilateral and contralateral site within each group. For NO generation (**Figure 3.1A**), significant differences were found when compared 0 hr, 4 hrs brain tissue with sham and 7 days brain tissue post FPI ($F(3, 24) = 165.4$, $p<0.0001$). And ipsilateral site had significant higher generation of NO at 0 hr and 4 hrs, when NO was reduced after 7 days post FPI in the injured brain ($F(1, 24) = 127.1$, $p<0.0001$). Meanwhile, Superoxide generation was significant higher in the ipsilateral site, at 0 hr, 4 hrs and 7 days post FPI ($F(3, 15) = 39.78$, $p<0.0001$). At 0 hr and 4 hrs post FPI, superoxide expression was much higher in the ipsilateral site compared with contralateral site ($F(1, 15) = 395.9$, $p<0.0001$). Even though O_2^- generation was reduced, it still showed a significant difference with sham group at day 7 post FPI (**Figure 3.1B**).

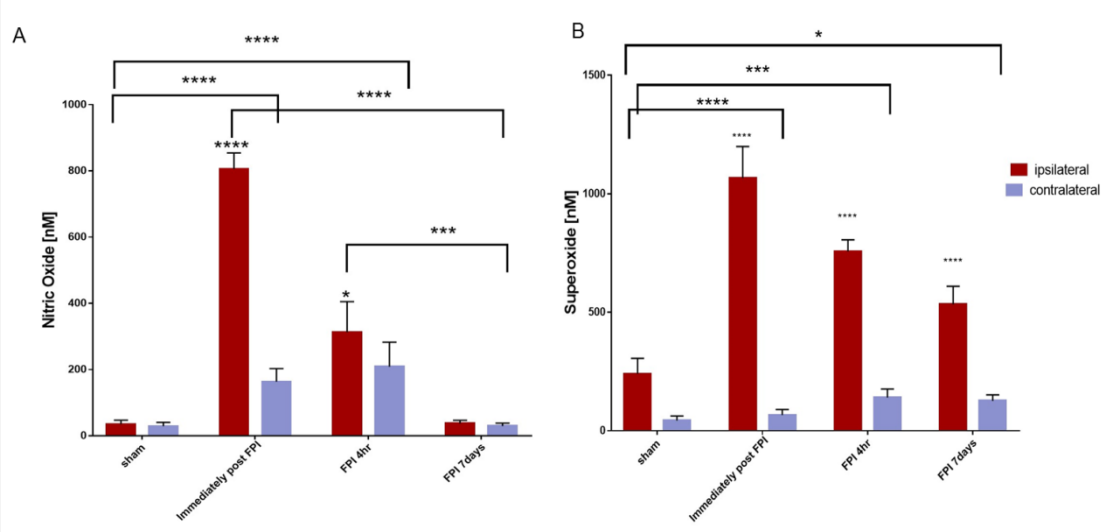

Figure 3.1 Nitric oxide and hydrogen superoxide generation at different time post FPI. Real-time NO (A) and O_2^- (B) production were detected in live rat brain tissue by Free Radical Analyzer. Live brain tissues were cultured in oxygenated CSF. Values are mean ±SEM. *p<0.05, **p<0.01, ***p<0.001, ****p<0.0001 versus sham (N = 7).

3.3.2 Oxidative/Nitrosative Damage in Perivascular Space and Propagated after Injury

To further examine the oxidative/nitrosative stress, the ROS/RNS generating enzymes were investigated by NADPH oxidase 1 (NOX1), and inducible nitric oxide synthase (iNOS), respectively. Corresponding oxidative damage marker 4-Hydroxynonenal (4-HNE), and nitrosative damage marker 3-Nitrotyrosine (3-NT) were examined in parallel with the enzyme markers. Significant higher expression of iNOS (**Figure 3.2A**) and 3-NT (**Figure 3.2B**) were observed in the ipsilateral site at 4 hrs post FPI. By co-localization of 3-NT with tight junction protein Zonula occludens-1 (ZO-1), it showed that nitrosative damage occurred in blood brain barrier at 4 hrs post FPI (**Figure 3.2C**). Western blot results showed the quantification analysis of iNOS and 3-NT in sham and the ipsilateral site at 4 hrs, 3 days and 7 days post FPI. Significant increase was found at 4 hrs for both RNS

generating enzyme and nitrosative stress marker, and then they both decreased after 3 days and 7 days (**Figure 3.2D-E**). There was no significant difference between 3 days/7 days post FPI with sham control.

ROS generating enzyme NOX-1 and oxidative stress marker 4-HNE was evaluated by immunostaining and western blot, respectively (**Figure 3.3**). Increased expression of NOX-1 and 4-HNE was observed in the ipsilateral site, compared with sham and the contralateral site at 4 hrs post FPI. With co-localization of tight junction protein claudin5, oxidative stress was found in blood brain barrier. Interestingly, even though both oxidative/nitrosative enzymes and stress markers showed similar trends with a decrease after 3 days and 7 days post-FPI, the ROS generation enzyme NOX1 and damage marker 4-HNE in injured brain at day3 and day7 were still significantly higher than sham control.

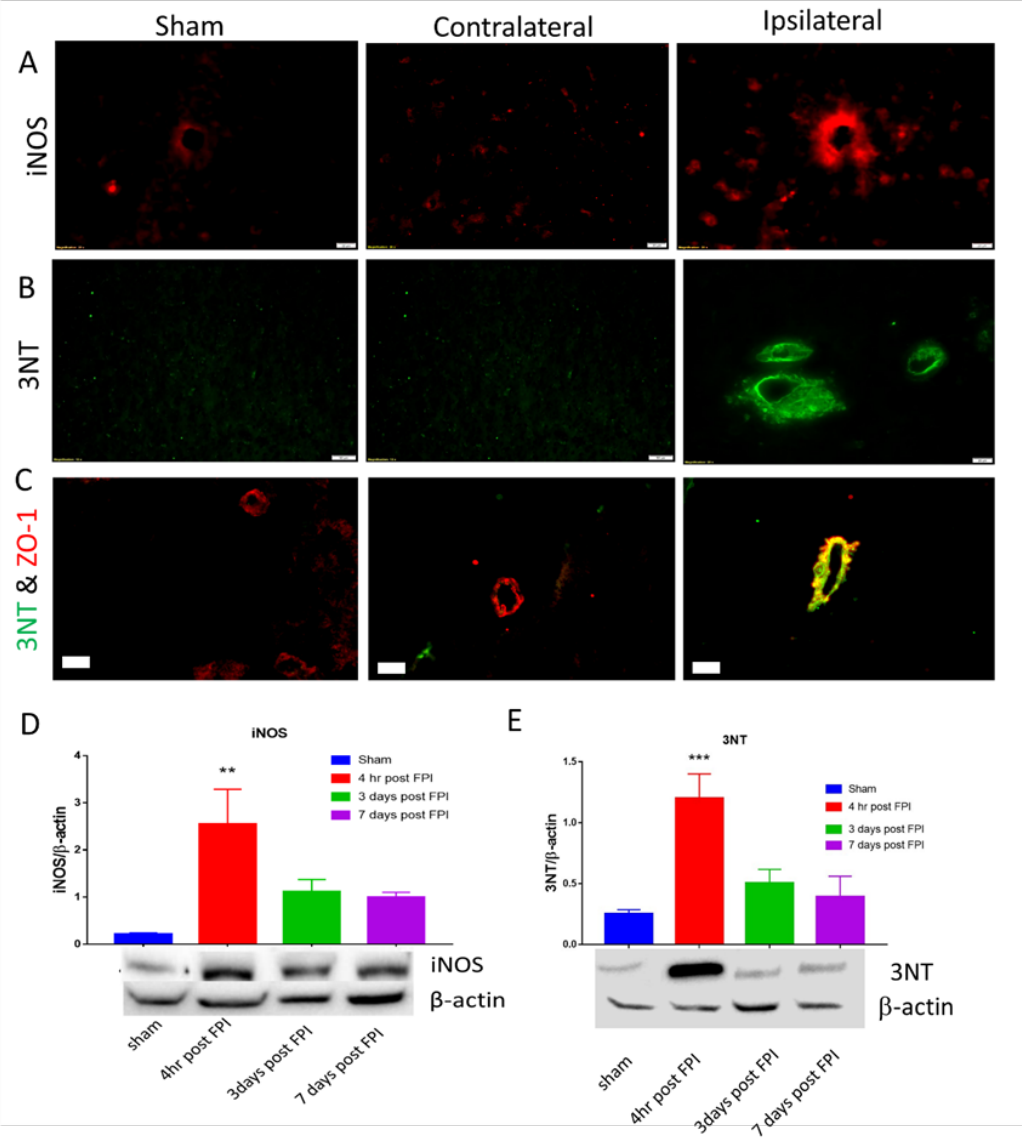

Figure 3.2 FPI induced nitrosative stress in the blood brain barrier. (A) shows RNS generation enzyme iNOS expression in sham, injured brain contralateral and ipsilateral site at 4 hrs post FPI, (B) is the nitrosative stress marker 3-NT staining in the injured brain contralateral and ipsilateral site, compared with sham brain at 4 hrs post FPI. (C) Co-localization of 3-NT with tight junction protein Zonula occludens-1 in the injured brain contralateral and ipsilateral site, compared with sham brain at 4 hrs post FPI. Scale bar is 20 μm. (D) and (E) are western blot results of iNOS and 3-NT, in sham brain and injured brain ipsilateral tissue after 4hrs, 3 days and 7 days post FPI, respectively. Values are mean ±SEM, one-way ANOVA was used, $F(3, 20)=18.15$, $^{**}p<0.01$, $^{***}p<0.001$, versus sham (N = 6).

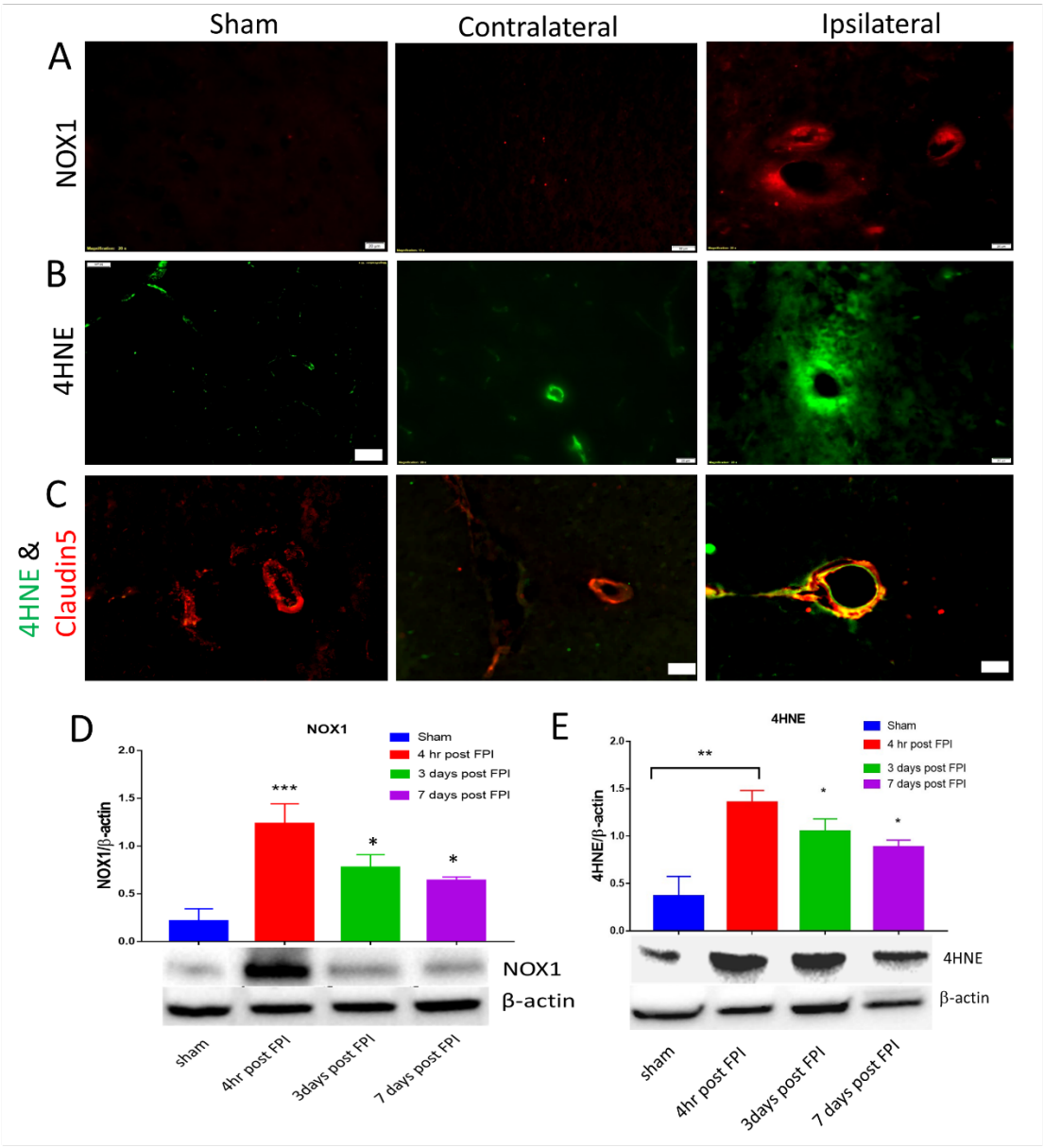

Figure 3.3 FPI induced oxidative stress in the blood brain barrier. (A)ROS generation enzyme NOX1 expression in sham, injured brain contralateral and ipsilateral site at 4 hrs post FPI, (B) Representative Immunostaining of 4-HNE in sham, injured brain contralateral and ipsilateral site at 4 hrs post FPI. (C) Oxidative stress marker 4-HNE co-localized with tight junction marker Claudin-5 in sham, contralateral and ipsilateral brain. Scale bar is 20 µm. (D) and (E) are western blot results of NOX1 and 4-HNE, in sham brain and injured brain ipsilateral tissue after 4hrs, 3 days and 7 days post FPI, respectively. Values are mean ±SEM. One-way ANOVA was used, $F(3, 20)=25$, *$p<0.05$, **$p<0.01$, ***$p<0.001$, versus sham ($N = 6$).

3.3.3 Cerebrovascular Disruption and Immune Cells Infiltration

Blood brain barrier (BBB) integrity and immune cell reactions were then examined at the hemorrhage site after 4 hrs and 7 days post FPI. Antibody to CD11b and CD68 were used for detection of immune cells, as described in **Chapter 2.3 Results**. Co-localization of CD11b with tight junction protein Occludin in **Figure 3.4** showed an enhanced acute aggregation of CD11b positive cells through BBB at 4 hrs post-FPI, in injury site compared with sham control. An increased infiltration of CD68 positive cells (monocytes/macrophages) through BBB was also observed in brain tissue sections at 4 hrs post-TBI compared with sham controls (**Figure 3.5)**. Interestingly, co-localization of the blood-brain barrier tight junction anchoring protein zonula occluden-1 (ZO-1) with CD68 indicated a significant aggregation of monocytes or macrophages around perivascular space in the injured brain tissue compared with sham controls (**Figure 3.5C)**.

At 7 days post FPI, immune cells were still significantly accumulated at the impacted site, and infiltrated through BBB (**Figure 3.6**). CD11b positive immune cells were observed in the ipsilateral site (**Figure 3.6A**), co-localization of CD68 with ZO-1 at 7 days post-FPI showed the monocytes/macrophages infiltration through BBB (**Figure 3.6A**). These evidence indicated the prolonged immune reactions after TBI, paralleled with BBB disruption.

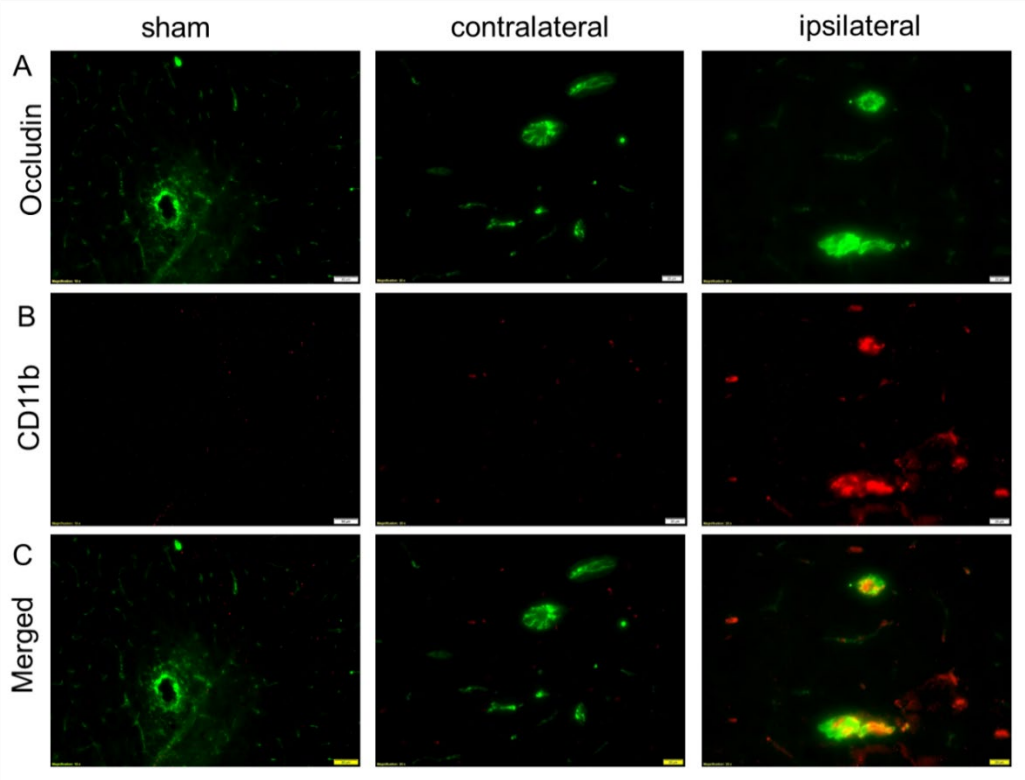

Figure 3.4 CD11b positive immune cells infiltration at 4 hrs post FPI. Tight junction protein occludin (A) and CD11b (B) in sham, FPI brain contralateral site and ipsilateral site. (C) Co-localization of CD11b with occludin shows CD11b positive cells infiltration through BBB. Scale bar is 20 μm.

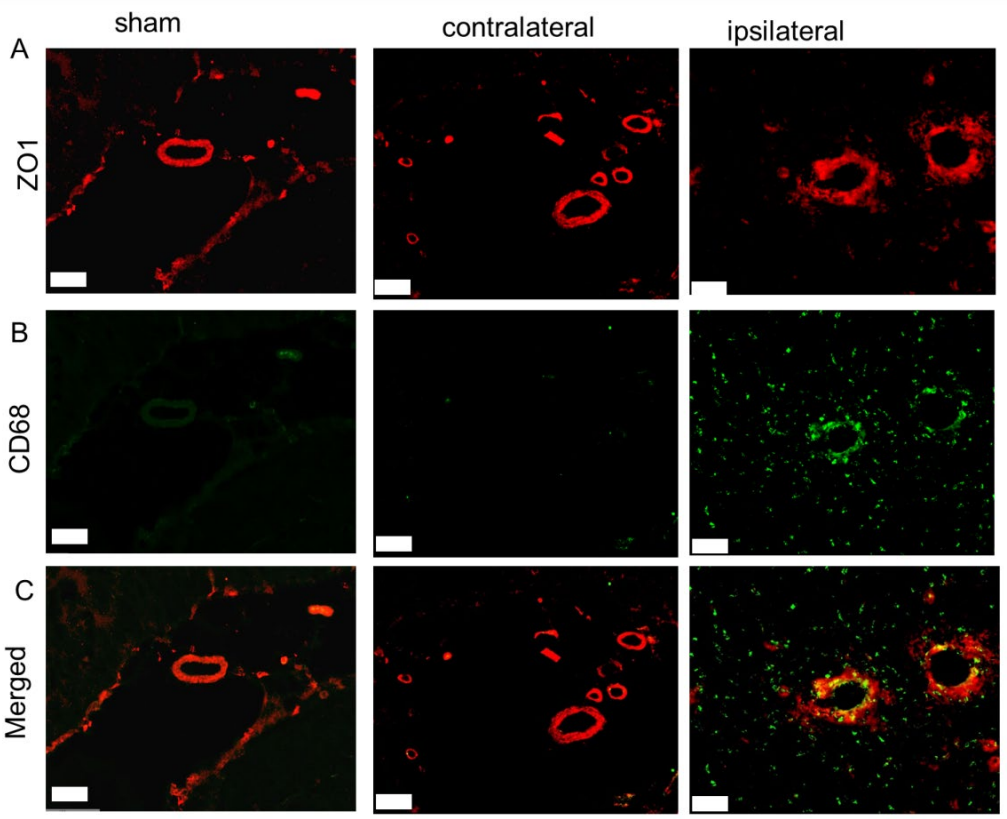

Figure 3.5 CD68 positive immune cells infiltration at 4 hrs post FPI. (A) Tight junction protein ZO-1 and pan-macrophages marker CD68 (B) in sham, FPI brain contralateral site and ipsilateral site. (C) Co-localized images indicate the infiltration of CD68 positive immune cells through blood brain barrier. And BBB integrity was impaired. Scale bar is 20 μm.

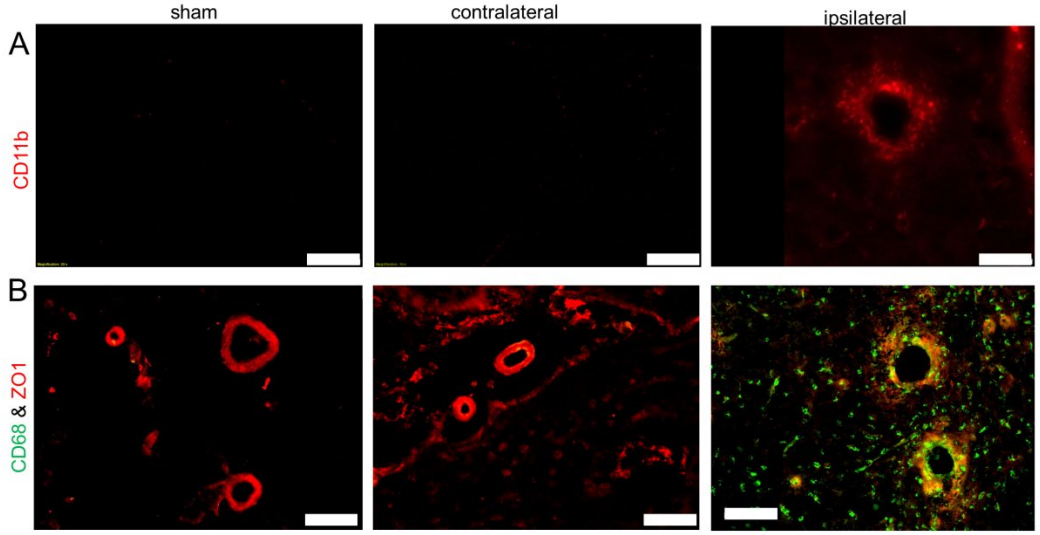

Figure 3.6: Prolonged immune cells accumulation at 7 days post FPI. (A) Representative image for CD11b positive cells in sham, FPI brain contralateral and ipsilateral site. (B) Co-localization of CD68 (green) with ZO-1 (red) indicates the persistent aggregation of monocytes/macrophages through blood brain barrier. Scale bar is 50 μm.

3.3.4 Microglial and Astrocytes Activates after Traumatic Brain Injury

As the resident macrophages in the brain, microglia were expected to react to acute immune cell infiltration and hemorrhage. And astrocytes may also be activated to aid in the maintenance of the BBB. Thus gliosis was examined after FPI by GFAP (Glial fibrillary acidic protein) and IBA-1 (ionized calcium binding adaptor molecule-1) as the markers for astrocytes and microglial, respectively. In **Figure 3.7**, microglial and astrocytes were activated at 4hrs post FPI, especially in the cortex and around BBB at the ipsilateral site. By comparison with sham brain sections, GFAP and IBA-1 positive cells were highly expressed in the ipsilateral site (**Figure 3.7A-B**). In the merged images of GFAP and IBA-1, increased astrocytes and activated microglia in amoeboid form were observed in the ipsilateral site, surrounding BBB and in the impact cortex (**Figure 3.7C**).

To further investigate the phenotype of microglia at different time points post FPI, iNOS and IL-6 were used for co-localization with IBA-1, to identify M1 phenotype at different time points post FPI. In **Figure 3.8**, IBA-1 positive cells were found to be significantly co-localized with iNOS at the impact site and in the ipsilateral cortex at 4 hrs post FPI. After 7 days post-FPI, with the reduction of RNS enzyme iNOS and decreased amoeboid microglia, the co-localization of IBA-1 with iNOS was difficult to observe. Meanwhile, microglia remained inactivated form in the contralateral site at both 4 hrs and 7 days post FPI.

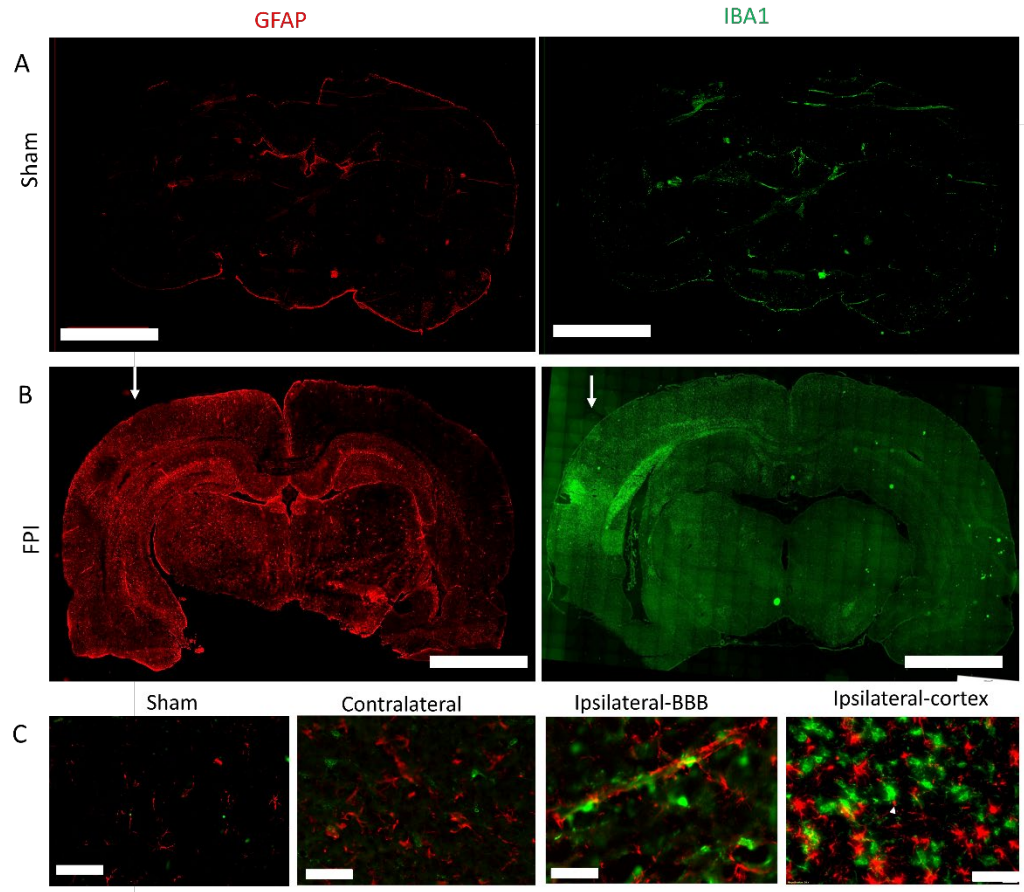

Figure 3.7 Microglia and astrocytes active after FPI. (A) - (B) show whole brain section for microglia (IBA-1) and astrocytes (GFAP) activity in sham and FPI brain sections at 4 hrs post FPI. White arrow indicates the injury site. Scale bar: 3 mm. (C) Merged images of IBA-1 and GFAP in sham, contralateral, ipsilateral site-blood brain barrier and cortex. Activated microglia and astrocytes are highly presented around blood brain barrier and at injured site compare with sham and contralateral site. White arrow head indicates the amoeboid form of microglia. Scale bar: 20 µm.

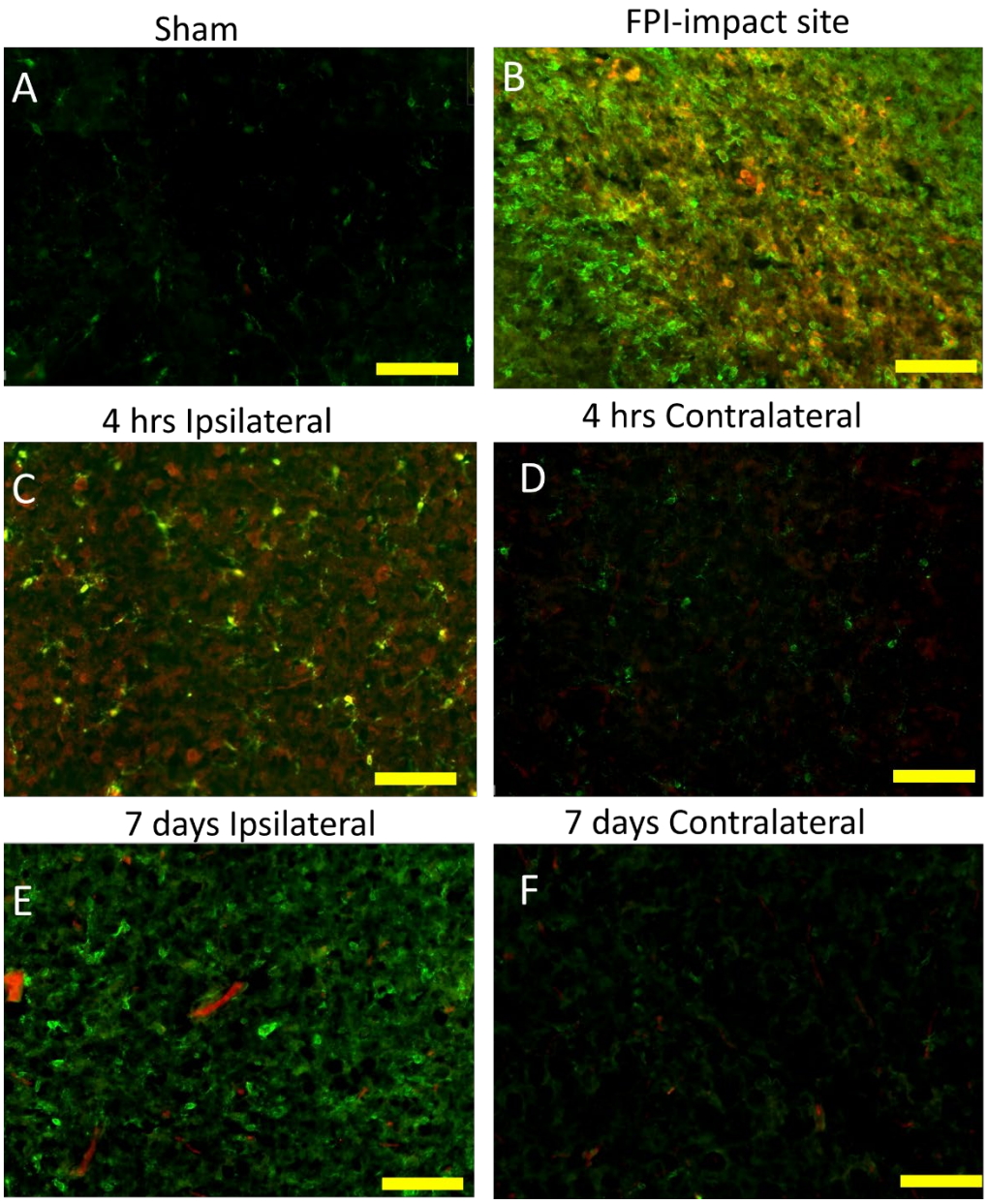

Figure 3.8 Co-localization of IBA-1 (green) with inducible nitric oxide synthase iNOS (red) at 4 hours and 7 days post-FPI. Merged images in sham (A), FPI 4hrs brain impact site (B), 4 hrs (C-D) and 7 days (E-F) in the ipsilateral and contralateral. Scale bar is 60 µm.

In the current study, IL-6 was highly expressed in the ipsilateral site at 4 hrs post FPI, compared with sham and contralateral site, and reduced but still substantially expressed in the ipsilateral site after 7 days. Meanwhile, the number of amoeboid

microglia was decreased after 7 days post FPI, so were the co-localized microglia with IL-6 (**Figure 3.9**).

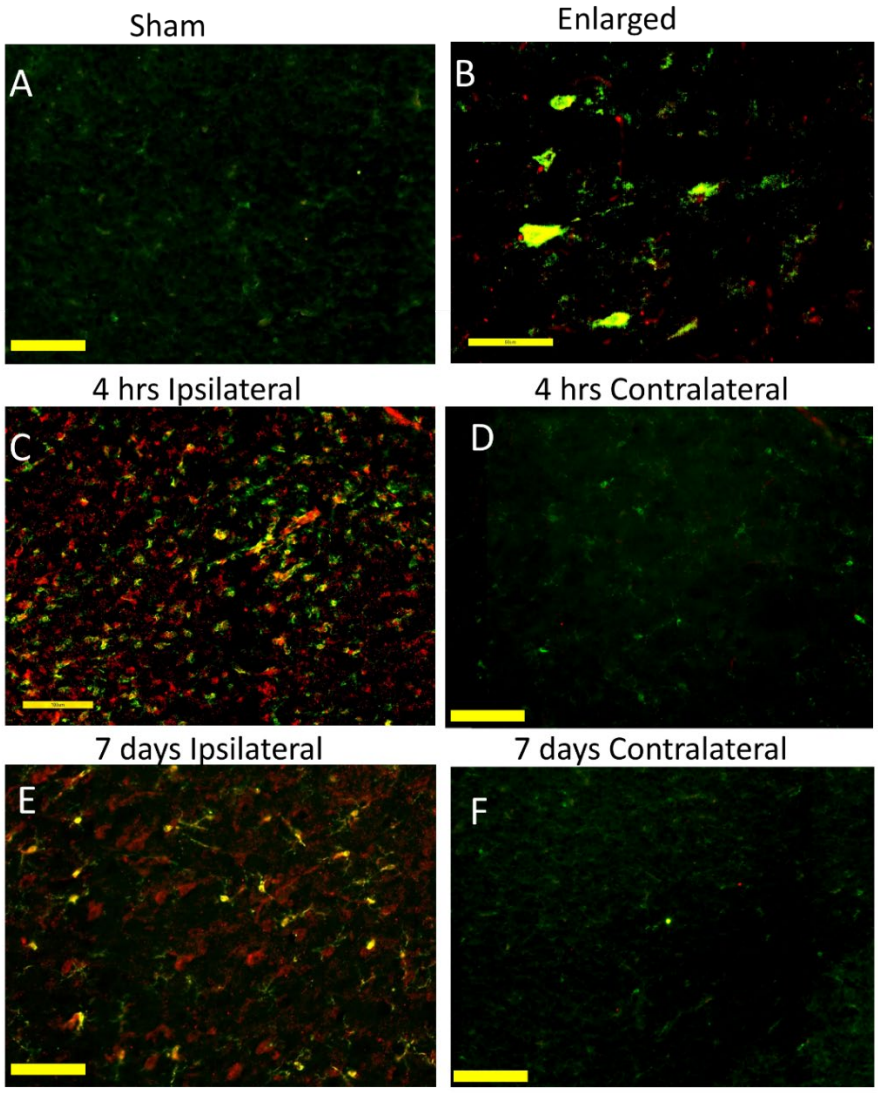

Figure 3.9 Co-localization of IBA-1 (green) with Interleukin 6 (IL-6, red) at 4 hours and 7 days post-FPI. Merged images in sham (A), enlarged amoeboid microglia expressing IL-6 (B) at 4 hrs at the impact site, 4 hrs (C-D) and 7 days (E-F) in ipsilateral and contralateral. Scale bar for A, C-F is 60 µm, for B is 30 µm.

3.3.5 Tau-protein Phosphorylation and Apoptosis after Brain Injury

To track cell death following neuroinflammation, immunofluorescence staining was used for apoptosis marker Caspase-3. Caspase-3 was upregulated in the ipsilateral

site, indicating the ongoing programmed cell death at 7 days post FPI (**Figure 3.10G-I**). Tauopathy was also investigated as an indication of neuronal dysfunction, as the phosphorylated tau can induce microtubule instability that results in cell death. Hyper-phosphorylation of tau protein was found in perivascular space, and accumulated surrounding vasculature structure (**Figure 3.10**). Western blot showed quantification results of total tau protein marker Tau-5 and phosphorylated tau protein marker Ser202 (**Figure 3.10J-K**). Both of them peaked at 4 hrs post FPI, then decreased after 3 days post FPI, and only 4 hrs was significantly different to sham.

NeuN immunostaining was then used to indicate the neuronal loss in the injured cortex site at day 7 post FPI (**Figure 3.10**). By qualitative staining images and quantitative positive NeuN cell counting, significant neuronal loss was observed at day 7 in the injury site.

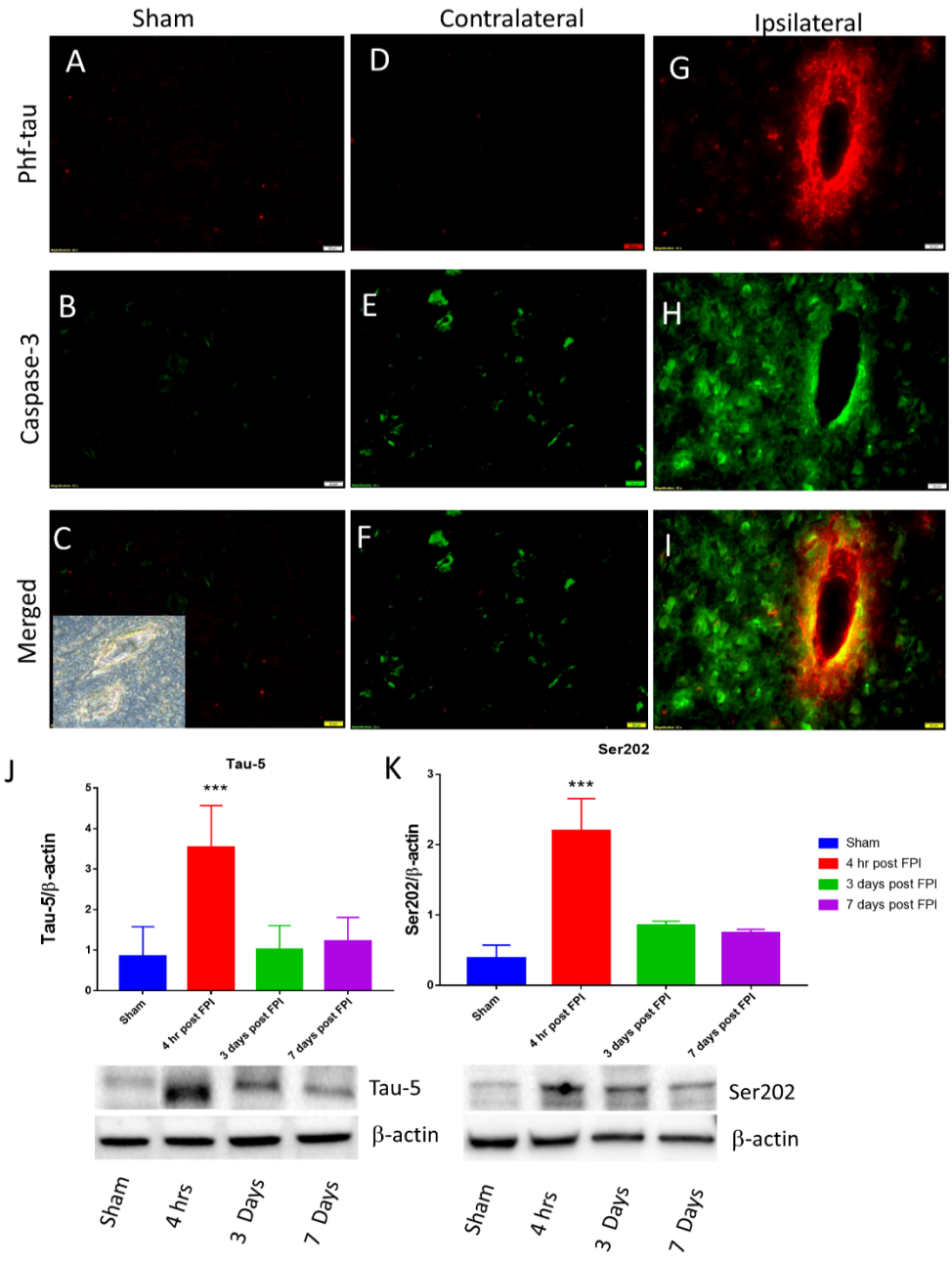

Figure 3.10 Tauopathy and apoptosis after FPI. Co-localization of phosphorylated-tau Ser202 (phf-tau) (red) & Caspase-3 (green) in sham (A-C), FPI contralateral (D-F) and ipsilateral (G-I) brain after 7 days post FPI. Bright field image in (C) was taken at the same region of the immunostaining image in the same brain section. Scale bar: 20 µm in A-I. (D-E) show western blot results for total-tau protein Tau-5 and phf-tau Ser202 at different time point in the ipsilateral site, compared with sham control. Values are mean ±SEM. One-way ANOVA was used, $F(3, 20)=30$, ***$p<0.001$, versus sham (N = 6).

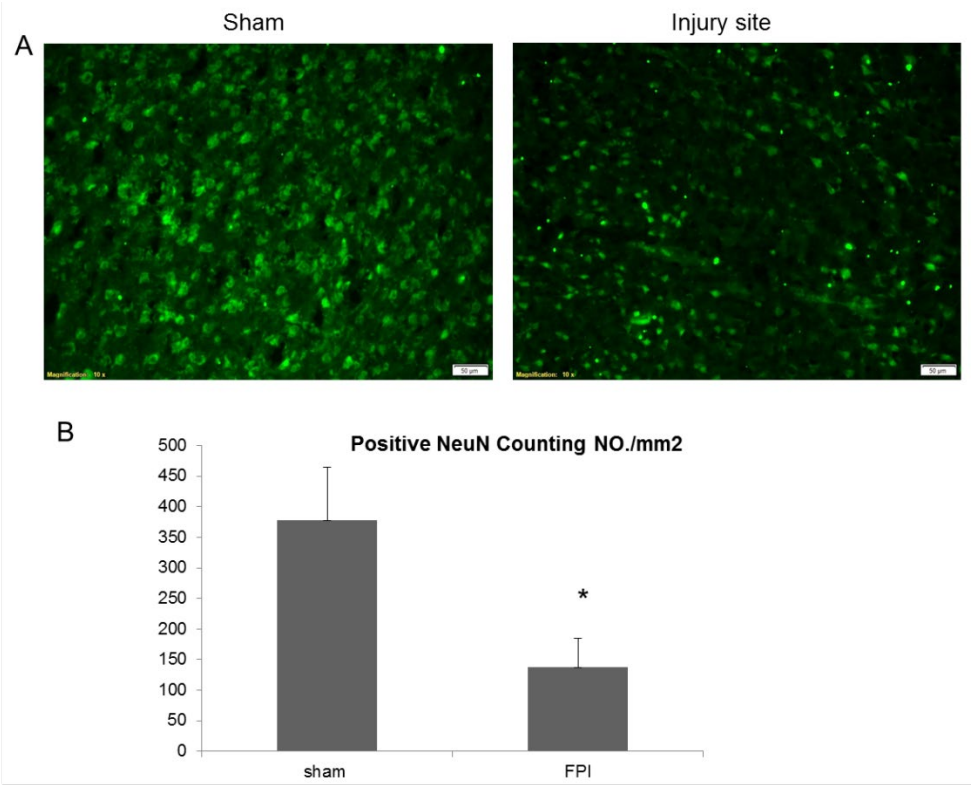

Figure 3.11 Neuronal loss in the injured cortex after 7 days post FPI. (A) Representative immunostaining of NeuN in sham and FPI injury site. Scale bar is 50 µm. (B) Neuronal cells counting in cortex for NeuN staining in sham and FPI injury site cortex. N=12. **$p < 0.01$.

3.4 Discussion

In the present study, oxidative/nitrosative damage was examined in blood brain barrier at the injury site, followed by the prolonged gliosis, cytokine release, immune cells accumulation, apoptosis, tauopathy and neuronal loss. The nature of sustained cerebrovascular disruption was oxidative/nitrosative damage, which might be initiated by ROS/RNS via the induction of NOX1 and iNOS. The signature of oxidative damage (4-HNE) and nitrated protein (3-NT) in the vasculature was correlated with the induction of NOX1/iNOS. The expression of these markers both peaked at 4 hrs post FPI and reduced after 3 days post FPI. In the context of these

findings, it was emphasized that cerebrovascular oxidative injury may precede the development of neuroinflammation.

From previous studies in our group, the authors have reported BBB leakage with the evidence of tight junction protein disruption (occludin, claudin-5, and zonula occludin 1) post mild TBI in primary blast animal model [119]. Recently from Chandra's group, a thorough investigation of cell-type dependent increase in NOX isoforms at different brain regions was reported in the blast shock-wave rodent model [132]. Oxidative damage has been found not only in BBB [133, 134], but also in neurons, astrocytes and microglia. As the future direction for blunt TBI, it will be beneficial to examine the cell-type dependent increase of ROS/RNS.

Meanwhile, zonula occludin 1 (ZO-1) and occludin were used as the tight junction protein markers to investigate BBB integrity. When co-localized with immune cells marker CD68 and CD11b, the results indicated a significant aggregation and accumulation of neutrophils, monocytes and macrophages from blood circulation to the brain parenchyma, as well as impairment of tight junction proteins. In the previous study, our group reported the acute immune cells infiltration at 4 hrs post FPI [135], which causes inflammation as the secondary event following vascular rupture and hemorrhage. Here, it was further indicated that after 7days post FPI, the infiltration of immune cells was prolonged. It was probably resulted from the persistent oxidative damage in the BBB and the vascular disruption.

In response of immune cells accumulation, microglial activation was observed at 4 hrs and 7 days post FPI at the injury site. Microglia phenotypes can be identified by co-localization with other markers [129], here, iNOS and IL-6 were used as M1

phenotype markers. A significant co-localization of IBA-1 positive cells with iNOS was observed at the impact site at 4 hrs post FPI (**Figure 3.8B**), nevertheless, some of the IBA-1 positive cells were round shape, which should be monocytes and were unlikely to be microglia. To separate these two types of cells, further study is needed with the use of CD45 for monocytes [125]. The number of amoeboid microglia was reduced after 7 days post FPI, but still substantial in the ipsilateral cortex, showing a prolonged inflammation and the process of phagocytosis to clear cell debris and coagulation. However, the conclusion cannot be made that M1/M2 phenotypes changed in temporal, previous studies reported the uncertainty that microglia have both phenotypes in acute and long-term post TBI [125, 129, 136].

With the finding of the prolonged neuroinflammation, as a result, neurodegeneration happens following the events of inflammation. In deed, the current findings validated that Caspase-3 activation and cell apoptosis were observed mostly around the perivascular region of the brain, suggesting the ongoing apoptosis in parallel with gliosis and immune cells infiltration after 7 days post FPI. Moreover, the significantly higher phosphorylation of tau protein around perivascular space showed the indication of neurodegeneration and can be a hallmark of injury pathology. Interestingly, phosphorylated tau protein Ser202 and total tau Tau-5 were both found to increase significantly at 4 hrs post FPI and return to sham level after 3 days and 7 days in the current study, while tauopathy is the hallmark for chronic traumatic encephalopathy (CTE) which is typically found after months or even years post TBI [11, 71]. But similar trends of results were also reported in other studies for rapid accumulation of tau oligomers in FPI model [136, 137]. The evidence of acute

accumulation and reduction after 3 days for tau/phosphorylated-tau, could be paralleled with the pattern of oxidative damage, and the gliosis in this study. In the recent years, microglial activation has been well established that it is tightly associated with prolonged neuroinflammation and neurodegeneration in CTE, Alzheimer's disease and Parkinson's disease [111, 136, 138, 139]. With the current finding of microglial robust M1 phenotype at 4hrs and prolonged amoeboid form after 7 days post TBI, it can be postulated here that the acute tau hyperphosphorylation is likely to be associated with gliosis and oxidative damage. The immune system may attempt to protect CNS and clean the neurotoxic debris/ waste metabolites in short-time, but fail in long-term with the sustained neuroinflammation and thus lead to chronic neurodegeneration.

All together, these findings in the current study validated the correlation of oxidative/nitrosative damage with cerebrovascular disruption in moderate FPI model, as well as the secondary injury propagated as the prolonged neuroinflammation and neurodegeneration in longer term.

CHAPTER 4

REGENERATIVE TREATMENT WITH ANGIOGENIC SELF-ASSEMBLING PEPTIDE HYDROGEL

4.1 Introduction

A major concern of traumatic brain injury (TBI) is the direct damage to the cerebral vasculature. Hemorrhage, blood–brain barrier (BBB) disruption, edema, and blood flow abnormalities occur in the early stage following the insult, these are commonly observed in TBI patients and recapitulated in animal models of TBI [77, 78, 81]. At a cellular level, the cerebral vasculature contributes several key components to the expanded neurovascular unit (eNVU), consisting of endothelial cells, smooth muscle cells, neurons, astrocytes, and pericytes [75]. Disruption of the vascular tree precedes ischemia, immune cell infiltration, altered delivery of metabolites, hypoxia and tissue death [85]. These suggest that treatments which promote neoangiogenesis of mature and stabilized vessels, may allow enhanced recovery for TBI.

Clinical trials in TBI to date have not specifically targeted angiogenesis and neurogenesis in situ [140]. Preclinical studies in cerebral ischemia are replete with strategies that deliver vascular endothelial growth factor, sildenafil, atorvastatin, carbamylated erythropoietin (EPO) and EPO monotherapy, to name a few [141-146]. Treatments with growth factors also contribute to eNVU remodeling, improving outcomes after ischemic brain injury [146]. However, these systemic or local treatments are cleared by the body in a matter of minutes to hours and do not have a durable localized effect. Further, few strategies report the generation of a supportive in situ microenvironment for wound healing [147]. In previous studies, Kumar's group have generated a self-assembling peptide hydrogel (SAPH) appended with a

potent mimic of VEGF-165, QK [148]. Vascular endothelial growth factor (VEGF) is angiogenic and neuroprotective that can promote neurogenesis in the repair process after brain injury [149-152]. This angiogenic peptide hydrogel termed SLanc, assembles into fibers displaying the QK epitope in very high density [148, 153-159]. Owing to non-covalent interactions, these peptides rapidly assemble and dissemble upon needle shear. Injectable gels have been examined in *in vitro* assays for cytocompatibility, angiogenesis, recovery from hind limb ischemia, and management of a number of ischemic tissue diseases [153-155].

In the current study, the angiogenic SAPH termed SLanc was tested in the impact site post FPI, for its angiogenic and neuroprotective effect in the injured rat brain. A lateral fluid percussion injury model (FPI) was used to induce a moderate blunt TBI, with physical vascular disruption and tissue deformation [94]. SLanc peptide hydrogels were injected into the injury site immediately after FPI, and the bio-distribution along with histological recovery (angiogenesis and neuronal survivability) were evaluated at day 7 and day 14 post injury.

4.2 Methods and Materials

4.2.1 Synthesis and Characterization of Peptides

SLanc was designed and prepared by Dr. Vivek Kumar's laboratory. It was prepared as previously described [148, 155]. Briefly, SLanc was synthesized by a standard Fmoc solid-phase peptide synthesis protocol and purified through dialysis against DI water for 2 days. The dialyzed peptide was frozen, lyophilized and stored in the powder form at –80°C until formulation. The peptide hydrogel was prepared initially at a

concentration of 20 mg/ml (2 w. %) in sterile 298 mM sucrose with pH adjusted to 7. To obtain the final concentration of 10 mg/ml, the same volume of sterile 1X HBSS sucrose solution was added. This formulation was easily injectable with a 25G needle.

Table 4.1 Primary Sequences of Peptides Used in this Study

Name	Sequence
SLanc	$K(SL)_3RG(SL)_3K$–G–KLTWQELYQLKYKGI
F-SLanc	Carboxyfluorescein-$K(SL)_3RG(SL)_3K$–G–KLTWQELYQLKYKGI

4.2.2 Cytocompatibility of SLanc on Primary Neurons

1% (w/v) SLanc was placed into the wells of a 96-well plate (100 µL/well) and incubated at 37ºC for 2 hrs to gel. Complete neurobasal medium containing 2% Gibco B27 supplement with antioxidants (50X), 1% penicillin-streptomycin, and 0.2% glutamate was added and incubated at 37ºC for 2 hrs to condition the SLanc. Primary neuronal cells were obtained by neuronal isolation. Briefly, cortices were extracted from the embryos of a Sprague Dawley pregnant rat (Charles River) at day 16 gestation. Cortices were then digested in trypsin-EDTA (0.25%) at 37°C for 30 mins. Primary cortical neurons were separated by straining with 70 µm and 40 µm pore filters. Neurons were seeded at a density of 50,000 cells/cm^2 on top of the SLanc and supplemented with complete neurobasal medium. Cell morphology and neurite growth was observed over time by microscopy.

4.2.3 Animal Handling

Adult male and pregnant female Sprague-Dawley and Wistar rats were purchased from Charles River Laboratory (Wilmington, MA). The animals were kept with free access

to food and water in a 12 hrs dark-light cycle at room temperature. All procedures were followed in accordance with guidelines established in the Guide for the Care and Use of Laboratory Animals and were approved by the NJIT-Rutgers-Newark Institutional Animal Care and Use Committee.

4.2.4 Fluid Percussion Injury

Sprague Dawley male rats (250-300 g; 8–11 weeks old) were randomly selected and subjected to lateral FPI for a moderate TBI [25]. Sham-injured cases served as control. 5 rats were used for each group (Sham, FPI+PBS, FPI+SLanc). All rats were anesthetized with a mixture of ketamine (100 mg/kg), and xylazine (10 mg/kg) administered via intraperitoneal injection and placed in a stereotaxic frame. Craniotomy (3.0 mm) was performed over the left parietal skull, 2.5 mm lateral from the midline and 3.0 mm caudal from bregma, with the dura intact. A Luer-lock hub was positioned according to the craniotomy and secured with cyanoacrylate gel on the skull. The hub was secured by application of methyl-methacrylate (Henry Schein, Melville, NY, USA). One day after surgery, animals were randomly selected to receive either sham or FPI. Sham animals were subjected to all surgical procedures except the induction of the injury. For induction of FPI, the pendulum hammer was released onto the piston of the fluid filled cylinder to induce a water pulse. For a moderate injury (1.6-1.8 atm.), the recorded apnea and righting reflex time were 10-12 s and 6-8 min, respectively.

4.2.5 Therapeutic Intervention and Bio-distribution of Peptide

After FPI and anesthesia, the rats were placed in a stereotaxic frame to be treated with 5 µl SLanc peptide hydrogel, Fluorescent-tagged SLanc peptide, or PBS as the injury control. The location of injection according to the stereotaxic coordinates was: AP= -3, L= -2.5 from Bregma, dorsoventral (DV) = 0.5 mm. Then the injury hub was removed, and the head was sutured. The rats recovered on a heating pad and then they were returned to their cage.

4.2.6 Tissue Processing

3, 7, 14 days after FPI/FPI + treatment, the rats were euthanized via slow transcardial perfusion with ice cold phosphate buffered saline (PBS), followed by ice cold 4% paraformaldehyde in PBS. Brain tissues were immersed in 4% paraformaldehyde overnight, followed by cryoprotection in 30% sucrose containing PBS. 20 µm thick coronal sections were processed from each sample and stored at −80°C for further analysis.

4.2.7 Immunofluorescence and Microscopy

Both *in vitro* and *in vivo* constructs were analyzed through immunofluorescence. Coverslips with cells were fixed in 4% paraformaldehyde for 15 mins at room temperature, followed by washing with 0.1% Triton X-100 in PBS for 5 mins at room temperature. Brain tissue sections were washed with PBS and fixed in acetone-methanol (1:1 volumetric ratio) for 10 mins at –20°C for immunofluorescence staining. Fixed slides were then blocked with 3% bovine serum albumin at 25°C for 1

h in the presence of 0.1% Triton X- 100. Slides were incubated with the primary antibodies shown in **Table 4.2** overnight at 4°C for probing the respective antigens. Sample slides were washed with PBS and then incubated with Alexa Fluor 488 or Alexa Fluor 594 conjugated with anti-mouse/goat/rabbit/sheep immunoglobulin-G (IgG) for 1 h. After washing with PBS, sample slides were mounted on immunomount containing DAPI (Thermo Fisher, Waltham, MA). Whole brain tissue sections were scanned (20x magnification) by Leica Aperio Versa 200 digital pathology grade slide scanner, and detailed regional fluorescence images were captured by a fluorescence microscope (IX81 DSO; Olympus, Somerset, NJ). Cell counting was performed by using Image J to measure positive stained Neurons, and presented as numbers/ square mm.

Table 4.2 Sources, Catalogue Numbers, and Dilution Factors for Antibodies Used in Immunofluorescence Staining and Western Blot Analysis.

Antibody	Marker for	Company	Catalogue #	Dilution for IF	Dilution for WB
Rabbit anti-MBP	Myelin basic protein	Abcam	Ab40390	1:150	--
Mouse anti-NeuN	Neurons	Abcam	Ab104224	1:200	--
Rabbit anti-Von Willebrand Factor	Endothelial cells	Abcam	Ab6994	1:200	1:1000
Mouse anti-alpha smooth muscle actin	Smooth muscle cells	Abcam	Ab7817	1:200	--
Goat VEGF-Receptor 2	VEGF-R2	Abcam	Ab10972	1:200	1:1000

4.2.8 Western Blot

Fresh brain tissue was homogenized with CellLytic-M (Sigma) lysis buffer (500 uL buffer for every 10 mg of tissue) on ice using sonication (2 mins at 180 watts in rounds of 10 seconds sonication/ 10 seconds rest). After 30 mins incubation on ice, this homogenization was centrifuged at 13,000 rpm for 20 mins at 4ºC and supernatant was collected and assessed for protein concentration by the bicinchoninic

acid (BCA) method (Thermo Fisher). Protein was loaded 20 ug/lane in 4–15% SDS-PAGE gradient gels (Thermo Fisher), transferred on nitrocellulose membranes, blocked with 5% milk, incubated overnight with primary antibodies at 4ºC, washed, and incubated with respective horse-radish peroxidase conjugated secondary antibodies (1:10000 dilution) for 1 hr. at room temperature. Immunoreactive bands were detected by West Pico chemiluminescence substrate (Thermo Fisher). Data was quantified as densitometry intensity using ImageJ software.

4.2.9 Statistical Analysis

All results are expressed as the mean ± SEM. Statistical analysis of the data was performed using GraphPad Prism 7 (Sorrento Valley, CA, USA). Comparisons between samples were performed by one-way ANOVA with Tukey's multiple comparison tests. Differences were considered significant at $p<0.05$.

4.3 Results

4.3.1 Peptide Hydrogel Properties

Previous work has established the self-assembly, cytocompatibility, and angiogenic potential of SLanc *in vitro* and *in vivo* (subcutaneously and in a rodent hind limb ischemia model) [148, 155, 156]. In this study, the efficacy of this facile strategy was critically analyzed in wound recovery subsequent to traumatic brain injury (TBI). As previously established, SLanc was synthesized via conventional Fmoc solid phase peptide synthesis and purified by dialysis and HPLC. Peptides, in aqueous buffer, undergo self-assembly into a nanofibrous hydrogel through simultaneous hydrogen

bond formation and hydrophobic packing (**Figure 4.1A**). Previous work showed that SLanc promotes wound healing [148] in *in-vitro* endothelial scratch assays. Germane to this work, cytocompatibility of SLanc with primary rat neurons showed neurite outgrowth with SLanc hydrogel, **Figure 4.1B**, prior to evaluation in the rat TBI model, **Figure 1C**.

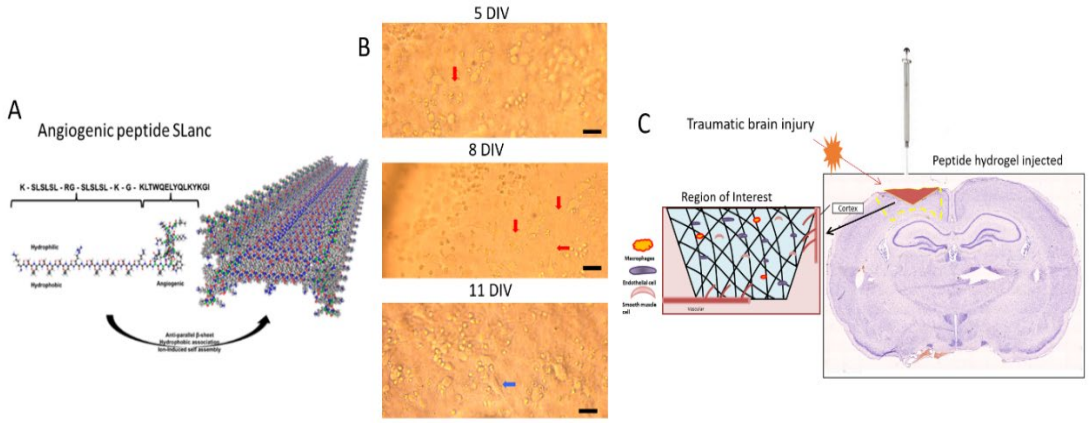

Figure 4.1 Schematic of angiogenic peptides *in vitro* and in FPI. (A) Injectable hydrogels consisting of self-assembled peptides – sequence and assembly schematic (adapted from Kumar et al [148], reprinted with permission from ACS ®). Of critical importance is cytocompatibility with primary rat cortex neuron cultures (B), arrows indicate neurons spreading out; cytocompatibility with SLanc is demonstrated over a 14 day period with primary neurons in culture that show minimal neuronal loss, with concomitant neurite growth, scale bar 30 μm. (C) Fluid percussion injury on the exposed dura resulted in tissue deformation at the impact site (Right image of Nissl stained whole brain section). Hydrogels assemble into an ECM-mimetic niche for cellular infiltration and neo-angiogenesis (Left image).

4.3.2 Sustained Angiogenic Moiety Presentation from Peptide Hydrogels Increases Blood Vessel Density in the Injured Brain

To examine the bio-distribution of the peptide hydrogel in situ at the impact site, fluorescently tagged SLanc was injected intracranially directly after FPI in the injury site. The peptide hydrogel exhibited thixotropic shear thinning and near instantaneous recovery into a hydrogel in situ after injection [148]. While the bulk of

the gel remained localized, some of the SLanc migrated to the cortex and the hippocampus (**Figure 4.2A**). After 14 days post treatment, the implanted hydrogel showed modest biodegradation, and distribution in the cortex, hippocampus, and partially in the ventricles. Post-TBI, Hematoxylin & Eosin (H&E) stained brain sections clearly showed cellular infiltration and angiogenesis (**Figure 4.2B-E**), in SLanc treated FPI brain (**Figure 4.2D**) vs. the injury-control brain (**Figure 4.2C**) and sham (**Figure 4.2B**). Vasospasm was observed in the injury control with enlarged perivascular space as shown in **Figure 4.2C** at 7 days post FPI. In the enlarged figure (**Figure 4.2E**), clear angiogenesis and increased cell infiltration were observed, indicating vascular regeneration by angiogenic SAPH.

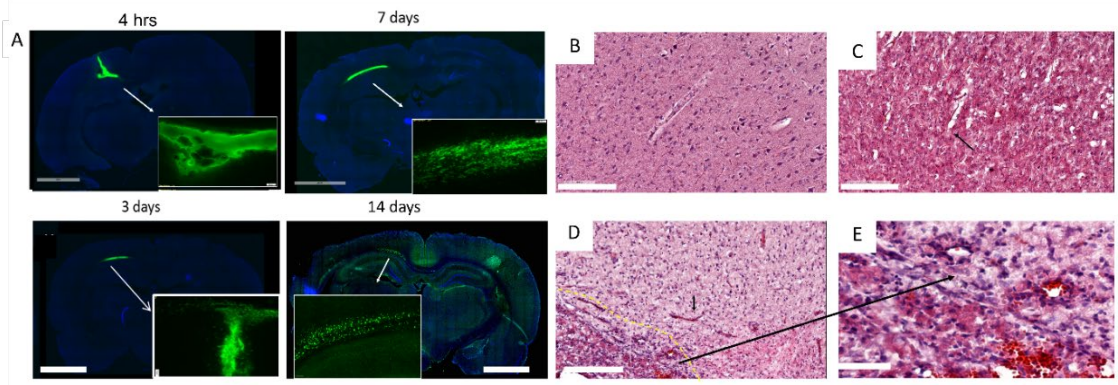

Figure 4.2 Self-assembly of peptides and promotion of angiogenesis in the brain. (A) Fluorescently tagged SLanc (1:10 ratio with untagged SLanc) showed localization and localized spreading from the injected bolus site. Representative whole brain sections from different rats at 4hrs – 14 days shows persistence of SLanc hydrogels in the brain, scale bar 3 mm. (B-E) Promotion of material driven angiogenesis in cranial tissue was first observed using H&E staining of whole rat brain sections at day7 post TBI; sham (B) or injured control (C) did not show significant angiogenesis. Black arrow in C showed vasospasm in the injured brain without treatment. Scale bar 200 µm. The SLanc treated brain (D) showed a significant increase of new blood vessels (black arrows in D). Enlarged figure (E) clearly displayed the new blood vessels structure, scale bar 50 µm.

4.3.3 Angiogenesis is Promoted by Regenerative Treatment Post Brain Injury

Mechanistic understanding of the angiogenic process was determined by VEGF-Receptor 2 immunostaining, **Figure 4.3**. SLanc treatment resulted in significantly higher VEGF-R2 expression at day 7 post injury, compared with injury control and sham brain, especially in the cortex and perivascular space, **Figure 4.3**. Previous studies have shown VEGF-R2 upregulation in the injured brain as a native response to repair the damaged vascular, as well as attempts to recapitulate this niche [150, 160-162]. But the angiogenic peptide activated significantly more VEGF-R2 to promote the angiogenesis than the native wound healing process (**Figure 4.5A**).

Critical to the formation of vasculature is their nascency/ maturity, permeability and ability to therapeutically revascularize ischemic tissue. This was observed by staining for nascent capillary based endothelial cells using von-Willebrand factor (vWF), and mature arteriole/ venules marker smooth muscle cell marker (α-smooth muscle actin), **Figure 4.4**. An increased number of endothelial cells and higher immunostaining density of α-smooth muscle actin were observed in and around SLanc hydrogel implants at the impact site after 7 days post FPI (**Figure 4.4A-B**). Western blots of vWF showed significantly higher recruitment of endothelial cells in the FPI+SLanc brain, compared with FPI without treatment and sham (**Figure 4.5B**).

To explore the regeneration mechanism with angiogenic SAPH, BrdU (Bromodeoxyuridine / 5-bromo-2'-deoxyuridine) assay was used as a nucleotide analog to identify proliferating cells. When co-localized with VEGF-R2, it confirmed that proliferating endothelial cells were attached to vasculature for neovascularization (**Figure 4.6**).

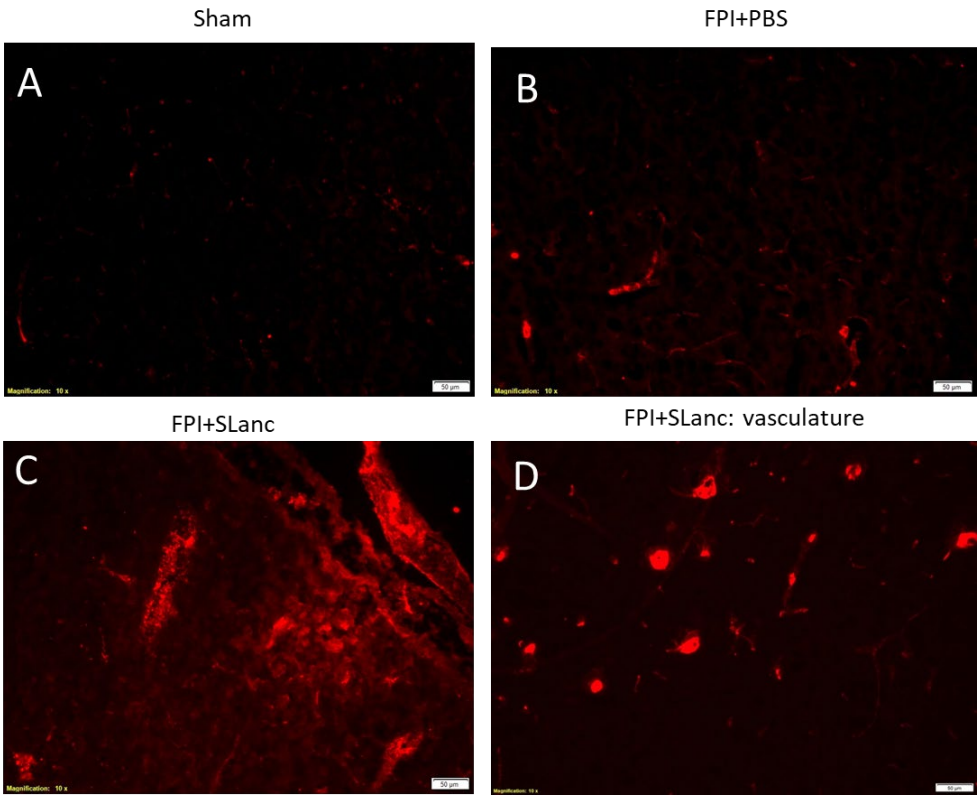

Figure 4.3 Upregulation of angiogenic receptor VEGF-R2. The canonical marker of upregulated angiogenesis was studied by VEGFR2 at 7 days after the treatment. Immunostaining of VEGF-receptor 2 shows an increase in the SLanc treated brain, at the ipsilateral site (C) and expanded to the blood brain barriers (D), compared with sham (A) and the FPI injury control (B). Scale bar is 50 μm.

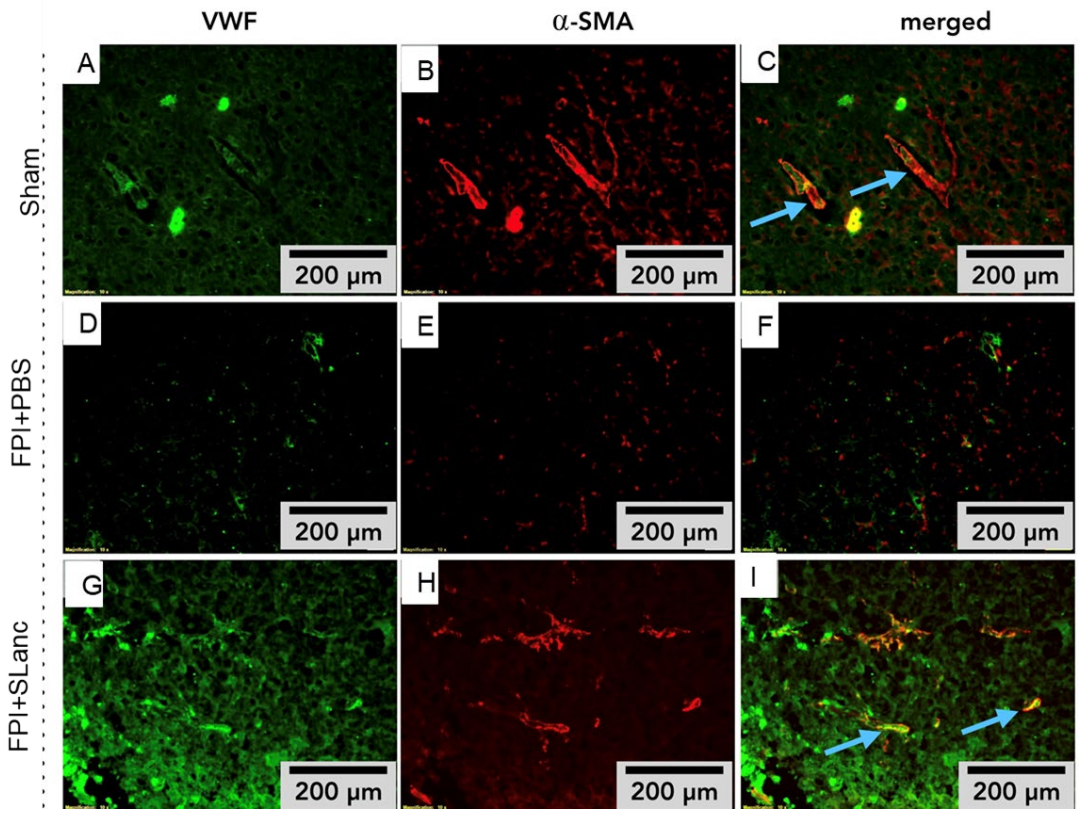

Figure 4.4 Higher expression of vascular markers in the SLanc treated injury brain. There is increased endothelial cells adhesion (vWF in green) and α-smooth muscle cells (red) in SLanc treated FPI brains (G-I), compared with sham (A-C) and FPI injury control (D-F). T=7 days post FPI, Scale bar 200 μm.

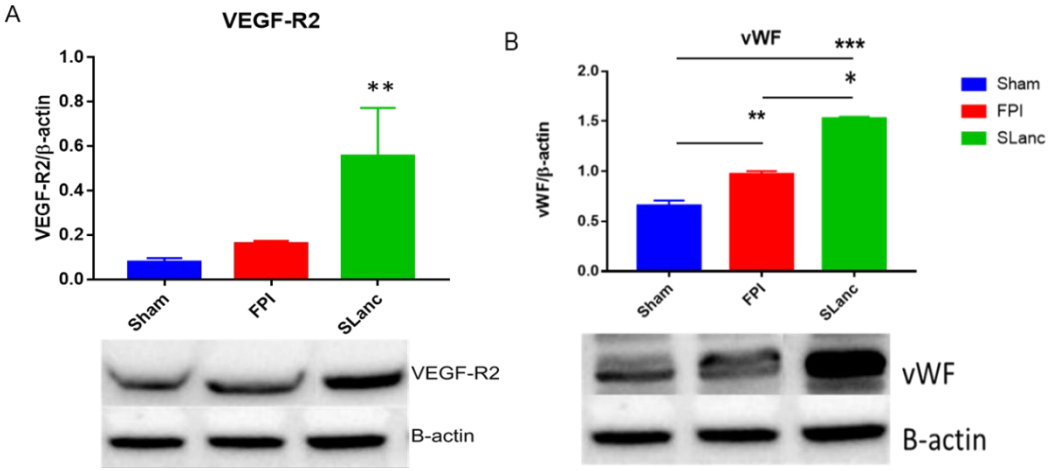

Figure 4.5 Angiogenic receptor and endothelial cell upregulation. (A) Western blot quantified VEGF-R2 expression in the ipsilateral treated brain tissue lysis, compared with FPI injured brain without treatment and sham. T=7 days post FPI, Values are mean ±SEM (n = 5), **p < 0.01. (B) Western blot shows significant increase of vWF in SLanc treated FPI brain than sham and FPI injury control, at 7 days post FPI. Values are mean ±SEM (n = 5), *p < 0.05, **p< 0.01, ***p< 0.001.

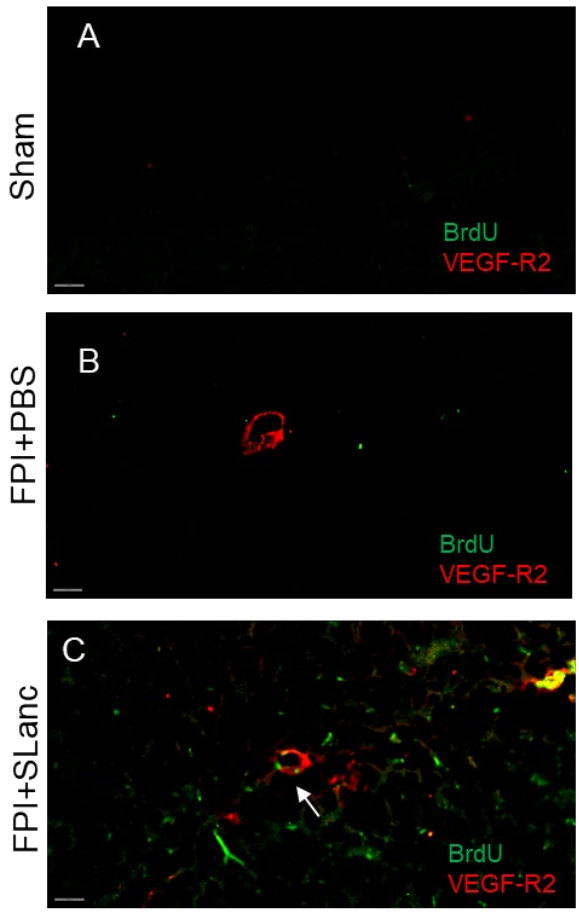

Figure 4.6 Co-localization of BrdU and VEGF-R2 immunoreactivity, in sham (A), FPI untreated brain (B), and FPI+SLanc (C) in the injury site, at 7 days post FPI. The white arrow shows proliferating endothelial cells. Scale bar is 60 μm.

4.3.4 Angiogenic Treatment Reduces Coagulation and is Potentially Neuroprotective

It was hypothesized that therapeutic angiogenesis promoted by SLanc treatment, may translate to improved neuronal survivability in the injured brain. From previous studies in Chapter 2, it was found that coagulation was significantly increased after FPI with the blood platelets marker CD42d. In **Figure 4.7**, the co-localization of the large molecular tracer FITC (in perivascular space) with tight junction protein ZO-1 showed that SLanc repaired the blood brain barrier (BBB) and recovered the distribution of tracer in the CSF pathway. Moreover, coagulation in the injured brain

was found to be significantly reduced by angiogenic peptide SLanc after 7 days post FPI, in western blot quantification (**Figure 4.7**). Immunostaining and cell counting of sections using NeuN as a neuronal marker and Myelin basic protein (MBP) as a myelin sheath marker were used for neuronal rescue examination at day 7 post injury (**Figure 4.8**). Reduced immunodensity of MBP staining and NeuN staining were observed at the impact site in the FPI untreated brain sections. Neuron cell counting showed FPI induced a significant neuronal loss in FPI untreated brain, even though SLanc increased the immunodensity of NeuN staining, it was not significantly different with FPI control by one-way ANOVA analysis. However, co-localization of MBP with F-SLanc at 14 days post treatment validated that the SLanc peptide hydrogel has the potential to benefit myelination recovery (**Figure 4.9**).

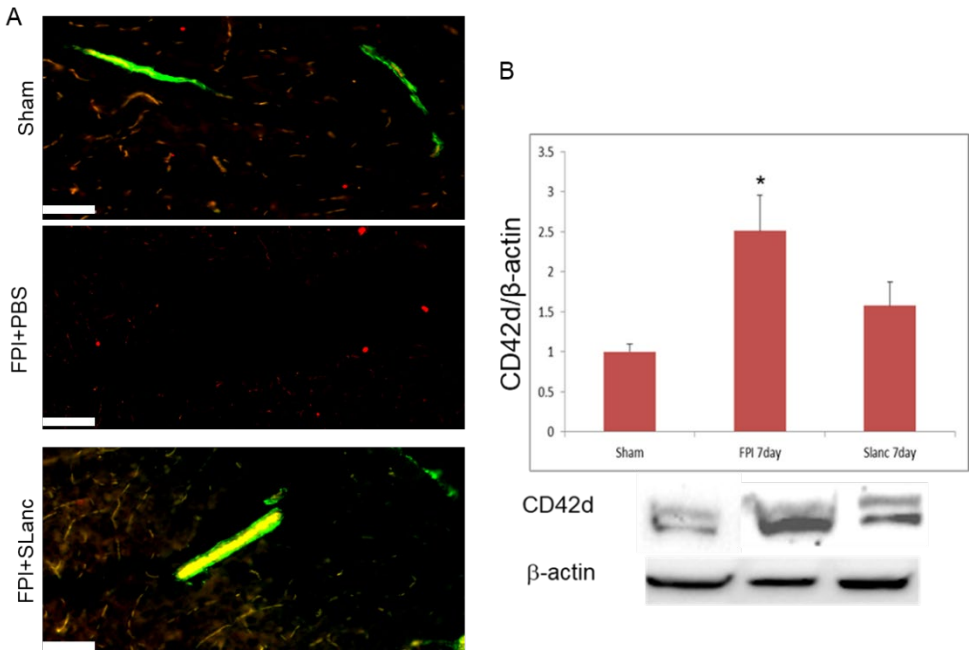

Figure 4.7 Angiogenic peptide hydrogel repairs blood brain barrier and reduces coagulation. (A) Co-localization of FITC tracer (green) with tight junction protein (ZO-1, red) in sham, FPI+PBS and FPI+SLanc brain. Scale bar is 40 μm, T= 7days post FPI. (B) Western blot quantification results show that coagulation persisted after 7 days post-FPI, with angiogenic treatment SLanc, blood platelets (CD42d) was significantly reduced.

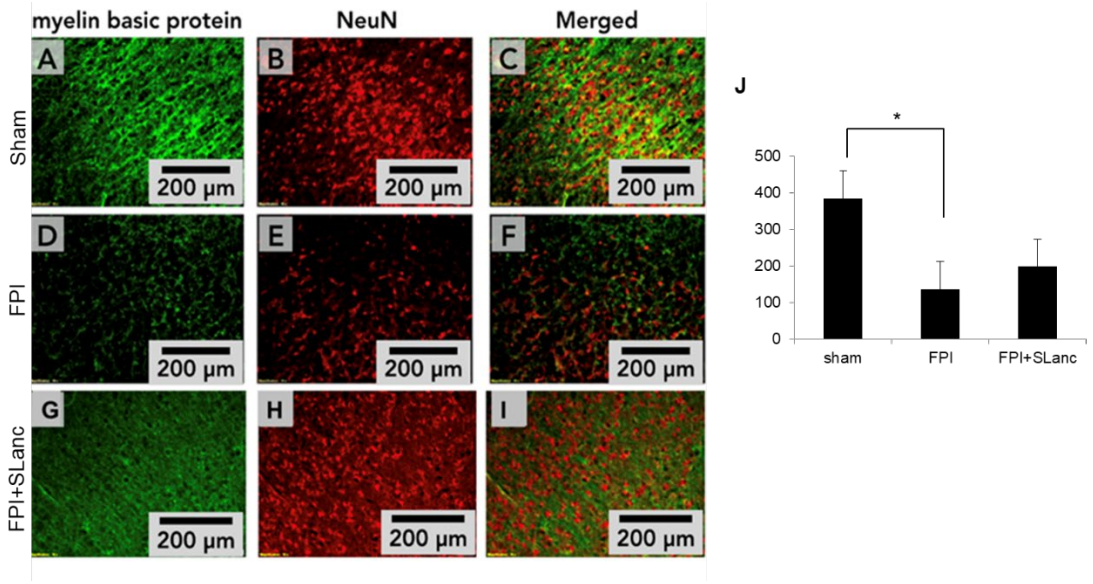

Figure 4.8 Angiogenic peptide is potentially neuroprotective. NeuN and Myelin basic protein (MBP) were used to investigate neuronal survival and axons at 7 days post FPI. Immunostaining in sham brain (A-C), FPI untreated brain (D-F) and FPI+SLanc (G-I) shows SLanc has the potential to improve neural survival. But neuron cell counting (J) shows FPI induced a significant neuronal loss in the FPI group, even though SLanc increased the neurons number, it was not significantly different with the FPI group. Values are mean ±SEM (n = 5), *p < 0.05. Scale bar 200 µm.

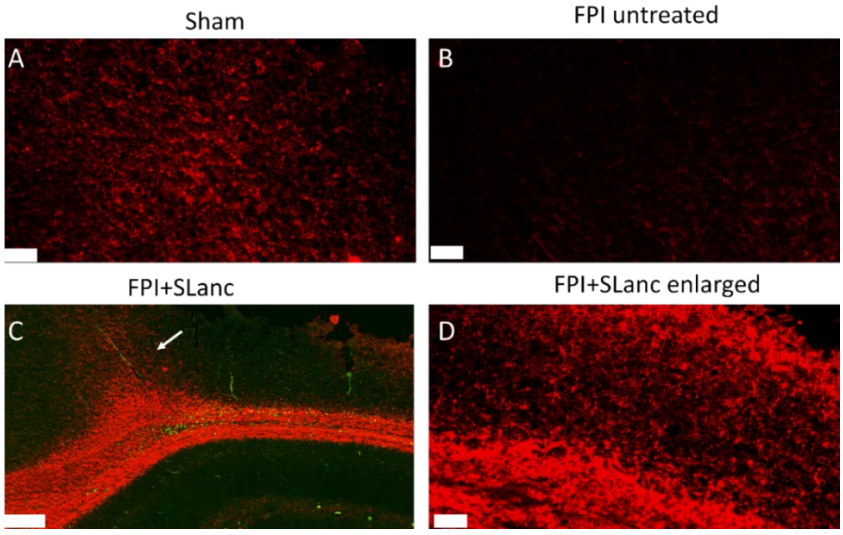

Figure 4.9 Myelin basic protein is upregulated around the angiogenic peptide post FPI. MBP staining in sham (A), FPI untreated brain (B) and co-localization of MBP with F-SLanc (C) indicate that the angiogenic peptide promotes myelin production (white arrow) in the injured brain at 14 days post FPI. (D) Enlarged image captured surrounding fluorescein-angiogenic peptide. Scale bar in A-B and D is 60 µm, in C is 200 µm.

4.5 Discussion

SAPH have been utilized in a number of preclinical applications over the past decade [153-158, 163-167]. Angiogenic SAPH has previously demonstrated angiogenic potential on human endothelial cells; promoting rapid vascularization of subcutaneous bolus implants, and rapid recovery in a hind limb ischemia model [148, 154, 155]. The injured brain presents added complexity from eNVU disruption due to both vasculature damage and neuronal loss. Further driving the urgency of therapeutic developments is the lack of successful clinical modalities [168]. An understudied aspect of TBI treatment is cerebrovascular repair and angiogenesis; critical milestones have focused on whole growth factor therapies, vasodilators, statins and promotors of red blood cell production [150, 152, 169, 170]. In the current study, a self-assembling peptide based injectable hydrogel (SLanc) was used, which contains a VEGF-165 mimic that can promote angiogenesis. VEGF-165 is a main endogenous mediator of recovery following CNS damage, with a role in neuronal protection, angiogenesis and neurogenesis [151, 171]. The hydrogel can be injected into the injury site post FPI and provide a consistent healing microenvironment for regeneration of the eNVU. Our results suggest that sustained presentation of a VEGF mimic, through the use of SAPH in a hydrogel implant can guide axonal projections and angiogenesis after injury of the native brain ECM. Histological staining and immunostaining of the endothelium and smooth muscle indicated a robust angiogenic response induced by the angiogenic SAPH in and surrounding the hydrogel implant. Further, the initiation of angiogenesis was found to be the activation and upregulation of VEGF-receptor 2 in the treated ipsilateral

brain tissue. This was observed concomitant to a significant increase of endothelial cells and smooth muscle cells. It has been established that the activation of VEGF-R2 drives the neuroprotective actions according to the direct activation of neuronal intracellular signaling pathway P13-K/Akt, as well as MARK ERK kinase/extracellular signal-regulated kinase pathway [171]. Moreover, in an ischemia animal model, overexpression of VEGF was shown to reduce infarct volume by promoting neurogenesis and neuromigration [149].

Axonal injury was commonly reported in clinical TBI reports and experimental models [96]. It was demonstrated that targeting angiogenesis can also induce neurogenesis and thus improve cognitive impairment [152, 161, 170]. As angiogenesis was activated by SLanc SAPH at 7 days post injury and treatment, the neuronal survivability and myelination recovery were further examined at day 7 and day 14 post injury & treatment, respectively. Even though the number of neurons was not significantly increased comparing with FPI brain at 7 days with SLanc treatment, the integrity of myelination was found to be reversed surrounding the angiogenic SAPH, indicating a potential neuroprotective efficacy by SLanc in long-term.

CHAPTER 5

CONCLUSIONS AND FUTURE DIRECTIONS

The objective of this dissertation was to understand the layer-structured events in blunt TBI, and to find a therapeutic target for the potential treatment, through a moderate FPI rat model. To achieve this goal, this study was separated into three specific aims.

Aim 1 was to examine the primary event of vascular damage directly from the mechanical insult in TBI, followed by hemorrhage, coagulation and necrotic cell death as the acute sequela. The large molecule tracer (FITC) in the CSF pathway, and small molecule tracer (Texas red) in the blood circulation were used to indicate cerebral vascular disruption. The CSF pathway blockage shown by FITC tracer revealed the pattern of coagulation in the subarachnoid and along the perivascular space at the injury site. The blockage was correlated well with the expression of coagulation factor XII, thrombin and blood platelets, indicating the pattern of hemorrhage and coagulation after physical disruption of the cerebro-vasculature. Furthermore, necrotic cell death and onsite immune cell accumulation were observed in the short-term in and around the hemorrhagic area, leading to neurodegeneration and neuroinflammation in the acute phase.

Even though Aim 1 revealed the layer-structured events post-FPI, further studies are still needed to build a connection between thrombosis and necrotic cell death pathways. Here, it was attempted to show thrombotic necrosis according to pathology in H&E staining, as there is no biomarker to indicate this specific necrosis

so far [172]. However, a better methodology is needed to demonstrate thrombotic necrosis. For example, a laser-induced hemorrhage model would simplify the injury into the specific vascular damage related events. Another limitation in Aim 1 is lacking the further study of the necrosis pathway, which will be improved by examining other necrosis markers, including RIPK3 and MLKL.

In Aim 2, secondary events following vascular disruption were investigated for prolonged neuroinflammation and neurodegeneration in longer term. Two pathways were evaluated following tissue deformation and vascular damage: 1) Free radical generation and oxidative/nitrosative damage in blood brain barrier, 2) immune cells aggregation and gliosis. According to the results, persistent immune cells aggregation and BBB disruption was found after 7 days post-FPI, as well as gliosis, tau hyperphosphorylation and apoptosis.

Further investigation is needed for Aim 2, to investigate which apoptosis pathway is involved following neuroinflammation. Co-localization of current marker Caspase 3 with Caspase9/8 would help to understand whether it is the intrinsic or extrinsic pathway. And better quantification methods are necessary to further demonstrate the origin cell types that express ROS/RNS after TBI, at different injury severity levels. Cell counting according to the co-localized ROS/RNS with different cell type markers will be the potential method for this purpose.

For Aim 3, an angiogenic SAPH was investigated in the injured brain tissue. The injectable self-assembling peptide hydrogel (SAPH) with vascular endothelial growth factor mimic (VEGF-165 mimic) delivers the persistent angiogenic signal to the injury site, while providing a matrix for tissue infiltration and regeneration.

Angiogenesis was further validated by immunohistochemistry and biomarkers for vasculature and the VEGF-receptor 2. Angiogenic SAPH was shown to activate angiogenesis by inducing proliferating endothelial cells and upregulation of VEGF-R2. However, the neuronal cell counting in the injured cortex did not show a significant difference at 7 days post treatment, compared with the FPI injured brain. But the myelin basic protein staining at day 14 indicated a myelination recovery in and around the angiogenic SAPH, suggesting that repair of the neurovascular unit might be beneficial for neuroprotection.

The study in Aim3 examined the efficacy of angiogenic SAPH at the injury site, targeting cerebral vascular repair and neuroprotection potential in a moderate FPI model to mimic blunt TBI. However, longer-term studies that track neuronal protection, functional recovery and behavioral outcomes are needed for the further step in preclinical and translational medicine research.

APPENDIX A

REAGENTS RECIPES

This appendix includes all the recipes for the reagents used in this dissertation. These reagents were stored at 4 °C refrigerator.

Artificial Cerebrospinal Fluid:

For 1L volume flask:

Reagent	Amount to add	Final concentration in 10× ACSF	Final concentration in 1× ACSF
NaCl	73.05 g	1.25 M	125 mM
NaHCO3	21.843 g	260 mM	26 mM
NaH2PO3	1.725 g	12.5 mM	1.25 mM
KCl	1.864 g	25 mM	2.5 mM
$MgCl_2$	5 mL of a 2M $MgCl_2$ stock	10 mM	1 mM

Standard 1 mM H_2O_2 Solution:

Acetanilide (Sigma-Aldrich 397237)	67.5 mg
DI water	250 ml
2-4% H_2O_2 (Sigma-Aldrich 323381)	231 µl

100 µM Standard SNAP Solution:

This reagent was stored in amber bottle in dark.

EDTA	5.0 mg

MilliQ water	250 ml
Crystalline SNAP	5.6 mg

APPENDIX B

SELF-ASSEMLING PEPTIDE HYDROGELS FOR NEUROPROTECTION IN TRAUMATIC BRAIN INJURY

In Appendix B, the self-assembling peptide hydrogel with neurogenic growth factor will be injected in the injured brain to investigate neuroprotective treatment.

B.1 Introduction

Traumatic brain injuries (TBI) cause neuronal death and glial scarring, which may lead to cognitive deficits years or even decades later. The surge of extracellular glutamate level after TBI has been linked to increased neuronal death [173, 174]. The neurons in the brain are post-mitotic and have muted intrinsic regenerative potential. Unlike those in the peripheral nervous system, neurons in the central nervous system (CNS) cannot regenerate axons following axonal tear [175], which often results from the mechanical impact of TBI [176].

In the absence of a strong physiological regenerative response, therapies that promote the survival of existing neuronal networks could be useful in managing the impact of TBI, especially in the acute phase (1–7 days). Neurotrophic factors such as nerve growth factor (NGF) and brain-derived neurotrophic factor (BDNF) can aid in the neuronal survival in vivo. Peptide-based hydrogels have been used to deliver loaded neurotrophic growth factors for a sustained period [177] and aid axonal regeneration in the CNS [178]. One pronounced disadvantage of such drug delivery strategies is that the neurotrophic factors can diffuse away from the delivery site, leading to time-dependent attenuation of activity. This problem can be sidestepped by encoding the bioactive neuroprotective epitopes directly onto the sequence of the

therapeutic peptides that self-assemble into nanofibrous hydrogels [148, 155]. This strategy enables sustained epitope presentation, while maintaining the favorable material properties of the implanted matrix. Thus, if we conjugate a domain to a self-assembling peptide that activates intracellular neurotrophic pathways similar to NGF and BDNF, the resulting biomaterial could have beneficial neuroprotective effects. Self-assembling peptides based on β-sheet motif can form high-aspect-ratio nanofibers, resulting in ECM-mimetic thixotropic hydrogels [154]. These scaffolds have been evaluated for drug delivery, wound healing, and modulation of angiogenesis, dentinogenesis, and inflammation [154, 165, 179]. We designed a neuroprotective peptide SLen containing a central β-sheet-forming peptide backbone [131] [148], attached to a neuroprotective peptide domain KKDGDGDFAIDAPE (referred to as CMX-9236). CMX-9236 is a 14 amino acid portion of ependymin, a neuroprotective extracellular glycoprotein [180]. CMX-9236 promotes neuronal survival in ischemic rat models [180], by activating the transcription factor AP-1 (a heterodimer of leucine zipper proteins Fos and Jun), which regulates CREB (cAMP response element-binding protein) and promotes synaptic plasticity and neurite growth [181, 182]. Neurotrophic factors exert their neuroprotective effect and modulate synaptic functions, in part, by activating AP-1 [183]. In vitro, CMX-9236 blocks excitotoxic effects of glutamate in primary rat cortical neuron cultures [180]. However the small peptides such as CMX-9236 are not suitable for persistent effect in vivo as they are prone to rapid clearance [184]. Attaching the peptide moiety to a self-assembling domain ensures that the peptide is physically retained (as a hydrogel) in the injury site days after implantation. As the neuroprotective moiety is negatively

charged, we designed the self-assembling domain to be negatively charged as well (glutamate residues are negatively charged at neutral pH), resulting in a net negative charge (–5) for the entire self-assembling peptide (SL)6-E-G-KKDGDGDFAIDAPE in physiological conditions. The net charge on SLen confers flexibility in the storage and formulation of the peptide. The peptide is soluble in low ionic strength conditions, as the net charge of the building blocks prevent self-assembly into nanofibers, due to electrostatic repulsion among the building blocks. In presence of multivalent positively charged ions (such as Ca+2), due to shielding of like-charge repulsion among the building blocks [185], SLen self-assembled into β-sheet nanofibers, which form a thixotropic hydrogel.

B.2 Materials and Methods

B.2.1 Synthesis and Characterization of Peptides

SLen was synthesized by standard Fmoc solid-phase peptide synthesis protocol and purified by high-performance liquid chromatography and dialysis. The dialyzed peptide was lyophilized and stored in the powder form at –80°C until formulation. The peptide hydrogel was formulated as: 20 mg/mL SLen (6.6 mM); 16.5 mM $CaCl_2$; 298 mM sucrose; pH 7.

B.2.2 Effects of SLen on Glutamate-mediated Excitotoxicity *in vitro*

Cortices were extracted from the embryos of a Sprague Dawley timed pregnant rat (Charles River) at Day 16 gestational period. Cortices were digested in trypsin-EDTA (0.25%) at 37°C for 30 min and agitated with a pipette to release cells, then

strained with 70 µm and 40 µm pore filters to separate out primary cortical neurons. Neurons were counted and seeded at a density of 50,000 cells/cm^2 on coverslips (diameter: 12 mm) coated with 10 µg/mL poly-D-lysine and supplemented with neurobasal medium with 2% Gibco B27 AO+ neuronal culture system (50X), 1% penicillin-streptomycin, and 0.2% glutamate. Neurons were cultured in the neurobasal media for 12 days with media changes every 2 days. At Day 12, neurons exhibited neurite branching (**Figure B.1C**). Neurons were then incubated with 100 µM L-glutamic acid for 24 h to induce excitotoxicity. Previous work demonstrated a range of concentrations and incubation times for L-glutamic acid to induce excitotoxicity [186, 187]. After performing a dose response assessment, we found that 100 µM L-glutamate with 24 h incubation caused severance of synapses and fragmentation of neurites.

Our preliminary data indicated that SLen exerts observable effects specifically on neurite integrity and growth. After performing a dose response assessment, we found that 0.005 mM concentration of SLen did not have any protective effects on the injured neurons and 0.5 mM concentration caused neurons to aggregate into large neuro-spheres, but 0.05 mM SLen exhibited beneficial effects. After removal of the L-glutamic acid, neurobasal media supplemented with 0.05 mM SLen was added and media was changed every day for 3 days. At Day 16, the Live/Dead cell viability kit (Invitrogen) was used to evaluate the neuronal survival. Four images were taken per hydrogel (n= 4 wells per condition, and in vitro assay was repeated 4 times of neurons isolation.), and the number of live and dead cells was counted per image.

B.2.3 Fluid Percussion Injury (FPI)

This step is described in Chapter 2.2 Methods. For a moderate injury (1.8–2.0 atm.), the recorded apnea and righting reflex time were 15–20 s and 8–10 min, respectively.

B.2.4 Therapeutic Intervention

After FPI and anesthesia, the rats were placed in a stereotaxic frame to be treated with 5 μL **SLen** hydrogel. The location of injection according to the stereotaxic coordinates were: AP=−3, L=−2.5 from Bregma, dorsoventral (DV) = 0.5 mm. Then the injury hub was removed, and the head sutured. The rats were returned to a heating pad until they were ambulatory and subsequently they were returned to their home cage.

B.2.5 Tissue Processing

7 days after FPI, the rats were deeply anesthetized and euthanized via slow trans-cardial perfusion with ice cold phosphate buffered saline (PBS), followed by ice cold 4% paraformaldehyde in PBS. Brain areas involved in the traumatic foci were recut from the whole brain and immersed in 4% paraformaldehyde overnight, followed by cryoprotection in 30% sucrose containing PBS. Coronal sections of 20 μm thickness were sectioned from each sample and stored at −80°C for further analysis.

B.2.6 Immunofluorescence and Microscopy

Both the in vitro and in vivo constructs were analyzed through immunofluorescence. Coverslips with cells were fixed in 4% paraformaldehyde for 15 min at room

temperature, followed by washing with 0.1% Triton X-100 in PBS for 5 mins at room temperature. Brain tissue sections (20 μm thick) containing the external and internal microvessels were washed with PBS and fixed in acetone-methanol (1:1 volumetric ratio) for 10 minutes at –20°C for immunofluorescence staining. Fixed slides were then blocked with 3% bovine serum albumin at 25°C for 1 h in the presence of 0.1% Triton X- 100. Slides were then incubated with the following primary antibodies: rabbit anti-vWF (vWF: von Willebrand factor), anti-NeuN, anti-Myelin Basic protein, mouse anti-alpha smooth muscle actin, anti-neurofilament, anti-s100 overnight at 4°C for probing the respective antigens. Sample slides were washed with PBS and then incubated with Alexa Fluor 488 or Alexa Fluor 594 conjugated with anti-mouse or anti-goat or anti-rabbit or anti-sheep immunoglobulin-G (IgG) for 1 h. After washing with PBS, sample slides were mounted on immunomount containing DAPI (Thermo-Fisher). Fluorescence micro-photographs were captured by fluorescent microscopy (Eclipse TE2000-U, Nikon microscope, Melville, NY) using NIS elements (Nikon, Melville, NY) software.

B.2.7 Evaluation Methodology and Statistical Analyses

All results are expressed as the mean ± standard error of mean. Statistical analysis of the data was performed using SPSS 24 (IBM). Percentage of live cells differed significantly among conditions (one-way ANOVA, $F(3,8) = 69.47$, $\eta 2 = 0.96$, $p < 0.001$). *Post hoc* independent samples were tested with Student's t test, with Bonferroni correction (α adjusted to 0.013). Positive NeuN count differed significantly among conditions (Kruskal-Wallis chi-squared = 27.42, df = 3, $p <$

0.001). *Post hoc* two-sample Wilcoxon tests, with Bonferroni correction were carried out (α adjusted to 0.013).

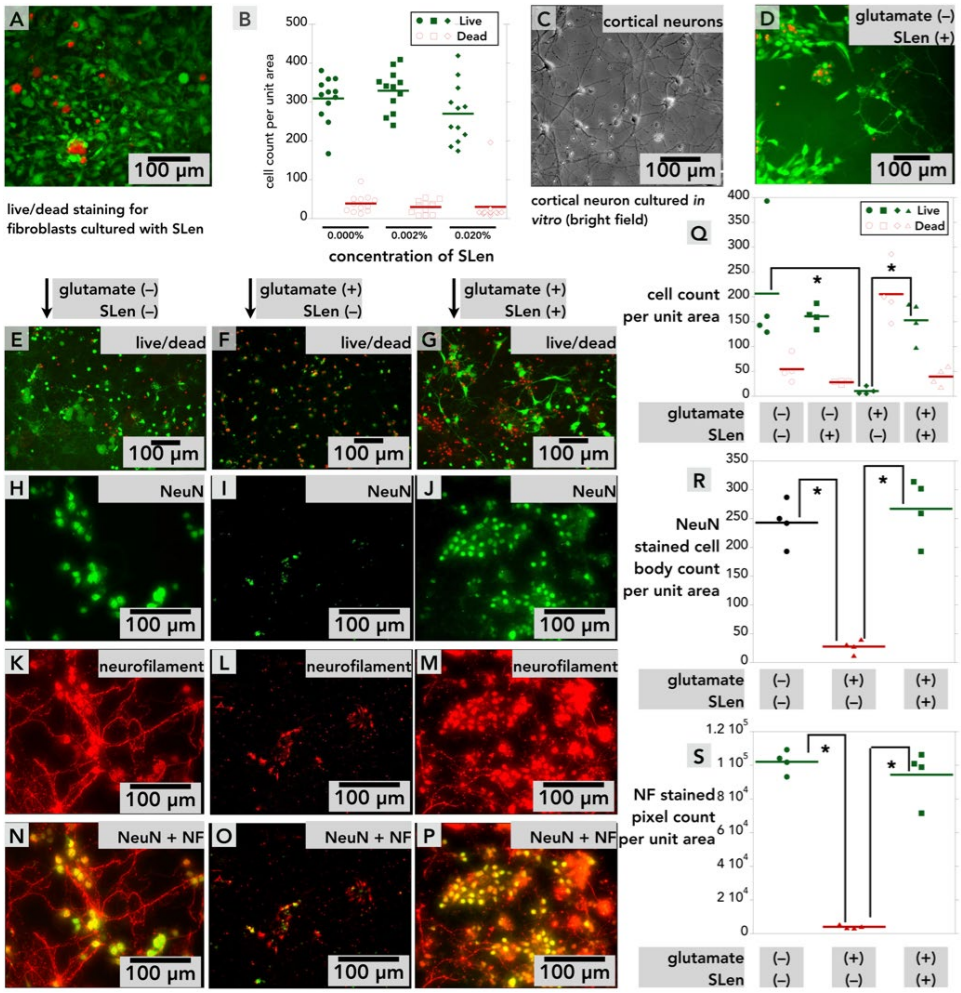

Figure B.1 In vitro assays for cytocompatibility and neuroprotective properties of SLen. (A) Live/dead staining for cytocompatibility of SLen in fibroblasts, and, (B) quantification of live versus dead cells at different concentration of SLen. (C) Bright-field image of primary cortical neurons cultured in vitro, (D) live/dead staining for cortical neurons cultured with SLen. (E–G) Live/dead staining indicate SLen is neuroprotective against L-glutamate-mediated excitotoxicity in the in vitro model of primary cortical neurons. Representative immunostaining of (H–J) the neuronal marker NeuN (green), and (K–M) the neurofilament protein (red); (N–P) merged images of NeuN and neurofilament staining. (Q) Quantification of live/dead staining in control neurons, control neurons + SLen, L-glutamate exposed neurons, and L-glutamate acid exposed neurons + SLen (representative images in panel E, F, and G). (R) Cell counting of positive NeuN staining, and (S) quantification of Neurofilament staining fluorescence intensity show a significant difference between L-glutamate exposed neurons with and without SLen. Data were analyzed using one-way ANOVA post-hoc independent-samples t-tests with Bonferroni correction (N=6). Scale bar: 100 µm. (*$p < 0.05$). We can put arrows to highlight the effect on neurite growth.

B.3 Results

B.3.1 Cytocompatibility and Neuroprotection in-vitro

SLen's potential cytotoxicity was evaluated dose-dependently in NIH 3T3 fibroblasts (**Figure B.1A–B**), by Live/dead staining. Then the effect of the peptide on primary cortical neurons was examined by an excitotoxicity assay (**Figure B.1C**). Firstly, by live/dead staining, SLen was shown to be neuro-compatible in vitro (**Figure B.1D, Q**). Predictably, excitotoxic insult by L-glutamate leads to death of most of the neurons. However, the presence of 0.05 mM SLen in culture exerted a neuroprotective effect even in the presence of a toxic amount of extracellular glutamate (**Figure B.1G**). To further reveal the underling neuroprotective mechanism of SLen, we examined neuronal cell bodies (NeuN) and the axonal projections (neurofilament) by immunostaining after excitotoxicity assay (**Figure B.1E–P**). Excitotoxic glutamate damage led to a significant loss of neuronal cell bodies (**Figure B.1R**) and disrupted neuronal branches, both of which can be prevented in the presence of SLen (**Figure B.1R–S**). The in vitro assays suggested that SLen has a protective effect on neuronal bodies and branches against glutamate-mediated excitotoxicity. The safety assessment and excitotoxicity methodology in-vitro indicated the cytocompatibility of SLen and unraveled the neuroprotective mechanism of SLen. Based on the results in-vitro, the in-vivo SLen efficacy was further evaluated, to circumvent these issues.

B.3.2 Effect of the Peptide Hydrogel on Injured Brain Microenvironment

Fluid percussion injury (FPI) is an established TBI model that mimics human concussion in real scenarios [25]. It's a mixed injury model which produces focal damage including perisomatic axotomy and vascular disruption, as well as diffuse injury of axonal damage, leading to impaired axonal transport and neuronal atrophy [25]. In this study, a moderate level of FPI led to a drastic loss in the number of neuronal cells (NeuN and myelin basic protein staining) at day 7 after the injury (**Figure B.2**). Significant decrease of neurons in the cortex was detected by counting cell bodies stained by NeuN. Some of the neuronal loss can be prevented with the peptide hydrogel SLen injection into the injury site after FPI. As an indication of white matter/axonal damage, staining of the myelin basic protein (MBP) following TBI revealed that TBI results in a high degree of disorganization of myelin in the rat cortex compared to sham. SLen injection following TBI attenuated the disruption of myelin organization. The signal embedded in the sequence of the peptides cannot diffuse away rapidly after implantation, since the epitopes are immobilized covalently in the hydrogels.

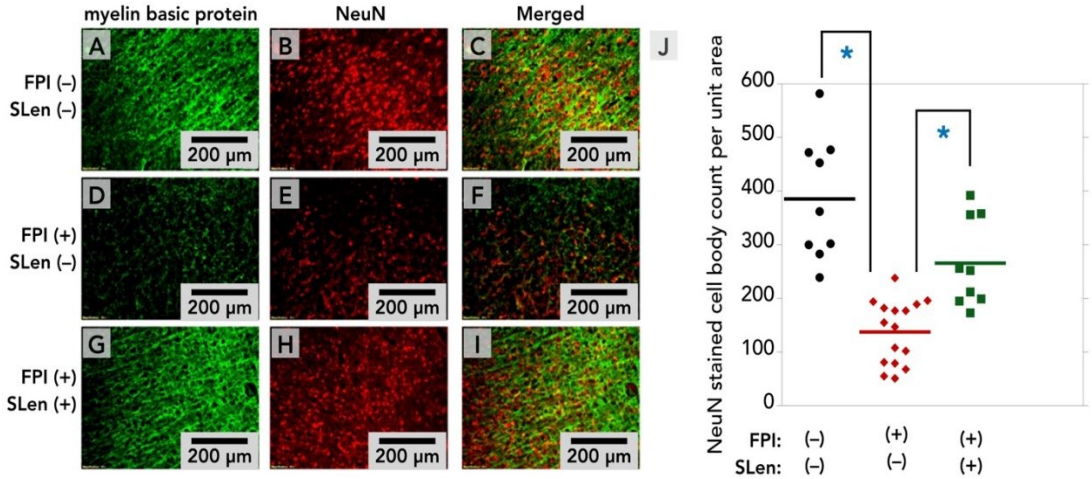

Figure B.2 *In vivo* response to SLen. Representative images of brain sections immunostained for Myelin basic protein (A, D, G), NeuN (B, E, H) and merged images (C, F, I) in Sham, FPI, and FPI treated with SLen, (J) Neuronal cell counting in cortex for NeuN staining in sham, FPI, FPI+ SLen. N=12 (twelve animals for each condition). Scale bar: 200 µm. *$p < 0.05$.

REFERENCES

1. Thurman, D.J., et al., *Traumatic Brain Injury in the United States: A Public Health Perspective.* The Journal of head trauma rehabilitation, 1999. **14**(6): p. 602-15.

2. Faul, M. and V. Coronado, *Epidemiology of Traumatic Brain Injury.* Handbook of clinical neurology, 2015. **127**: p. 3-13.

3. Taylor, C.A., et al., *Traumatic Brain Injury-Related Emergency Department Visits, Hospitalizations, and Deaths - United States, 2007 and 2013.* MMWR Surveill Summ, 2017. **66**(9): p. 1-16.

4. Dewan, M.C., et al., *Estimating the Global Incidence of Traumatic Brain Injury.* Journal of neurosurgery, 2018: p. 1-18.

5. Arciniegas, D.B., K. Held, and P. Wagner, *Cognitive Impairment Following Traumatic Brain Injury.* Current treatment options in neurology, 2002. **4**(1): p. 43-57.

6. Barman, A., A. Chatterjee, and R. Bhide, *Cognitive Impairment and Rehabilitation Strategies after Traumatic Brain Injury.* Indian journal of psychological medicine, 2016. **38**(3): p. 172-81.

7. Chen, Y. and W. Huang, *Non-Impact, Blast-Induced Mild Tbi and Ptsd: Concepts and Caveats.* Brain injury, 2011. **25**(7-8): p. 641-50.

8. Bryant, R., *Post-Traumatic Stress Disorder Vs Traumatic Brain Injury.* Dialogues in clinical neuroscience, 2011. **13**(3): p. 251-62.

9. Prasad, K.N. and S.C. Bondy, *Common Biochemical Defects Linkage between Post-Traumatic Stress Disorders, Mild Traumatic Brain Injury (Tbi) and Penetrating Tbi.* Brain research, 2015. **1599**: p. 103-14.

10. Johnson, V.E., W. Stewart, and D.H. Smith, *Widespread Tau and Amyloid-Beta Pathology Many Years after a Single Traumatic Brain Injury in Humans.* Brain pathology (Zurich, Switzerland), 2012. **22**(2): p. 142-9.

11. Hay, J., et al., *Chronic Traumatic Encephalopathy: The Neuropathological Legacy of Traumatic Brain Injury.* Annual review of pathology, 2016. **11**: p. 21-45.

12. Stern, R.A., et al., *Long-Term Consequences of Repetitive Brain Trauma: Chronic Traumatic Encephalopathy.* PM & R : the journal of injury, function, and rehabilitation, 2011. **3**(10 Suppl 2): p. S460-7.

13. DeGrauw, X., et al., *Epidemiology of Traumatic Brain Injury-Associated Epilepsy and Early Use of Anti-Epilepsy Drugs: An Analysis of Insurance Claims Data, 2004-2014.* Epilepsy research, 2018. **146**: p. 41-49.

14. Semple, B.D., et al., *Affective, Neurocognitive and Psychosocial Disorders Associated with Traumatic Brain Injury and Post-Traumatic Epilepsy.* Neurobiology of disease, 2018.

15. Fleminger, S., et al., *Head Injury as a Risk Factor for Alzheimer's Disease: The Evidence 10 Years on; a Partial Replication.* Journal of neurology, neurosurgery, and psychiatry, 2003. **74**(7): p. 857-62.

16. Salib, E. and V. Hillier, *Head Injury and the Risk of Alzheimer's Disease: A Case Control Study.* International journal of geriatric psychiatry, 1997. **12**(3): p. 363-8.

17. Guo, Z., et al., *Head Injury and the Risk of Ad in the Mirage Study.* Neurology, 2000. **54**(6): p. 1316-23.

18. Blyth, B.J. and J.J. Bazarian, *Traumatic Alterations in Consciousness: Traumatic Brain Injury.* Emergency medicine clinics of North America, 2010. **28**(3): p. 571-94.

19. Gaetz, M., *The Neurophysiology of Brain Injury.* Clinical neurophysiology : official journal of the International Federation of Clinical Neurophysiology, 2004. **115**(1): p. 4-18.

20. Bramlett, H.M. and W.D. Dietrich, *Progressive Damage after Brain and Spinal Cord Injury: Pathomechanisms and Treatment Strategies.* Progress in brain research, 2007. **161**: p. 125-41.

21. Narayan, R.K., et al., *Clinical Trials in Head Injury.* Journal of neurotrauma, 2002. **19**(5): p. 503-57.

22. Menon, D.K., *Unique Challenges in Clinical Trials in Traumatic Brain Injury.* Critical care medicine, 2009. **37**(1 Suppl): p. S129-35.

23. Morales, D.M., et al., *Experimental Models of Traumatic Brain Injury: Do We Really Need to Build a Better Mousetrap?* Neuroscience, 2005. **136**(4): p. 971-89.

24. Briones, T.L., *Chapter 3 Animal Models of Traumatic Brain Injury: Is There an Optimal Model That Parallels Human Brain Injury?* Annual review of nursing research, 2015. **33**: p. 31-73.

25. Ma, X., et al., *Animal Models of Traumatic Brain Injury and Assessment of Injury Severity.* Molecular neurobiology, 2019.

26. Maas, A.I. and H.F. Lingsma, *New Approaches to Increase Statistical Power in Tbi Trials: Insights from the Impact Study.* Acta neurochirurgica. Supplement, 2008. **101**: p. 119-24.

27. Lu, J., et al., *A Method for Reducing Misclassification in the Extended Glasgow Outcome Score.* Journal of neurotrauma, 2010. **27**(5): p. 843-52.

28. Gennarelli, T.A., *Animate Models of Human Head Injury.* Journal of neurotrauma, 1994. **11**(4): p. 357-68.

29. Thompson, H.J., et al., *Lateral Fluid Percussion Brain Injury: A 15-Year Review and Evaluation.* Journal of neurotrauma, 2005. **22**(1): p. 42-75.

30. Ziebell, J.M., et al., *Experimental Diffuse Brain Injury Results in Regional Alteration of Gross Vascular Morphology Independent of Neuropathology.* Brain injury, 2016. **30**(2): p. 217-24.

31. Cernak, I., *Animal Models of Head Trauma.* NeuroRx : the journal of the American Society for Experimental NeuroTherapeutics, 2005. **2**(3): p. 410-22.

32. McIntosh, T.K., et al., *Traumatic Brain Injury in the Rat: Characterization of a Lateral Fluid-Percussion Model.* Neuroscience, 1989. **28**(1): p. 233-44.

33. Floyd, C.L., et al., *Craniectomy Position Affects Morris Water Maze Performance and Hippocampal Cell Loss after Parasagittal Fluid Percussion.* Journal of neurotrauma, 2002. **19**(3): p. 303-16.

34. Sanders, M.J., W.D. Dietrich, and E.J. Green, *Cognitive Function Following Traumatic Brain Injury: Effects of Injury Severity and Recovery Period in a Parasagittal Fluid-Percussive Injury Model.* Journal of neurotrauma, 1999. **16**(10): p. 915-25.

35. O'Connor, W.T., A. Smyth, and M.D. Gilchrist, *Animal Models of Traumatic Brain Injury: A Critical Evaluation.* Pharmacol Ther, 2011. **130**(2): p. 106-13.

36. Alder, J., et al., *Lateral Fluid Percussion: Model of Traumatic Brain Injury in Mice.* Journal of visualized experiments : JoVE, 2011(54).

37. Hicks, R., et al., *Temporal and Spatial Characterization of Neuronal Injury Following Lateral Fluid-Percussion Brain Injury in the Rat.* Acta neuropathologica, 1996. **91**(3): p. 236-46.

38. Bramlett, H.M. and W.D. Dietrich, *Quantitative Structural Changes in White and Gray Matter 1 Year Following Traumatic Brain Injury in Rats.* Acta neuropathologica, 2002. **103**(6): p. 607-14.

39. Liu, Y.R., et al., *Progressive Metabolic and Structural Cerebral Perturbations after Traumatic Brain Injury: An in Vivo Imaging Study in the Rat.* Journal of nuclear medicine : official publication, Society of Nuclear Medicine, 2010. **51**(11): p. 1788-95.

40. Hamm, R.J., *Neurobehavioral Assessment of Outcome Following Traumatic Brain Injury in Rats: An Evaluation of Selected Measures.* Journal of neurotrauma, 2001. **18**(11): p. 1207-16.

41. Pierce, J.E., et al., *Enduring Cognitive, Neurobehavioral and Histopathological Changes Persist for up to One Year Following Severe Experimental Brain Injury in Rats.* Neuroscience, 1998. **87**(2): p. 359-69.

42. Wahab, R.A., et al., *Fluid Percussion Injury Device for the Precise Control of Injury Parameters.* J Neurosci Methods, 2015. **248**: p. 16-26.

43. Kabadi, S.V., et al., *Fluid-Percussion-Induced Traumatic Brain Injury Model in Rats.* Nat Protoc, 2010. **5**(9): p. 1552-63.

44. Prins, M.L., et al., *Fluid Percussion Brain Injury in the Developing and Adult Rat: A Comparative Study of Mortality, Morphology, Intracranial Pressure and Mean Arterial Blood Pressure.* Brain research. Developmental brain research, 1996. **95**(2): p. 272-82.

45. Eakin, K., R.K. Rowe, and J. Lifshitz, *Modeling Fluid Percussion Injury: Relevance to Human Traumatic Brain Injury*, in *Brain Neurotrauma: Molecular, Neuropsychological, and Rehabilitation Aspects*, F.H. Kobeissy, Editor. 2015: Boca Raton (FL).

46. Bhowmick, S., V. D'Mello, and P.M. Abdul-Muneer, *Synergistic Inhibition of Erk1/2 and Jnk, Not P38, Phosphorylation Ameliorates Neuronal Damages after Traumatic Brain Injury.* Molecular neurobiology, 2018.

47. Shultz, S.R., et al., *A Single Mild Fluid Percussion Injury Induces Short-Term Behavioral and Neuropathological Changes in the Long-Evans Rat: Support for an Animal Model of Concussion.* Behavioural brain research, 2011. **224**(2): p. 326-35.

48. Griesbach, G.S., D.A. Hovda, and F. Gomez-Pinilla, *Exercise-Induced Improvement in Cognitive Performance after Traumatic Brain Injury in Rats Is Dependent on Bdnf Activation.* Brain research, 2009. **1288**: p. 105-15.

49. Chitturi, J., et al., *Early Behavioral and Metabolomic Change after Mild to Moderate Traumatic Brain Injury in the Developing Brain.* Neurochemistry international, 2018. **120**: p. 75-86.

50. Li, Y., et al., *Toll-Like Receptor 4 Enhancement of Non-Nmda Synaptic Currents Increases Dentate Excitability after Brain Injury.* Neurobiology of disease, 2015. **74**: p. 240-53.

51. Kinoshita, K., et al., *Interleukin-1beta Messenger Ribonucleic Acid and Protein Levels after Fluid-Percussion Brain Injury in Rats: Importance of Injury*

Severity and Brain Temperature. Neurosurgery, 2002. **51**(1): p. 195-203; discussion 203.

52. Vitarbo, E.A., et al., *Tumor Necrosis Factor Alpha Expression and Protein Levels after Fluid Percussion Injury in Rats: The Effect of Injury Severity and Brain Temperature.* Neurosurgery, 2004. **55**(2): p. 416-24; discussion 424-5.

53. D'Ambrosio, R., et al., *Post-Traumatic Epilepsy Following Fluid Percussion Injury in the Rat.* Brain : a journal of neurology, 2004. **127**(Pt 2): p. 304-14.

54. Sanders, M.J., et al., *Chronic Failure in the Maintenance of Long-Term Potentiation Following Fluid Percussion Injury in the Rat.* Brain research, 2000. **861**(1): p. 69-76.

55. Schmidt, R.H. and M.S. Grady, *Regional Patterns of Blood-Brain Barrier Breakdown Following Central and Lateral Fluid Percussion Injury in Rodents.* Journal of neurotrauma, 1993. **10**(4): p. 415-30.

56. Morehead, M., et al., *Histopathologic Consequences of Moderate Concussion in an Animal Model: Correlations with Duration of Unconsciousness.* Journal of neurotrauma, 1994. **11**(6): p. 657-67.

57. Zeeshan, M., et al., *The Novel Oral Anticoagulants (Noacs) Have Worse Outcomes Compared to Warfarin in Patients with Intracranial Hemorrhage after Tbi.* The journal of trauma and acute care surgery, 2018.

58. Vanderploeg, R.D., et al., *Health Outcomes Associated with Military Deployment: Mild Traumatic Brain Injury, Blast, Trauma, and Combat Associations in the Florida National Guard.* Archives of physical medicine and rehabilitation, 2012. **93**(11): p. 1887-95.

59. Otis, J.D., et al., *Complicating Factors Associated with Mild Traumatic Brain Injury: Impact on Pain and Posttraumatic Stress Disorder Treatment.* Journal of clinical psychology in medical settings, 2011. **18**(2): p. 145-54.

60. Levin, H.S. and R.R. Diaz-Arrastia, *Diagnosis, Prognosis, and Clinical Management of Mild Traumatic Brain Injury.* The Lancet. Neurology, 2015. **14**(5): p. 506-17.

61. Godoy, D.A., et al., *Moderate Traumatic Brain Injury: The Grey Zone of Neurotrauma.* Neurocritical care, 2016. **25**(2): p. 306-19.

62. Dijkland, S.A., et al., *Prognosis in Moderate and Severe Traumatic Brain Injury: A Systematic Review of Contemporary Models and Validation Studies.* Journal of neurotrauma, 2019.

63. Edlow, B.L., et al., *Early Detection of Consciousness in Patients with Acute Severe Traumatic Brain Injury.* Brain : a journal of neurology, 2017. **140**(9): p. 2399-2414.

64. Tang, Q., et al., *Prevalence of Persistent Vegetative State in Patients with Severe Traumatic Brain Injury and Its Trend During the Past Four Decades: A Meta-Analysis.* NeuroRehabilitation, 2017. **40**(1): p. 23-31.

65. Iverson, K.M., C.M. Dardis, and T.K. Pogoda, *Traumatic Brain Injury and Ptsd Symptoms as a Consequence of Intimate Partner Violence.* Comprehensive psychiatry, 2017. **74**: p. 80-87.

66. Omalu, B., et al., *Chronic Traumatic Encephalopathy in an Iraqi War Veteran with Posttraumatic Stress Disorder Who Committed Suicide.* Neurosurgical focus, 2011. **31**(5): p. E3.

67. Goldstein, L.E., et al., *Chronic Traumatic Encephalopathy in Blast-Exposed Military Veterans and a Blast Neurotrauma Mouse Model.* Science translational medicine, 2012. **4**(134): p. 134ra60.

68. Cantu, R.C., et al., *Overview of Concussion Consensus Statements since 2000.* Neurosurg Focus, 2006. **21**(4): p. E3.

69. Ray, J.W., et al., *Current Concepts in Concussion: A Review.* Journal of the California Dental Association, 2017. **45**(6): p. 285-89.

70. Bailes, J.E. and R.C. Cantu, *Head Injury in Athletes.* Neurosurgery, 2001. **48**(1): p. 26-45; discussion 45-6.

71. McKee, A.C., et al., *Chronic Traumatic Encephalopathy in Athletes: Progressive Tauopathy after Repetitive Head Injury.* Journal of neuropathology and experimental neurology, 2009. **68**(7): p. 709-35.

72. Goldberg, A.S., et al., *Injury Surveillance in Young Athletes: A Clinician's Guide to Sports Injury Literature.* Sports medicine (Auckland, N.Z.), 2007. **37**(3): p. 265-78.

73. Bazarian, J.J., et al., *Mild Traumatic Brain Injury in the United States, 1998--2000.* Brain injury, 2005. **19**(2): p. 85-91.

74. Leibson, C.L., et al., *Incidence of Traumatic Brain Injury across the Full Disease Spectrum: A Population-Based Medical Record Review Study.* Epidemiology (Cambridge, Mass.), 2011. **22**(6): p. 836-44.

75. Bhowmick, S., et al., *Impairment of Pericyte-Endothelium Crosstalk Leads to Blood-Brain Barrier Dysfunction Following Traumatic Brain Injury.* Experimental neurology, 2019. **317**: p. 260-270.

76. Persidsky, Y., et al., *Blood-Brain Barrier: Structural Components and Function under Physiologic and Pathologic Conditions.* Journal of neuroimmune pharmacology : the official journal of the Society on NeuroImmune Pharmacology, 2006. **1**(3): p. 223-36.

77. Perel, P., et al., *Intracranial Bleeding in Patients with Traumatic Brain Injury: A Prognostic Study.* BMC emergency medicine, 2009. **9**: p. 15.

78. Hochstadter, E., et al., *Subarachnoid Hemorrhage Prevalence and Its Association with Short-Term Outcome in Pediatric Severe Traumatic Brain Injury.* Neurocritical care, 2014. **21**(3): p. 505-13.

79. Faust, K., et al., *Blood Pressure Changes after Aneurysmal Subarachnoid Hemorrhage and Their Relationship to Cerebral Vasospasm and Clinical Outcome.* Clinical neurology and neurosurgery, 2014. **125**: p. 36-40.

80. Kooijman, E., et al., *Long-Term Functional Consequences and Ongoing Cerebral Inflammation after Subarachnoid Hemorrhage in the Rat.* PloS one, 2014. **9**(6): p. e90584.

81. Maegele, M., et al., *Coagulopathy and Haemorrhagic Progression in Traumatic Brain Injury: Advances in Mechanisms, Diagnosis, and Management.* The Lancet. Neurology, 2017. **16**(8): p. 630-647.

82. Robba, C., et al., *Coagulation Management in Patients Undergoing Neurosurgical Procedures.* Current opinion in anaesthesiology, 2017. **30**(5): p. 527-533.

83. Skrifvars, M.B., et al., *Venous Thromboembolic Events in Critically Ill Traumatic Brain Injury Patients.* Intensive care medicine, 2017. **43**(3): p. 419-428.

84. Schwarzmaier, S.M., et al., *Temporal Profile of Thrombogenesis in the Cerebral Microcirculation after Traumatic Brain Injury in Mice.* Journal of neurotrauma, 2010. **27**(1): p. 121-30.

85. Stein, S.C., et al., *Association between Intravascular Microthrombosis and Cerebral Ischemia in Traumatic Brain Injury.* Neurosurgery, 2004. **54**(3): p. 687-91; discussion 691.

86. Gaasch, J.A., et al., *Brain Iron Toxicity: Differential Responses of Astrocytes, Neurons, and Endothelial Cells.* Neurochemical research, 2007. **32**(7): p. 1196-208.

87. Dietrich, W.D., et al., *Widespread Hemodynamic Depression and Focal Platelet Accumulation after Fluid Percussion Brain Injury: A Double-Label Autoradiographic Study in Rats.* Journal of cerebral blood flow and metabolism : official journal of the International Society of Cerebral Blood Flow and Metabolism, 1996. **16**(3): p. 481-9.

88. Albert-Weissenberger, C., et al., *How Is the Formation of Microthrombi after Traumatic Brain Injury Linked to Inflammation?* Journal of neuroimmunology, 2019. **326**: p. 9-13.

89. Allingstrup, M., et al., *Antithrombin Iii for Critically Ill Patients: A Systematic Review with Meta-Analysis and Trial Sequential Analysis.* Intensive care medicine, 2016. **42**(4): p. 505-520.

90. Grenander, A., et al., *Antithrombin Treatment in Patients with Traumatic Brain Injury: A Pilot Study.* Journal of neurosurgical anesthesiology, 2001. **13**(1): p. 49-56.

91. Shen, X., et al., *A Systematic Review of the Benefits and Risks of Anticoagulation Following Traumatic Brain Injury.* The Journal of head trauma rehabilitation, 2015. **30**(4): p. E29-37.

92. Stein, S.C., et al., *Intravascular Coagulation: A Major Secondary Insult in Nonfatal Traumatic Brain Injury.* Journal of neurosurgery, 2002. **97**(6): p. 1373-7.

93. Stein, S.C., et al., *Erythrocyte-Bound Tissue Plasminogen Activator Is Neuroprotective in Experimental Traumatic Brain Injury.* Journal of neurotrauma, 2009. **26**(9): p. 1585-92.

94. Lyeth, B.G., *Historical Review of the Fluid-Percussion Tbi Model.* Frontiers in neurology, 2016. **7**: p. 217.

95. Lifshitz, J., et al., *Clinical Relevance of Midline Fluid Percussion Brain Injury: Acute Deficits, Chronic Morbidities and the Utility of Biomarkers.* Brain injury, 2016. **30**(11): p. 1293-1301.

96. Xiong, Y., A. Mahmood, and M. Chopp, *Animal Models of Traumatic Brain Injury.* Nature reviews. Neuroscience, 2013. **14**(2): p. 128-42.

97. Iliff, J.J., et al., *Cerebral Arterial Pulsation Drives Paravascular Csf-Interstitial Fluid Exchange in the Murine Brain.* The Journal of neuroscience : the official journal of the Society for Neuroscience, 2013. **33**(46): p. 18190-9.

98. Ma X, et al., *Hemorrhage Associated Mechanisms of Neuroinflammation in Experimental Traumatic Brain Injury.* Journal of Neuroimmune Pharmacology, forthcoming 2019.

99. Rhind, S.G., et al., *Prehospital Resuscitation with Hypertonic Saline-Dextran Modulates Inflammatory, Coagulation and Endothelial Activation Marker Profiles in Severe Traumatic Brain Injured Patients.* Journal of neuroinflammation, 2010. **7**: p. 5.

100. Zehtabchi, S., et al., *The Association of Coagulopathy and Traumatic Brain Injury in Patients with Isolated Head Injury.* Resuscitation, 2008. **76**(1): p. 52-6.

101. Liu, D.Z., et al., *Inhibition of Src Family Kinases Protects Hippocampal Neurons and Improves Cognitive Function after Traumatic Brain Injury.* Journal of neurotrauma, 2014. **31**(14): p. 1268-76.

102. Zhou, H., et al., *Moderate Traumatic Brain Injury Triggers Rapid Necrotic Death of Immature Neurons in the Hippocampus.* Journal of neuropathology and experimental neurology, 2012. **71**(4): p. 348-59.

103. Su, X., et al., *Necrostatin-1 Ameliorates Intracerebral Hemorrhage-Induced Brain Injury in Mice through Inhibiting Rip1/Rip3 Pathway.* Neurochemical research, 2015. **40**(4): p. 643-50.

104. Ndode-Ekane, X.E., et al., *T-Cell Infiltration into the Perilesional Cortex Is Long-Lasting and Associates with Poor Somatomotor Recovery after Experimental Traumatic Brain Injury.* Restorative neurology and neuroscience, 2018. **36**(4): p. 485-501.

105. Nguyen, R., et al., *The International Incidence of Traumatic Brain Injury: A Systematic Review and Meta-Analysis.* The Canadian journal of neurological sciences. Le journal canadien des sciences neurologiques, 2016. **43**(6): p. 774-785.

106. Xiong, Y., A. Mahmood, and M. Chopp, *Current Understanding of Neuroinflammation after Traumatic Brain Injury and Cell-Based Therapeutic Opportunities.* Chinese journal of traumatology = Zhonghua chuang shang za zhi, 2018. **21**(3): p. 137-151.

107. Timaru-Kast, R., et al., *Influence of Age on Brain Edema Formation, Secondary Brain Damage and Inflammatory Response after Brain Trauma in Mice.* PloS one, 2012. **7**(8): p. e43829.

108. Morganti, J.M., et al., *Age Exacerbates the Ccr2/5-Mediated Neuroinflammatory Response to Traumatic Brain Injury.* Journal of neuroinflammation, 2016. **13**(1): p. 80.

109. Charolidi, N., T. Schilling, and C. Eder, *Microglial Kv1.3 Channels and P2y12 Receptors Differentially Regulate Cytokine and Chemokine Release from Brain Slices of Young Adult and Aged Mice.* PloS one, 2015. **10**(5): p. e0128463.

110. Ofengeim, D., et al., *Ripk1 Mediates a Disease-Associated Microglial Response in Alzheimer's Disease.* Proceedings of the National Academy of Sciences of the United States of America, 2017. **114**(41): p. E8788-e8797.

111. Merlini, M., et al., *Fibrinogen Induces Microglia-Mediated Spine Elimination and Cognitive Impairment in an Alzheimer's Disease Model.* Neuron, 2019.

112. Merlini, M., D. Wanner, and R.M. Nitsch, *Tau Pathology-Dependent Remodelling of Cerebral Arteries Precedes Alzheimer's Disease-Related Microvascular Cerebral Amyloid Angiopathy.* Acta neuropathologica, 2016. **131**(5): p. 737-52.

113. Ling, H., J. Hardy, and H. Zetterberg, *Neurological Consequences of Traumatic Brain Injuries in Sports.* Molecular and cellular neurosciences, 2015. **66**(Pt B): p. 114-22.

114. Elder, G.A., et al., *Vascular and Inflammatory Factors in the Pathophysiology of Blast-Induced Brain Injury.* Frontiers in neurology, 2015. **6**: p. 48.

115. Haorah, J., et al., *Oxidative Stress Activates Protein Tyrosine Kinase and Matrix Metalloproteinases Leading to Blood-Brain Barrier Dysfunction.* Journal of neurochemistry, 2007. **101**(2): p. 566-76.

116. Abdul Muneer, P.M., et al., *The Mechanisms of Cerebral Vascular Dysfunction and Neuroinflammation by Mmp-Mediated Degradation of Vegfr-2 in Alcohol Ingestion.* Arteriosclerosis, thrombosis, and vascular biology, 2012. **32**(5): p. 1167-77.

117. O'Connell, K.M. and M.T. Littleton-Kearney, *The Role of Free Radicals in Traumatic Brain Injury.* Biological research for nursing, 2013. **15**(3): p. 253-63.

118. Mittal, M., et al., *Reactive Oxygen Species in Inflammation and Tissue Injury.* Antioxid Redox Signal, 2014. **20**(7): p. 1126-67.

119. Abdul-Muneer, P.M., et al., *Induction of Oxidative and Nitrosative Damage Leads to Cerebrovascular Inflammation in an Animal Model of Mild Traumatic Brain Injury Induced by Primary Blast.* Free radical biology & medicine, 2013. **60**: p. 282-91.

120. Alikunju, S., et al., *The Inflammatory Footprints of Alcohol-Induced Oxidative Damage in Neurovascular Components.* Brain, behavior, and immunity, 2011. **25 Suppl 1**: p. S129-36.

121. Grammas, P., *A Damaged Microcirculation Contributes to Neuronal Cell Death in Alzheimer's Disease.* Neurobiology of aging, 2000. **21**(2): p. 199-205.

122. Benveniste, E.N., V.T. Nguyen, and G.M. O'Keefe, *Immunological Aspects of Microglia: Relevance to Alzheimer's Disease.* Neurochemistry international, 2001. **39**(5-6): p. 381-91.

123. Wu, D.C., et al., *Nadph Oxidase Mediates Oxidative Stress in the 1-Methyl-4-Phenyl-1,2,3,6-Tetrahydropyridine Model of Parkinson's Disease.* Proceedings of the National Academy of Sciences of the United States of America, 2003. **100**(10): p. 6145-50.

124. Abdul-Muneer, P.M., N. Chandra, and J. Haorah, *Interactions of Oxidative Stress and Neurovascular Inflammation in the Pathogenesis of Traumatic Brain Injury.* Molecular neurobiology, 2015. **51**(3): p. 966-79.

125. Jeong, H.K., et al., *Brain Inflammation and Microglia: Facts and Misconceptions.* Experimental neurobiology, 2013. **22**(2): p. 59-67.

126. Donat, C.K., et al., *Microglial Activation in Traumatic Brain Injury.* Frontiers in aging neuroscience, 2017. **9**: p. 208.

127. Kumar, A., et al., *Microglial/Macrophage Polarization Dynamics Following Traumatic Brain Injury.* Journal of neurotrauma, 2016. **33**(19): p. 1732-1750.

128. Cherry, J.D., J.A. Olschowka, and M.K. O'Banion, *Neuroinflammation and M2 Microglia: The Good, the Bad, and the Inflamed.* Journal of neuroinflammation, 2014. **11**: p. 98.

129. Younger, D., et al., *Microglia Receptors in Animal Models of Traumatic Brain Injury.* Molecular neurobiology, 2019. **56**(7): p. 5202-5228.

130. Lively, S. and L.C. Schlichter, *Microglia Responses to Pro-Inflammatory Stimuli (Lps, Ifngamma+Tnfalpha) and Reprogramming by Resolving Cytokines (Il-4, Il-10).* Frontiers in cellular neuroscience, 2018. **12**: p. 215.

131. Cheng, Y., et al., *Alcohol Promotes Waste Clearance in the Cns Via Brain Vascular Reactivity.* Free radical biology & medicine, 2019. **143**: p. 115-126.

132. Rama Rao, K.V., et al., *A Single Primary Blast-Induced Traumatic Brain Injury in a Rodent Model Causes Cell-Type Dependent Increase in Nicotinamide Adenine Dinucleotide Phosphate Oxidase Isoforms in Vulnerable Brain Regions.* Journal of neurotrauma, 2018. **35**(17): p. 2077-2090.

133. Kuriakose, M., et al., *Temporal and Spatial Effects of Blast Overpressure on Blood-Brain Barrier Permeability in Traumatic Brain Injury.* Sci Rep, 2018. **8**(1): p. 8681.

134. Kuriakose, M., et al., *Synergistic Role of Oxidative Stress and Blood-Brain Barrier Permeability as Injury Mechanisms in the Acute Pathophysiology of Blast-Induced Neurotrauma.* Sci Rep, 2019. **9**(1): p. 7717.

135. Ma, X., et al., *Hemorrhage Associated Mechanisms of Neuroinflammation in Experimental Traumatic Brain Injury.* Journal of neuroimmune pharmacology : the official journal of the Society on NeuroImmune Pharmacology, 2019.

136. Kokiko-Cochran, O.N. and J.P. Godbout, *The Inflammatory Continuum of Traumatic Brain Injury and Alzheimer's Disease.* Frontiers in immunology, 2018. **9**: p. 672.

137. Hawkins, B.E., et al., *Rapid Accumulation of Endogenous Tau Oligomers in a Rat Model of Traumatic Brain Injury: Possible Link between Traumatic Brain Injury and Sporadic Tauopathies.* The Journal of biological chemistry, 2013. **288**(23): p. 17042-50.

138. McGeer, P.L., et al., *Reactive Microglia Are Positive for Hla-Dr in the Substantia Nigra of Parkinson's and Alzheimer's Disease Brains.* Neurology, 1988. **38**(8): p. 1285-91.

139. Ouchi, Y., et al., *Microglial Activation and Dopamine Terminal Loss in Early Parkinson's Disease.* Annals of neurology, 2005. **57**(2): p. 168-75.

140. Xiong, Y., A. Mahmood, and M. Chopp, *Angiogenesis, Neurogenesis and Brain Recovery of Function Following Injury.* Current opinion in investigational drugs (London, England : 2000), 2010. **11**(3): p. 298-308.

141. Beck, H. and K.H. Plate, *Angiogenesis after Cerebral Ischemia.* Acta neuropathologica, 2009. **117**(5): p. 481-96.

142. Wu, H., et al., *Induction of Angiogenesis and Modulation of Vascular Endothelial Growth Factor Receptor-2 by Simvastatin after Traumatic Brain Injury.* Neurosurgery, 2011. **68**(5): p. 1363-71; discussion 1371.

143. Xiong, Y., et al., *Delayed Administration of Erythropoietin Reducing Hippocampal Cell Loss, Enhancing Angiogenesis and Neurogenesis, and Improving Functional Outcome Following Traumatic Brain Injury in Rats: Comparison of Treatment with Single and Triple Dose.* Journal of neurosurgery, 2010. **113**(3): p. 598-608.

144. Xiong, Y., et al., *Effects of Posttraumatic Carbamylated Erythropoietin Therapy on Reducing Lesion Volume and Hippocampal Cell Loss, Enhancing Angiogenesis and Neurogenesis, and Improving Functional Outcome in Rats Following Traumatic Brain Injury.* Journal of neurosurgery, 2011. **114**(2): p. 549-59.

145. Wang, B., et al., *Effects of Atorvastatin in the Regulation of Circulating Epcs and Angiogenesis in Traumatic Brain Injury in Rats.* Journal of the neurological sciences, 2012. **319**(1-2): p. 117-23.

146. Thau-Zuchman, O., et al., *Subacute Treatment with Vascular Endothelial Growth Factor after Traumatic Brain Injury Increases Angiogenesis and Gliogenesis.* Neuroscience, 2012. **202**: p. 334-41.

147. Wang, T.W., et al., *Effects of an Injectable Functionalized Self-Assembling Nanopeptide Hydrogel on Angiogenesis and Neurogenesis for Regeneration of the Central Nervous System.* Nanoscale, 2017. **9**(42): p. 16281-16292.

148. Kumar, V.A., et al., *Highly Angiogenic Peptide Nanofibers.* ACS Nano, 2015. **9**(1): p. 860-8.

149. Wang, Y., et al., *Vegf-Overexpressing Transgenic Mice Show Enhanced Post-Ischemic Neurogenesis and Neuromigration.* Journal of neuroscience research, 2007. **85**(4): p. 740-7.

150. Guo, H., et al., *Vascular Endothelial Growth Factor: An Attractive Target in the Treatment of Hypoxic/Ischemic Brain Injury.* Neural regeneration research, 2016. **11**(1): p. 174-9.

151. Jin, K., et al., *Vascular Endothelial Growth Factor (Vegf) Stimulates Neurogenesis in Vitro and in Vivo.* Proceedings of the National Academy of Sciences of the United States of America, 2002. **99**(18): p. 11946-50.

152. Ortuzar, N., et al., *Vegf Reverts the Cognitive Impairment Induced by a Focal Traumatic Brain Injury During the Development of Rats Raised under Environmental Enrichment.* Behavioural brain research, 2013. **246**: p. 36-46.

153. Petrak, K., et al., *Challenges in Translating from Bench to Bed-Side: Pro-Angiogenic Peptides for Ischemia Treatment.* Molecules (Basel, Switzerland), 2019. **24**(7).

154. Sarkar, B., et al., *Angiogenic Self-Assembling Peptide Scaffolds for Functional Tissue Regeneration.* Biomacromolecules, 2018. **19**(9): p. 3597–3611.

155. Kumar, V.A., et al., *Treatment of Hind Limb Ischemia Using Angiogenic Peptide Nanofibers.* Biomaterials, 2016. **98**: p. 113-9.

156. Kumar, V.A., B.K. Wang, and S.M. Kanahara, *Rational Design of Fiber Forming Supramolecular Structures.* Experimental biology and medicine (Maywood, N.J.), 2016. **241**(9): p. 899-908.

157. Kumar, V.A., et al., *Nanofibrous Snake Venom Hemostat.* ACS biomaterials science & engineering, 2015. **1**(12): p. 1300-1305.

158. Kumar, V.A., et al., *Drug-Triggered and Cross-Linked Self-Assembling Nanofibrous Hydrogels.* Journal of the American Chemical Society, 2015. **137**(14): p. 4823-30.

159. Kumar, V.A., et al., *Self-Assembling Multidomain Peptides Tailor Biological Responses through Biphasic Release.* Biomaterials, 2015. **52**: p. 71-8.

160. Lafuente, J.V., E.G. Argandona, and B. Mitre, *Vegfr-2 Expression in Brain Injury: Its Distribution Related to Brain-Blood Barrier Markers.* Journal of neural transmission (Vienna, Austria : 1996), 2006. **113**(4): p. 487-96.

161. Lu, K.T., et al., *Hippocampal Neurogenesis after Traumatic Brain Injury Is Mediated by Vascular Endothelial Growth Factor Receptor-2 and the Raf/Mek/Erk Cascade.* Journal of neurotrauma, 2011. **28**(3): p. 441-50.

162. Krum, J.M., N. Mani, and J.M. Rosenstein, *Roles of the Endogenous Vegf Receptors Flt-1 and Flk-1 in Astroglial and Vascular Remodeling after Brain Injury.* Experimental neurology, 2008. **212**(1): p. 108-17.

163. Sarkar, B., et al., *Membrane-Disrupting Nanofibrous Peptide Hydrogels.* ACS biomaterials science & engineering, 2019. **5**(9): p. 4657-4670.

164. Nguyen, P.K., et al., *Self-Assembly of an Antiangiogenic Nanofibrous Peptide Hydrogel.* ACS Applied Bio Materials, 2018. **1**(3): p. 865-870.

165. Nguyen, P.K., et al., *Self-Assembly of a Dentinogenic Peptide Hydrogel.* ACS Omega, 2018. **3**(6): p. 5980-5987.

166. Hitscherich, P., et al., *Injectable Self-Assembling Peptide Hydrogels for Tissue Writing and Embryonic Stem Cell Culture.* Journal of biomedical nanotechnology, 2018. **14**(4): p. 802-807.

167. Shi, S., et al., *Development of Peptide Inhibitors of Hiv Transmission.* Bioactive materials, 2016. **1**(2): p. 109-121.

168. Hopp, S., et al., *Targeting Coagulation Factor Xii as a Novel Therapeutic Option in Brain Trauma.* Annals of neurology, 2016. **79**(6): p. 970-82.

169. Wu, H., et al., *Simvastatin-Mediated Upregulation of Vegf and Bdnf, Activation of the Pi3k/Akt Pathway, and Increase of Neurogenesis Are Associated with Therapeutic Improvement after Traumatic Brain Injury.* Journal of neurotrauma, 2008. **25**(2): p. 130-9.

170. Lee, C. and D.V. Agoston, *Vascular Endothelial Growth Factor Is Involved in Mediating Increased De Novo Hippocampal Neurogenesis in Response to Traumatic Brain Injury.* Journal of neurotrauma, 2010. **27**(3): p. 541-53.

171. Tovar-y-Romo, L.B., A. Penagos-Puig, and J.O. Ramirez-Jarquin, *Endogenous Recovery after Brain Damage: Molecular Mechanisms That Balance Neuronal Life/Death Fate.* Journal of neurochemistry, 2016. **136**(1): p. 13-27.

172. Mena, H., D. Cadavid, and E.J. Rushing, *Human Cerebral Infarct: A Proposed Histopathologic Classification Based on 137 Cases.* Acta neuropathologica, 2004. **108**(6): p. 524-30.

173. Folkersma, H., et al., *Increased Cerebral (R)-[(11)C]Pk11195 Uptake and Glutamate Release in a Rat Model of Traumatic Brain Injury: A Longitudinal Pilot Study.* Journal of neuroinflammation, 2011. **8**: p. 67.

174. Zipfel, G.J., et al., *Neuronal Apoptosis after Cns Injury: The Roles of Glutamate and Calcium.* Journal of neurotrauma, 2000. **17**(10): p. 857-69.

175. Brosius Lutz, A. and B.A. Barres, *Contrasting the Glial Response to Axon Injury in the Central and Peripheral Nervous Systems.* Dev Cell, 2014. **28**(1): p. 7-17.

176. Blennow, K., et al., *Traumatic Brain Injuries.* Nat Rev Dis Primers, 2016. **2**: p. 16084.

177. Song, B., et al., *Sustained Local Delivery of Bioactive Nerve Growth Factor in the Central Nervous System Via Tunable Diblock Copolypeptide Hydrogel Depots.* Biomaterials, 2012. **33**(35): p. 9105-16.

178. Anderson, M.A., et al., *Astrocyte Scar Formation Aids Central Nervous System Axon Regeneration.* Nature, 2016. **532**(7598): p. 195-200.

179. Nguyen, P.K., et al., *Self-Assembly of an Anti-Angiogenic Nanofibrous Peptide Hydrogel.* ACS Appl. Bio Mater., 2018. **1**(3): p. 865-870.

180. Shashoua, V.E., et al., *Neuroprotective Effects of a New Synthetic Peptide, Cmx-9236, in in Vitro and in Vivo Models of Cerebral Ischemia.* Brain research, 2003. **963**(1-2): p. 214-23.

181. Sanyal, S., et al., *Ap-1 Functions Upstream of Creb to Control Synaptic Plasticity in Drosophila.* Nature, 2002. **416**(6883): p. 870-4.

182. Ma, T.C., et al., *Camp-Responsive Element-Binding Protein (Creb) and Camp Co-Regulate Activator Protein 1 (Ap1)-Dependent Regeneration-Associated Gene Expression and Neurite Growth.* The Journal of biological chemistry, 2014. **289**(47): p. 32914-25.

183. Tuvikene, J., et al., *Ap-1 Transcription Factors Mediate Bdnf-Positive Feedback Loop in Cortical Neurons.* The Journal of neuroscience : the official journal of the Society for Neuroscience, 2016. **36**(4): p. 1290-305.

184. Di, L., *Strategic Approaches to Optimizing Peptide Adme Properties.* AAPS J, 2015. **17**(1): p. 134-43.

185. Sarkar, B., et al., *Membrane-Disrupting Nanofibrous Peptide Hydrogels.* ACS Biomat. Sci. Eng., 2019. **5**(9): p. 4657-4670.

186. Boeck, C.R., et al., *The Modulation of Ecto-Nucleotidase Activities by Glutamate in Cultured Cerebellar Granule Cells.* Neuroreport, 2000. **11**(4): p. 709-12.

187. Datusalia, A.K., et al., *Hyper-Insulinemia Increases the Glutamate-Excitotoxicity in Cortical Neurons: A Mechanistic Study.* Eur J Pharmacol, 2018. **833**: p. 524-530.